LAWRENCE
LIVERMORE
NATIONAL
LABORATORY

UCRL-TR-217193

DOE Project on Heavy Vehicle Aerodynamic Drag FY 2005 Annual Report

R. C. McCallen, K. Salari, J. Ortega, P. Castellucci, C. Eastwood, J. Paschkewitz, W. D. Pointer, L. J. DeChant, B. Hassan, F. Browand, C. Radovich, T. Merzel, D. Plocher, J. Ross, B. Storms, J. T. Heineck, S. Walker, C. J. Roy

November 18, 2005

This work was performed under the auspices of the U.S. Department of Energy by University of California, Lawrence Livermore National Laboratory under Contract W-7405-Eng-48.

DOE Project on Heavy Vehicle Aerodynamic Drag

Project Principal Investigator: R. C. McCallen
Lawrence Livermore National Laboratory
P.O. Box 808, Livermore, CA 94551-0808
(925) 423-0958; mccallen1@llnl.gov

Principal Investigator: K. Salari
Co-Investigators: J. Ortega, P. Castellucci, C. Eastwood, J. Paschkewitz
Lawrence Livermore National Laboratory
P.O. Box 808, Livermore, CA 94551-0808
(925) 424-4635; salari1@llnl.gov

Principal Investigator: W. D. Pointer
Argonne National Laboratory
9700 S. Cass Avenue, NE-208, Argonne, IL 60439
(630) 252-1052; dpointer@anl.gov

Principal Investigator: L. J. DeChant
Co-Investigators: B. Hassan
Sandia National Laboratories
P.O. Box 5800, MS 0825, Albuquerque, NM 87185-0825
(505) 844-4250 ljdecha@sandia.gov

Principal Investigator: F. Browand
Co-Investigators: C. Radovich, T. Merzel, D. Plocher
Aerospace & Mechanical Engineering, University of Southern California
RRB 203, Los Angeles CA 90089-1191
(213) 740-5359; e-mail: browand@spock.usc.edu

Principal Investigator: J. Ross
Co-Investigators: B. Storms, J.T. Heineck, S. Walker
NASA Ames Research Center
MS 260-1, Moffett Field, CA 94035
(650) 604-6722; jcross@mail.arc.nasa.gov

Principal Investigator: C. J. Roy
Auburn University
211 Aerospace Engineering Building
Auburn University, AL 36849-5338

(334) 844-5187 cjroy@eng.auburn.edu

Technology Development Manager: Lee Slezak
202-586-2335, Lee.Slezak@EE.DOE.GOV
Technical Program Manager: Jules Routbort
630-252-5065, routbort@anl.gov

Contractor: Lawrence Livermore National Laboratory, Sandia National Laboratories, Argonne National Laboratory, NASA Ames Research Center

Contract No.: W-7405-ENG-48, DE-AC04-94AL85000, W-31-109-ENG-38, DE-AI01-99EE50559

In Memory

Dr. Sidney ('Sid') Diamond

This document is dedicated to our DOE Program Manager, supporter, and dear friend Dr. Sid Diamond. This Consortium effort would not exist without Sid's vision, dedication, perseverance, and passion. His enthusiasm for this project, with his wonderful gusto for life, was contagious and pushed our effort forward. He will be dearly missed.

Objective

Class 8 tractor-trailers consume 11-12% of the total US petroleum use. At high way speeds, 65% of the energy expenditure for a Class 8 truck is in overcoming aerodynamic drag. The project objective is to improve fuel economy of Class 8 tractor-trailers by providing guidance on methods of reducing drag by at least 25%. A 25% reduction in drag would present a 12% improvement in fuel economy at highway speeds, equivalent to about 130 midsize tanker ships per year. Specific goals include:

- Provide guidance to industry in the reduction of aerodynamic drag of heavy truck vehicles.
- Establish a database of experimental, computational, and conceptual design information, and demonstrate the potential of new drag-reduction devices.

Approach

- Develop and demonstrate the ability to simulate and analyze aerodynamic flow around heavy truck vehicles using existing and advanced computational fluid dynamics (CFD) tools.
- Through an extensive experimental effort, generate an experimental data base for code validation.
- Using experimental data base, validate computations.
- Provide industry with design guidance and insight into flow phenomena from experiments and computations.
- Investigate aero devices (e.g., base flaps, tractor-trailer gap stabilizer, underbody skirts and wedges, blowing and acoustic devices), provide industry with conceptual designs of drag reducing devices, and demonstrate the full-scale fuel economy potential of these devices.

Accomplishments

A multi-laboratory, multi-university consortium has constructed a multi-year program plan with industry. The consortium has leveraged ASCI funds, utilized results of complimentary Laboratory, University and NASA internal supported efforts, in addition to buy-in, collaboration, and communications with truck industries and organizations. The Program has

- Demonstrated several concepts and devices which meet the 25% drag reduction goal and represent a savings of 4,200 million gals per year. This is equivalent to 130 midsize tanker ships per year!
- Insight from experiments and experimental data base has provided clear guidance to industry on reliable, predictable experimental techniques.
- Computational results provide clear guidance and caution warnings on the use of steady Reynolds-averaged Navier Stokes (RANS) models for CFD simulations.

Future Direction

- Getting devices on road
  - From understanding of key flow mechanisms, develop less obtrusive and optimized device concepts
  - Demonstration wind tunnel, track, and road tests by leveraging work with DANA/ORNL, National Research Council of Canada, TMA/DOE, and seek collaborative demonstrations with fleet owners and operators
- Economic/duty cycle evaluation with PSAT (ANL's system model)
  - Provide mechanistic data: strong variation in drag per yaw, speed, geometry/devices, environment, etc
  - Review road/track test plans, provide needed assistance in calibration/evaluation to DANA/ORNL
- Develop and transfer technology and information to industry
  - Collaborate with DOE Industrial Consortium who will be conducting fleet tests of advanced aerodynamic drag reduction devices. Schedule industry meetings to share findings and encourage consideration of effective design concepts for road testing.
  - Continue experimental data reduction and analysis for the generic conventional model (GCM).
  - Continue computations of flow around GCM, compare to experimental data, perform analyses, and provide guidance to industry on use of unsteady RANS and hybrid RANS/Large-Eddy Simulation (LES) methods.
- Address consequences with aerodynamic drag reduction and use of devices
  - Contouring the tractor hood reduces the grille area, also reducing coolant flow. In addition, underhood exhaust gas recirculation to meet EPA 2007 regulation requires more underhood cooling. Per industry encouragement, we are including underhood flow in aerodynamic drag computations to provide insight into the coupled flow phenomena.
  - Aerodynamic devices reduce moving resistance increasing braking distance and require more braking down hill, encouraging bake overheating. Underbody and near wheel aerodynamic devices can also restrict critical brake air cooling. We will continue our investigation of air flow around rotating tires for improved brake cooling, as well as drag reduction.
  - Trailer base devices and side skirts appear to enhance air upwash which is likely to enhance splash and spray. Per industry encouragement, we will continue our investigation of device and wheel aero related to splash and spray from tires and devices, pursuing ways to minimize this road safety hazard.
- Leverage Program work and seek funding from other agencies.

Introduction

Class 8 tractor-trailers consume 11-12% of the total US petroleum use. A modern Class 8 tractor-trailer can weigh up to 80,000 pounds and has a wind-averaged drag coefficient around $C_D = 0.6$. The drag coefficient is defined as the drag/(dynamic pressure × projected area). The higher the speed the more energy consumed in overcoming aerodynamic drag. At 70 miles per hour, a common highway speed today, overcoming aerodynamic drag represents about 65% of the total energy expenditure for a typical heavy truck vehicle. Reduced fuel consumption for heavy vehicles can be achieved by altering truck shapes to decrease the aerodynamic resistance (drag). Reducing aerodynamic drag by 25% improves fuel economy by about 12% at highway speeds. This would result in a savings of over 4,000 million gallons per year or up to 130 midsize tanker ships per year.

The project goal is to develop and demonstrate the ability to simulate and analyze aerodynamic flow around heavy truck vehicles using existing and advanced computational fluid dynamics (CFD) tools. Activities also include an extensive experimental effort to generate data for code validation and a design effort for developing drag reducing devices. The final products are specific device concepts that can significantly reduce aerodynamic drag, and thus improve fuel efficiency, in addition to an experimental data base and validated CFD tools. The objective is to provide industry with clear guidance on methods of computational simulation and experimental modeling techniques that work for predicting the flow phenomena around a heavy vehicle and add-on drag reducing devices. Development of effective drag reducing devices is also a major goal.

The following reports on the findings and accomplishments for fiscal year 2005 in the project's three focus areas

- Drag reduction devices
- Experimental testing
- Computational modeling

Detailed reports from each participating organization are provided in the appendices. Included are experimental results by NASA and USC, and complimentary computations by LLNL, ANL in Appendices A through D. The computational results from LLNL, ANL, and SNL/Auburn for the integrated tractor-trailer benchmark geometry called the Ground Transportation System (GTS) model and Generic Conventional Model (GCM) are used for the trailer wake and tractor-trailer gap flow investigations, turbulence model development, and benchmark simulations being investigated. Auburn University's task involves performing Detached Eddy Simulation (DES) computations on the GTS geometry. This effort is an extension of a Fiscal Year 2004 task which involved DES simulations on a truncated version of the GTS model. The FY04 computations were found to have mesh quality issues, and thus a new mesh of the full geometry has been generated. DES simulations for both 15 million cell and 30 million cell meshes are running on 72 processors and final results will be presented in the next Annual Report. USC is also providing wind tunnel test results for variable angle tractor side

extenders and a novel tire splash/spray device in Appendix B and LLNL presents vehicle and wheel computational results for splash and spray in Appendix A.

Drag Reduction Devices and Future Plans

There are three areas identified for aero drag reduction and several drag reduction devices have been investigated

- **Tractor-Trailer Gap**
  Stabilizing devices, cab extenders
- **Wheels/Underbody**
  Skirts/wedge and lowboy trailer
- **Trailer Base**
  Boattail plates, base flaps, rounded edges, and pneumatics

Over 12% increase in fuel economy is possible, e.g.,

> 4% trailer base-flaps
> 6% trailer skirts
> 2% gap splitter plate
> 12% Total

Unfortunately, these devices have operational and maintenance issues. With our understanding of the key flow mechanisms, we are developing less obtrusive and optimized innovative design concepts using computational fluid dynamics and experiments. In addition, to get devices on the road, consequences with aerodynamic improvements need to be addressed.

Contouring the tractor hood reduces the grille area, also reducing coolant flow. In addition, underhood exhaust gas recirculation to meet EPA 2007 regulation requires more underhood cooling. Per industry encouragement, we are including underhood flow in aerodynamic drag computations to provide insight into the coupled flow phenomena.

Aerodynamic devices reduce moving resistance increasing braking distance and require more braking down hill, encouraging bake overheating. Underbody and near wheel aerodynamic devices can also restrict critical brake air cooling. We will continue our investigation of air flow around rotating tires for improved brake cooling, as well as drag reduction.

Trailer base devices and side skirts appear to enhance air upwash which is likely to enhance splash and spray. Per industry encouragement, we will continue our investigation of device and wheel aero related to splash and spray from tires and devices, pursuing ways to minimize this road safety hazard.

Addressing these consequences of aerodynamic improvements is an important task in getting devices on the road. Fortunately, the task overlaps with our efforts in device optimization. In addition, these issues are of interest to other government agencies (e.g., DOT and EPA) and industry (i.e., Michelin is providing partial support for experiments at USC). The splash and spray effort will continue to receive complimentary support from industry and we will actively seek joint government funding.

APPENDIX A

Kambiz Salari, Rose McCallen, Jason Ortega, Craig Eastwood, John S. Paschkewitz, Paul Castelucci
Lawrence Livermore National Laboratory
7000 East Ave, L-098, Livermore, CA 94551
925-423-0958, Fax 925-422-3389, mccallen1@llnl.gov

Technology Development Manager: Lee Slezak
202-586-2335, Lee.Slezak@EE.DOE.GOV
Technical Program Manager: Jules Routbort
630-252-5065, routbort@anl.gov

Contractor: Lawrence Livermore National Laboratory
Contract No.: W-7405-ENG-48

LLNL's effort consists of two experimental and computational focus areas:

- Improve fuel economy through innovative, effective conceptual design of aerodynamic drag reduction devices utilizing computational studies of devices for a trailer underbody, gap, and base
- Get devices on the road by addressing consequences of aerodynamic drag reduction related to brake performance and splash/spray through computational studies of tire aerodynamics and spray dispersion in tire and heavy vehicle flow fields.

The following describes the objective, approach, accomplishments, and future directions for each of these focus areas.

A. Computational Fluid Dynamics Simulations of Heavy Vehicle Drag Reduction Devices

Objective

- Evaluate the performance of heavy vehicle drag reduction devices applied to the tractor-trailer gap, trailer underbody, and trailer base
- Determine if computational modeling can replicate the performance of drag reduction devices seen experimentally
- Understand how the drag reduction devices alter the flow field about a heavy vehicle

Approach

- Perform computational fluid dynamics (CFD) simulations of heavy vehicle geometries at both wind-tunnel and full-scale operating conditions
- Model the drag reduction performance of add-on devices placed in the gap between the tractor and trailer (splitter plate), on the trailer base (base flaps), and beneath the trailer (wedge-shaped skirt)
- Compare the simulated results with experimental data

- Analyze the computed velocity and pressure fields to yield a deeper insight into how the drag reduction devices function

Accomplishments

- Assessed the performance of add-on drag reduction devices using CFD
  - At lab-scale Reynolds numbers, both the tractor cab extenders and the trailer splitter plate produce a 5% drag reduction at large gap lengths
  - At full-scale Reynolds numbers, the addition of a trailer splitter plate decreases vehicle drag by 1% while maintaining vehicle side force
  - At full-scale Reynolds numbers, base flaps decrease the drag coefficient by 8-14%
  - At full-scale Reynolds numbers, the wedge-shaped skirt decreases the drag coefficient by 2%
- Observed that at full-scale Reynolds numbers, the increased vertical flow in the gap between the tractor and trailer alters the gap flow structures.
- Determined that base flaps function by increasing the pressure on the trailer base through the elimination of a recirculation zone on the trailer base
- Investigated the sensitivity of the drag coefficient reduction of the wedge-shaped skirt and base flaps to both grid refinement and steady versus unsteady simulations

Future Direction

- Investigate the effect of varying the splitter plate size and gap length on drag reduction
- Utilize a trailer splitter plate in combination with compact tractor cab extenders, base flaps, and a wedge-shaped skirt on a heavy vehicle
- Investigate design modifications of the base flaps to further enhance their performance
- Evaluate the performance of drag reduction devices at finite yaw angles
- Design and simulate alternate drag reduction concepts that alleviate the recirculation zone on the trailer base

---

Introduction

Computational fluid dynamics (CFD) simulations are used to determine whether or not the drag reduction from add-on devices can be replicated with computer modeling. Additionally, CFD simulations provide three-dimensional data on pertinent flow quantities, such as velocity, pressure, vorticity, turbulent kinetic energy, and dissipation, which are not readily accessible about the entire vehicle using experimental measurements. This added information gives a deeper insight into how the devices modify the flow about a heavy vehicle and identifies the means by which the devices can be further optimized. The targeted areas for drag reduction are the gap between the tractor and trailer, the trailer base, and the trailer underbody, all of which have been shown previously (Cooper (2003)) to contribute significantly to the overall heavy vehicle drag.

Base flaps (Figure 1a) are selected to alleviate the trailer base drag, a wedge-shaped skirt (Figure1b) for the trailer underbody drag, and a gap splitter plate (Figure 1c) and cab extenders (Figure 1d) for the gap drag. The base flaps are comprised of four angled, flat plates, which can be folded against the trailer sides, allowing access to the trailer cargo area.

Previous studies (Cooper (2003), Ortega, et al. (2004), Storms, et al. (2004)) have shown that the base flaps provide a relatively constant drag reduction, ΔC_d, on the order of $0.04 \leq \Delta C_d \leq 0.1$ with respect to the vehicle yaw angle. Recent full-scale tests (Browand (2004)) demonstrated that the base flaps provide over a 4% improvement in fuel economy. The wedge-shaped skirt is formed from two flat plates that are suspended from the trailer underside. The advantage of the wedge-shaped skirt over conventional side skirts is that it does not limit driver access to the trailer underside. Small-scale wind tunnel tests at NASA Ames (Ortega, et al. (2004)) showed that the wedge-shaped skirt is capable of reducing the wind-averaged drag coefficient by approximately 2%. Recent experiments utilizing a gap splitter plate on the front trailer face have shown that the plate reduces the separated flow entrained into the tractor-trailer gap and makes the flow distribution more symmetric across the gap. As part of the DOE Heavy Vehicle Aerodynamics Consortium, USC has compiled body force and flow field wind-tunnel data for a simplified tractor-trailer at varying yaw angles and gap lengths. Preliminary experimental results indicate that a single trailer splitter plate may be as effective as tractor cab extenders in reducing aerodynamic drag at yaw without increasing side force substantially.

Computational Setup

To evaluate the base flaps and the wedge-shaped skirt, the GCM heavy vehicle model (Storms, et al. (2004)) (Figure 2) is used as a platform for the simulations. A freestream velocity and a moving ground plane of 65 mph are specified upstream and beneath the GCM, respectively. The deflection angle for the base flaps is chosen to be 20^o, which Storms et al. (2004) showed to be the optimum angle for the GCM geometry at full-scale Reynolds numbers. The turbulent flow about the GCM is modeled using both the steady and unsteady Reynolds-averaged Navier-Stokes (RANS) approach. The simulations are performed with the CFD code, STAR-CD, on the parallel supercomputers at LLNL with multiple computational meshes ranging in size from 1.4 to 10.0 million cells.

The drag reduction devices employed in the tractor-trailer gap are modeled on a simplified heavy vehicle geometry referred to as the MGTS (Figure 3). The simulations of the gap devices are performed with NASA's OVERFLOW code, a compressible, control-volume based code using overset grids (Hariharan, et al. (1997)). Based on prior experience (Salari, et al. (2004)), the two-equation, Menter SST, steady RANS turbulence model (Menter (1994)) is used for all simulations. To ensure proper turbulence model performance, all surface grids are extruded such that off-the-wall y+ values are less than unity. The computational domain extends fifteen vehicle widths upstream, thirty widths downstream, and ten above and to the sides of the model. All walls, with the exception of the ground plane, are assigned slip wall boundary conditions. This is done to mimic the blockage experienced in the 3' by 4' Dryden wind tunnel at USC (Browand & Hammache (2005)); however, no attempt is made to model the tunnel sides or ceiling. In addition, the four posts that support the model above the tunnel floor are omitted from computations. Furthermore, the incoming boundary layer is eliminated in the experiment by applying suction through the test section floor. This effect is reproduced computationally by applying a fixed velocity boundary condition to the ground plane.

Results and Discussion

The resulting drag reduction of the base flaps and wedge-shaped skirt are shown in Figure 4. Although there is some sensitivity to the level of grid confinement, a

comparison of the values of C_d between similar sized grids indicates that the simulations predict levels of drag reduction comparable to those seen experimentally. *Another important observation from this plot is that the unsteady RANS simulations, which require a substantial amount of CPU power and storage space, predict nearly the same drag coefficient as that seen in the steady RANS simulations. This result could be of interest to tractor-trailer manufactures, who are concerned about accurately predicting C_d, but do not have the computational capability to perform high resolution, unsteady simulations.*

The simulations also highlight the manner in which the devices alter the flow field about the heavy vehicle. As can be seen in the velocity streamlines (Figure 5), the wedge-shaped skirt increases the upwash beneath the trailer. The base flaps produce an appreciable downwash, which has the effect of transporting high momentum fluid from the freestream into the trailer wake and reducing the overall wake size. Furthermore, it is evident that the base flaps reduce both the size and strength of the swirling flow structure on the bottom half of the trailer wake. As can be seen in Figure 6, this swirling flow structure is source of the low pressure region on the trailer base. By eliminating this structure, the base flaps remove the low pressure footprint, increase the pressure over the trailer base, and reduce the overall vehicle drag.

The baseline MGTS simulations at lab-scale Reynolds number and 6° yaw compare favorably to experiment for both body forces and flow structure, see Figures 7 and 8. These results add confidence in the use of overset grids with steady RANS turbulence models for predicting the flow around a simplified tractor-trailer with drag-reducing devices. The trailer splitter plate is nearly as effective as tractor cab extenders in reducing drag at relatively low, lab-scale Reynolds numbers. Both devices appear to suffer from increases in vehicle side force, although the splitter plate to a lesser extent. In addition, each device is found to be most effective reducing drag on the part of the vehicle it is mounted to. Furthermore, the splitter plate is most effective at larger gap lengths, where more flow is entrained into the gap and interacts with the trailer face. A summary of each device's performance at two gap lengths is plotted in Figures 9 and 10.

At a full-scale Reynolds number of 7 million, tractor cab extenders remain the more effective of the devices at reducing gap drag, but due mostly to the benefit received by the trailer. At larger gap lengths, one would expect the tractor cab extenders to lose some of their advantage to a trailer splitter plate in redirecting gap flow near the trailer. The fact that the addition of a trailer splitter plate is shown to simultaneously reduce both drag and side force, raises the question of vertical flow effects in the tractor-trailer gap. Unfortunately, no experimental data are available for MGTS lift, and any results would surely be sensitive to floor boundary layer reproduction. Regardless, for all simulations, the trailer splitter plate consistently reduces vehicle drag without a significant increase in side force. A summary of each device's performance is plotted in Figure 11.

Of the gap devices tested, the splitter plate is not as effective as cab extenders in reducing drag at lab or full-scale Reynolds numbers. However, drag reduction is comparable to tractor cab extenders, and improves with increasing gap length. Unlike tractor cab extenders, the trailer splitter plate does not appear to suffer from large increases in vehicle side force at yaw, perhaps even lessening side force while simultaneously reducing drag. Results indicate that for typical crosswinds, vehicle side force may be

50% larger than drag. Any device that serves to reduce drag without significant side force compensation may prove to be beneficial for both tire wear and vehicle stability. In addition, a vehicle equipped with a trailer splitter plate does not suffer from the reduced turning radii associated with cab extenders.

Summary

The following are the main accomplishments for the FY05 effort in heavy vehicle aerodynamic drag reduction:

1. Assessed the performance of add-on drag reduction devices using CFD
2. At lab-scale Reynolds numbers, both the tractor cab extenders and the trailer splitter plate produce a 5% drag reduction at large gap lengths
3. At full-scale Reynolds numbers, the addition of a trailer splitter plate decreases vehicle drag by 1% while maintaining vehicle side force
4. At full-scale Reynolds numbers, base flaps decrease the drag coefficient by 8-14%
5. At full-scale Reynolds numbers, the wedge-shaped skirt decreases the drag coefficient by 2%
6. Observed that at full-scale Reynolds numbers, the increased vertical flow in the gap between the tractor and trailer alters the gap flow structures.
7. Determined that base flaps function by increasing the pressure on the trailer base through the elimination of a recirculation zone on the trailer base
8. Investigated the sensitivity of the drag coefficient reduction of the wedge-shaped skirt and base flaps to both grid refinement and steady versus unsteady simulations

References

Browand, F., Radovich, C., & Boivin, M., "Fuel Saving by Means of Flaps Attached to the Base of a Trailer: Field Test Results," browand@spock.usc.edu, University of Southern California, 2004.

Browand, F., Hammache, M., Arcas, D., "Flow in the Gap Between Two Bluff Bodies with Application to Heavy Trucks", To be published, 2005.

Cooper, K.R., "Truck Aerodynamics Reborn—Lessons from the Past," SAE Paper No. 2003-01-3376, 2003.

Hariharan, N., Wang, Z.J., Buning, P., "Application of Conservative Chimera Methodology in Finite Difference Settings", AIAA-97-627, 1997.

Menter, F.R., "Two-equation Eddy-Viscosity Turbulence Models for Engineering Applications", AIAA Journal, 32.8 (1994): 1598-1605.

Ortega, J.M. & Salari, K., "An Experimental Study of Drag Reduction Devices for a Trailer Base and Underbody," AIAA Paper No. 2004-2253, 2004.

Salari, K., Ortega, J.M., Castellucci, P.J., "Computational Prediction of Aerodynamic Forces for a Simplified Integrated Tractor-Trailer Geometry", AIAA-2004-2253, 2004.

Storms, B.L., Satran, D.R., Heineck, J.T., & Walker, S.M., "A Study of Reynolds Number Effects and Drag-Reduction Concepts on a Generic Tractor-Trailer," AIAA Paper No. 2004-2251, 2004.

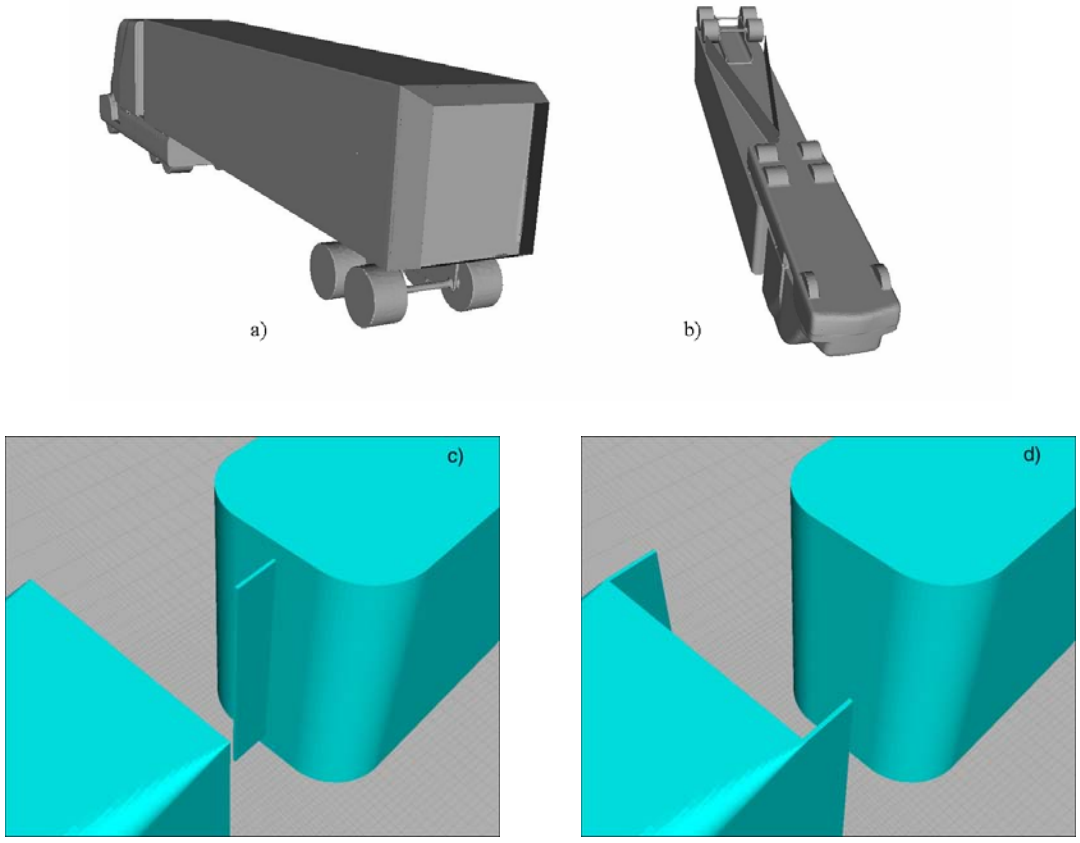

Figure 1. a) Base flaps b) Wedge-shaped skirt c) Splitter plate d) Cab extenders

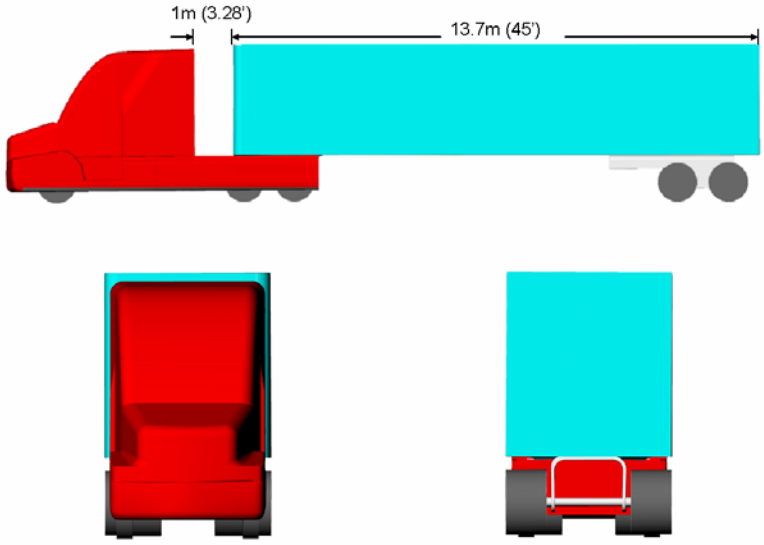

Figure 2. Generic conventional model (GCM) used in the CFD simulations.

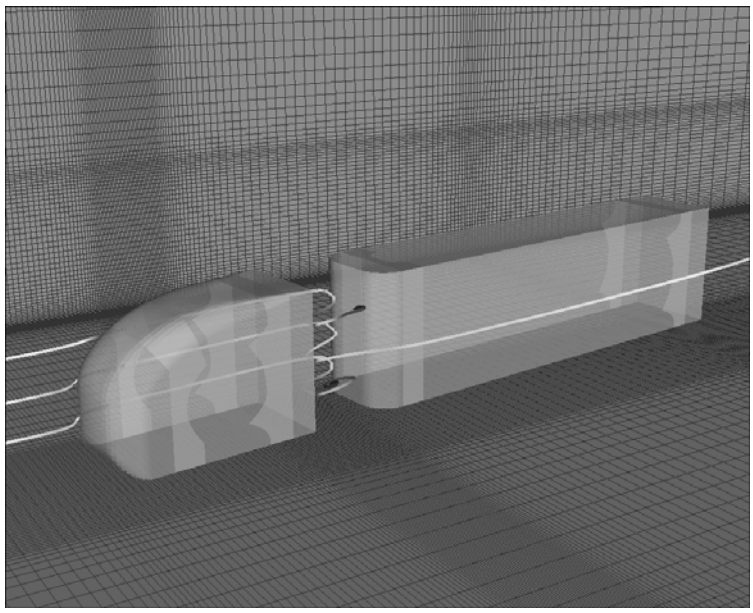

Figure 3. MGTS at 6° yaw with velocity-colored streamtraces.

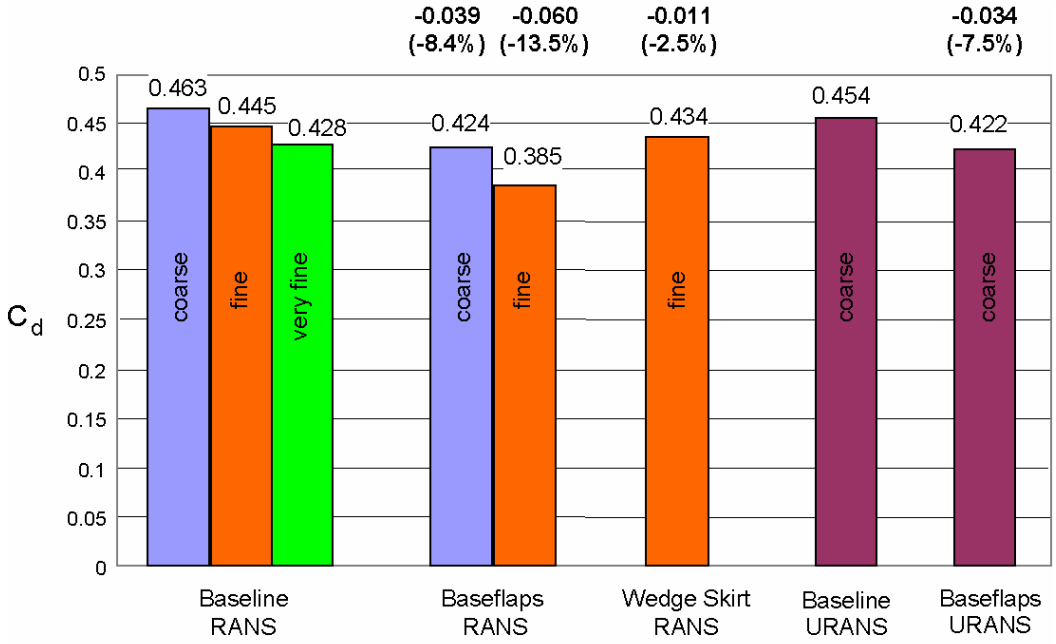

Figure 4. Drag coefficient for the baseline GCM with and without the drag reduction devices. The labels "coarse," "fine," and "very fine" refer to the level of grid refinement. The bold numbers at the top of the plot are the reductions in C_d with respect to the baseline configuration and the numbers in parenthesis are the percent reduction in C_d.

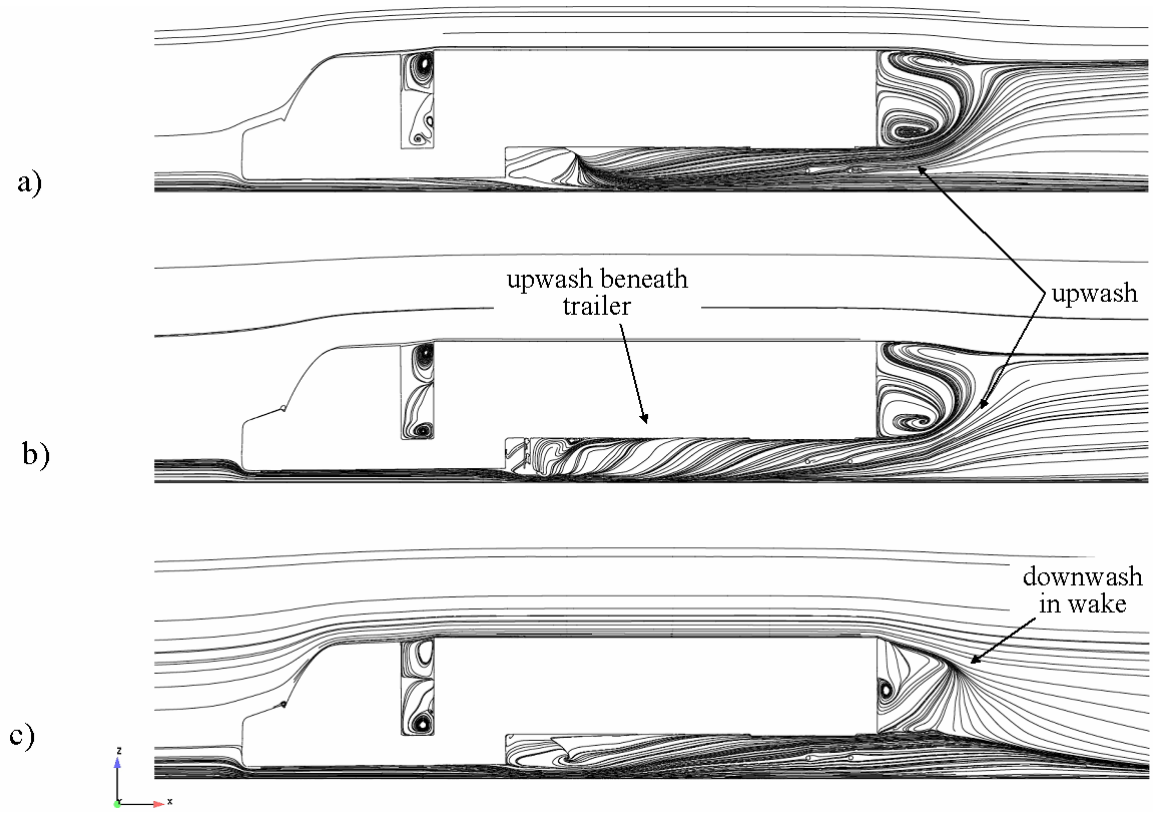

Figure 5. Velocity streamlines at the centerplane of the a) baseline GCM b) GCM with the wedge-shaped skirt c) GCM with base flaps.

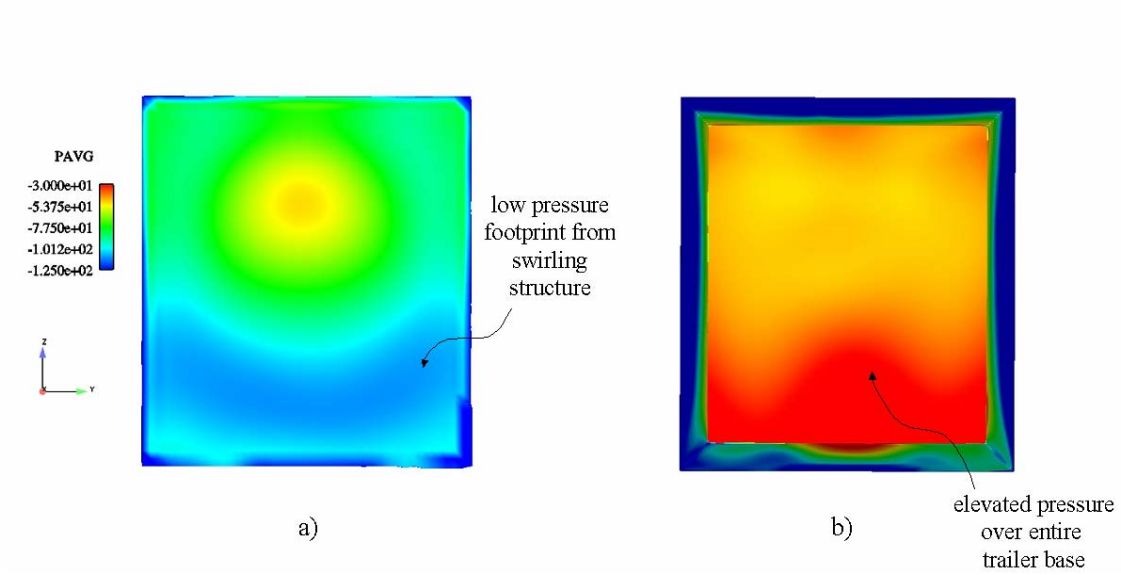

Figure 6. Pressure distribution over the trailer base of the a) baseline GCM b) GCM with base flaps.

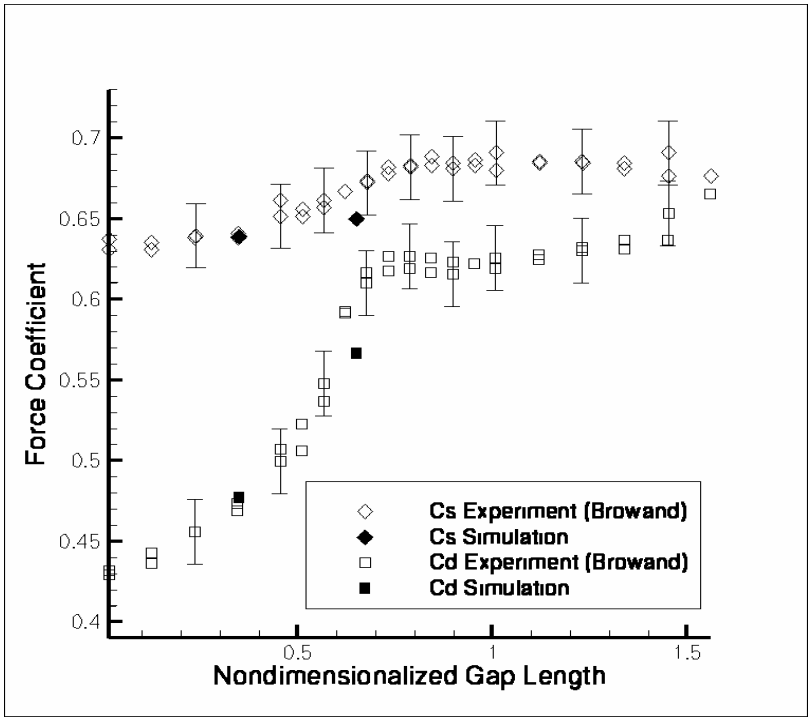

Figure 7. MGTS body force coefficients at 6° yaw and Re = 340,000

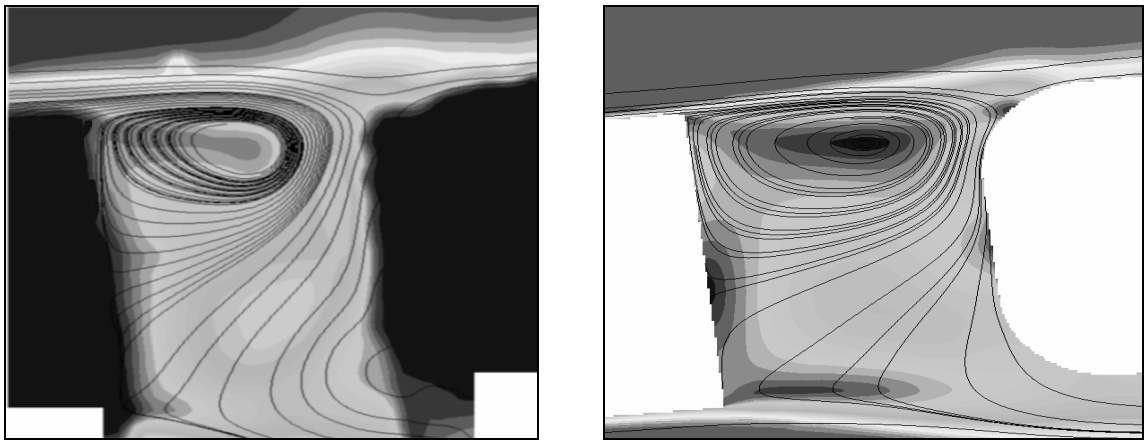

a) b)

Figure 8. Mid-height streamtraces and velocity magnitude contours for a) Experiment (Browand 2005) and b) Simulation at 6° yaw and Re = 340,000

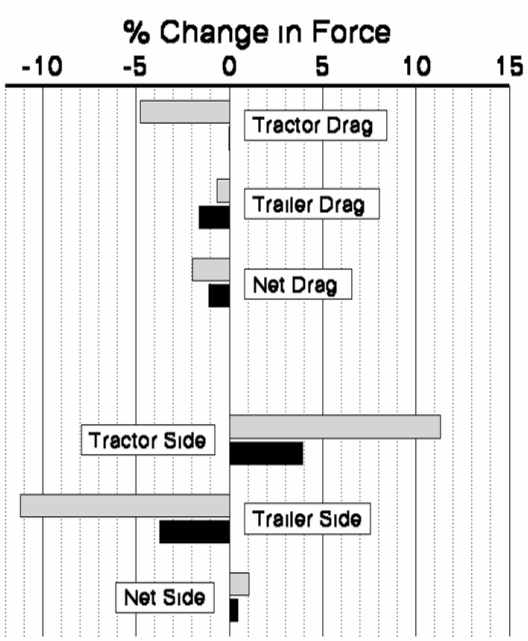

Figure 9. MGTS body force modification at 0.35 length gap, Re = 340,000:
Cab extenders – Gray, Splitter plate – Black

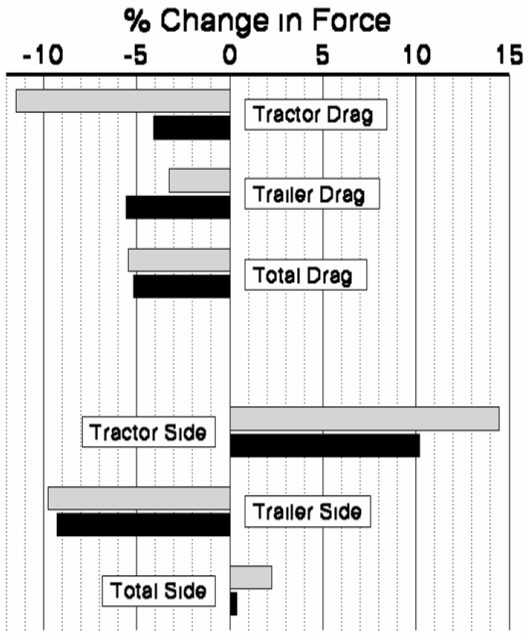

Figure 10. MGTS body force modification at 0.65 length gap, Re = 340,000:
Cab extenders – Gray, Splitter plate – Black

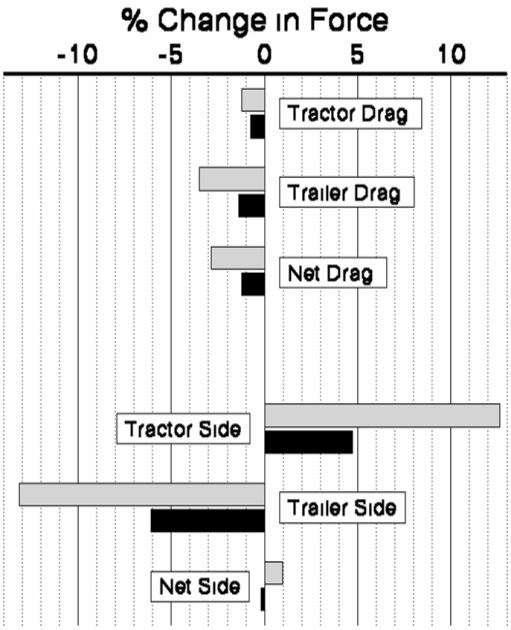

Figure 11. Full-scale MGTS body force modification at 0.38 length gap, Re = 7,000,000: Cab extenders – Gray, Splitter plate - Black

B. Computational modeling of spray dispersion in heavy vehicle and tire assembly wakes

Objective

- Analyze the formation and spread of spray clouds generated around and behind heavy vehicles using computational models
- Build and leverage understanding of tire aerodynamics required for detailed drag calculations to investigate spray dispersion
- Develop a set of predictive computational tools available to truck and tire manufacturers to estimate the effectiveness of splash and spray add-on devices while simultaneously determining the effects of aerodynamic drag.

Approach

- The commercial computational fluid dynamics (CFD) solver StarCD was used in combination with the mesh generation tool Harpoon to investigate water spray transport around truck and tire geometries.
- Droplets were injected into the flow distributions from multiple points on the truck or tire using rough estimates for initial velocity and size; empirical droplet breakup and collision models in StarCD were used to model spray generation processes resulting from both aerodynamic breakup as well as fine spray generation resulting from droplets hitting the truck or tire geometry.
- Quantitative estimates of the resulting spray dispersion, droplet size distributions and visibility impairment were obtained for the truck cases.
- Determine the differences between using the large eddy simulation (LES) and unsteady RANS turbulence modeling approaches on the predictions of spray transport.

Accomplishments

- Completed the only known simulations of the detailed, unsteady flow fields around realistic rotating tandem dual tires
- Completed the first CFD calculations of spray cloud generation and transport around truck and truck tire geometries
- Demonstrated that aerodynamic drag-reducing add-on devices such as base flaps may actually impair motorist visibility by focusing drops into "passing zone" behind and to the left of truck.
- Determined that truck spray is a fine mist with droplets having diameters less than 0.1 mm; larger droplets travel along ballistic trajectories and do not interact strongly with the flow field.
- Determined that aerodynamic breakup is minimal and that the primary source of small droplets is collisions with other parts of the truck or tire
- Discovered that the addition of fenders, fairings or mudflaps make little difference in the transport of the small droplets in the spray cloud; we speculate that collision of larger droplets with these additional surfaces may actually serve to generate *more* spray without some type of surface treatment.
- Investigated simple LES models in StarCD; compared the resulting spray transport in flows around a modified GTS geometry and demonstrated that URANS predicts substantially less dispersion than LES does

Future Direction

- Integrate understanding of spray transport dynamics into models of aerodynamic drag reducing devices
- Incorporate experimental data on spray formation from effort at USC into calculations
- Develop capability to model splash and integrate into existing models for spray transport
- Investigate more sophisticated models for droplet collision and breakup on absorbent surfaces

---

Introduction

The spray clouds generated around trucks in wet weather conditions reduce motorist visibility and are often cited by motorists as a major safety hazard. There have been numerous experimental studies over the last 30 years that have failed to conclusively demonstrate that any aftermarket add-on devices reduce truck spray. As discussed in the AAA Foundation for Traffic Safety report by Manser (2003), much of the work during the 1980's focused on what is still the best understanding of how spray is generated: water droplets are thrown from the tire treads and impact hard surfaces on the truck, breaking into small drops that get sucked into the vehicle wake. The more pronounced the vehicle wake, the greater the amount of droplet dispersion. Using a 1985 and 1997 Freightliner tractor, Manser demonstrated that the latter, more aerodynamic tractor generated less spray. These improvements can be attributed to streamlining of the tractor and the reduction of the size of the wake around the front of the vehicle. Manser reported that lower-drag tractor designs, in combination with *absorbent* mudflaps that extend fully to the ground (to minimize any breakup leading to mist formation) "definitely helped reduce spray cloud density."

It is less clear that the addition of drag-reducing add-on devices, especially on trailers, will have a similar effect. Droplets can exhibit what is known as "particle

focusing" in which small particles can get trapped in low pressure vortex cores. It is possible that devices that manipulate trailer aerodynamics could reduce motorist visibility by "pushing" spray into the path of a passing car.

As experiments in this area are both difficult and expensive to perform, a predictive computational capability would be of great value to understanding and designing spray reduction methods. Our objective over the past year has been to demonstrate the capability of computational fluid dynamics (CFD) tools to investigate this problem and to make the first steps towards developing a predictive capability.

Computational Methodology

The commercial CFD solver StarCD was used for all of the simulations presented here. The free-stream flow rate was set to a representative highway speed (29 m/s ~60 mph for the GCM cases; 20 m/s ~40 mph for the tire and GTS cases) and the resulting turbulent flow field around the geometry was calculated using the SST turbulence model with a wall function, except in the case of the LES simulations of the GTS, where the constant coefficient Smagorinsky LES model was used. In all cases, the simulations were completed in a time-dependent manner as droplet dispersion and breakup calculations are strongly dependent on the *dynamic* behavior of the flow they are exposed to. Meshes varied in size from approximately 1.5 million cells (GCM) to over 7 million cells (dual tire). For tire simulations, a local kinematic boundary condition was employed to account for the rotation of the tire and a moving ground plane was used. For truck simulations, the ground plane was specified to be moving at the same velocity as the free stream.

The primary thrust of this work was the integration of StarCD's droplet atomization and transport models into the CFD simulations. The droplets were modeled as point particles having finite mass, drag and velocity. Several empirical aerodynamic breakup models are available; the model of Pilch and Erdman was used since it accounts for the widest range of breakup modes. Particle-particle collisions were also accounted for but are generally rare events in the computations. Each computational particle (or parcel) represents a collection of particles with a fixed mass; if breakup occurs during flight the droplet size and number of particles represented by the parcel will change, but a new parcel will not be created. Collisions with surfaces, which are necessary to accurately model of the spray problem, were modeled using an empirical model derived for gasoline impingement on engine cylinders. While we anticipate that this model will not be quantitatively predictive for the problem at hand, it should illustrate qualitatively correct behavior. Note that new parcels *are* created as a result of droplet impacts using this model.

The initial conditions for the particles were difficult to specify without an experimental database with which to compare. As such, a distribution of particle sizes ranging from 5 microns to 1 mm was used and injection velocities were based on rough estimates: for example, droplets were injected near the base of the tires at a velocity equal to the tire rotational speed and an angle tangent to the tire tread.

Results and Discussion

Effect of drag-reducing devices on motorist visibility

A representative snapshot of the spray dispersion patterns in the wake of the baseline GCM is shown in Figure 1. We have observed the spray cloud is quantitatively more concentrated in the drag-reduced case (not shown). This effect is due to the focusing of droplets in the low pressure region in a vortex

core that is pronounced in the base flap case. We have also observed that remarkably little droplet breakup occurs due to aerodynamic forces by watching individual droplet traces; almost all the droplet breakup occurs when large drops hit truck or tire surfaces.

We can quantitatively define a measure of motorist visibility by examining the particle concentration in a representative passing zone shown as a box in Fig. 1 at a given simulation time. For the baseline GCM, the concentration is 2.15 particles/cubic meter while for the base flap case the concentration is 3.38 particles/cubic meter. This result suggests that the use of a drag reducing device such as *base flaps may actually decrease motorist visibility on rainy days*.

Detailed tire simulations and effect of fenders

All of the truck-like geometries considered in our CFD studies to date have used simple representations of the wheels. Here, we consider the aerodynamics of more realistic tire assemblies with spray models in StarCD (tires alone) or with massed particle traces in our post-processing software, which does not account for small droplets resulting from collisions but does illustrate the effectiveness of add-on devices for spray suppression. We have considered a simplified tandem dual slick tire arrangement representative of a trailer tire assembly both with and without fender add-ons.

As shown in Figure 2, we have been able to simulate a qualitatively realistic spray field using multiple droplet injectors. The flow field is quite complex and highly unsteady; the simulation presented here represents two iterations in mesh refinement to adequately resolve the fine scale structures on the front corners of the front tire, the gap between the tires and the wake region. As in the aforementioned GCM studies, the droplets that are most strongly transported by the flow field are on the order of 10 microns and are seen as dark drops along the top of the tire in the figure. Little aerodynamic breakup occurs but small droplets are created by collisions of large droplets from the front tire with the back tire.

In Figure 3, we present the results of massed particle traces for the case of a tandem dual tire with a fender. The lines represent the paths followed by water droplets having a diameter of 10 microns. It is clear that the fender has little effect on the transport of this fine mist. Larger particles (not shown) typically impact the fender and if a full spray simulation were completed, would lead to the generation of smaller droplets easily transported by the flow. We have also considered the case of a Reddaway-type fender (not shown), which has a small fairing across the top of the fender; in this case, the lateral spray transport is decreased but the spray is "pushed" to the inboard side of the wheels. We speculate that spray would likely be concentrated into the region directly behind the truck. While the visibility for a passing motorist may be improved, the visibility for a motorist following the vehicle might actually be degraded. *These simulations corroborate existing experimental data that demonstrate spray reducing add-on devices are ineffective but suggest that absorbent or breakup-suppressing surface treatments near the wheels may help mitigate the problem.*

Large Eddy Simulation (LES) turbulence modeling and effect on spray dispersion

All of the simulations presented thus far have utilized the unsteady Reynolds Averaged Navier-Stokes (URANS) methodology for turbulence modeling. While this approach is robust and captures the time-dependent nature of the flow, it has been well-established in the scientific literature that URANS models poorly predict the unsteady wakes behind bluff bodies such as tires and trucks. URANS fails to capture small-scale features through the Reynolds averaging process and can lead to erroneous predictions of transport of small particles or droplets that interact with them. To assess the possible error in our URANS simulations, we have completed some preliminary calculations of spray transport using an LES model and compared the results to those from a

URANS simulation. In Figure 4a, we present an instantaneous snapshot of the velocity contours and spray cloud in the LES case while in Fig. 4b we present the URANS case. It is obvious that the wake has a far different structure and the droplets are more strongly dispersed in the vertical direction in the LES case. We can quantify this by considering the root-mean-square (RMS) distance of the particles from the ground (vertical dispersion) or the centerline (horizontal dispersion). The results are shown in Fig. 5 for horizontal dispersion; we see similar results for vertical dispersion. *Our preliminary finding is that the URANS models appear to underestimate the amount of spray dispersion;* using LES would likely improve the accuracy of any predictions but comes at a considerable computational cost.

Summary

These are the highlights of the progress during FY 2005 in the area of simulation of heavy vehicle spray dispersion:

1. Using CFD, demonstrated drag-reducing add-on devices may make the spray problem worse
2. Completed investigation of detailed tandem dual tire aerodynamics with spray propagation
3. Illustrated fenders and fairings are ineffective at mitigating spray problem
4. Explored advanced turbulence models for spray dispersion modeling and showed that extra cost may lead to improved predictions

Conclusions

We have completed a preliminary computational investigation of spray propagation around truck and tire geometries. These simulations have demonstrated that motorist visibility may be adversely impacted by drag-reducing devices and fenders or fairings have minimal impact on spray transport. However, these results are dependent on the details of how the spray is injected and how droplet-wall collisions are modeled. The former will benefit strongly from experimental data from the work performed by Prof. Fred Browand at USC and the latter will require the development of more sophisticated computational tools. These same tools are also required to model the process of splash – the process by which water in a puddle is displaced by the tire and breaks up into droplets – which is quite challenging computationally and is currently the focus of several research efforts in the combustion atomization and spray community. With these tools in place, it will be possible to develop a predictive tool of use to truck and tire designers.

References

Manser, M., Koppa, R., & Mousley, P. "Evaluation of splash and spray suppression devices on large trucks during wet weather," AAA Foundation for Traffic Safety, www.aaafoundation.org/pdf/SplashSpray.pdf.

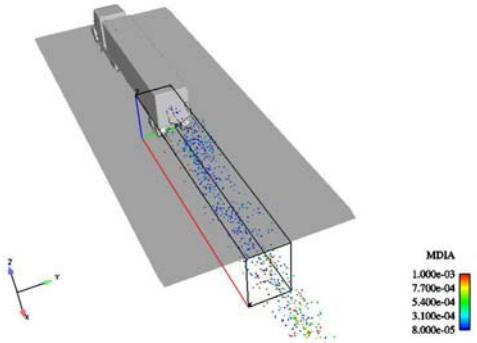

Figure 1: Sampling box for calculation of visibility reduction

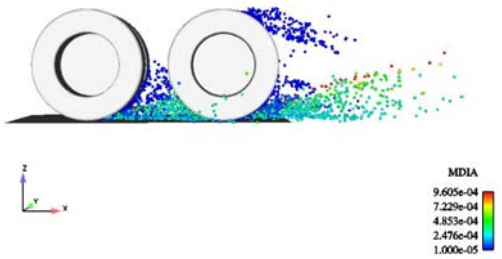

Figure 2: Droplet dispersion about tandem dual tire

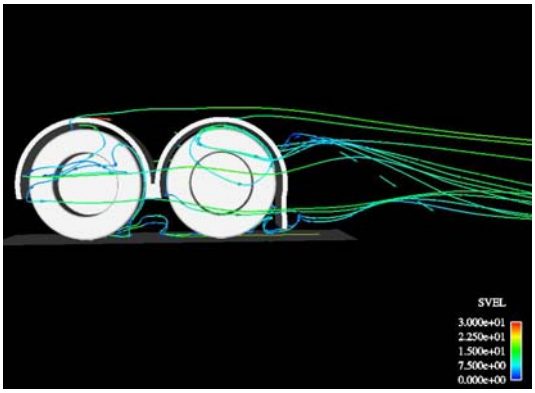

Figure 3: Massed particle traces in flow around tandem dual tire with fender

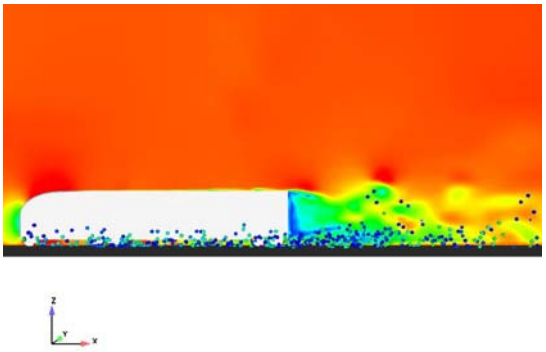

Figure 4a: Spray cloud behind MGTS predicted using LES

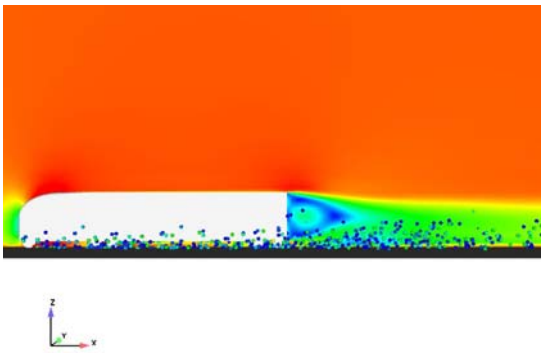

Figure 4b: Spray cloud behind MGTS predicted using URANS

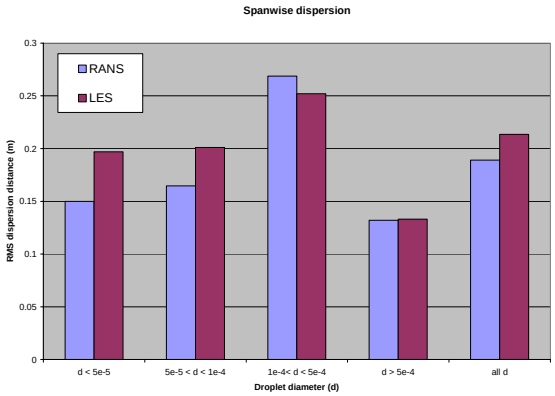

Figure 5: Horizontal spray dispersion in MGTS wake predicted using LES and URANS

APPENDIX B

Experimental Measurement of the Flow-field of Heavy Trucks

Principal Investigator: Fred Browand
Aerospace & Mechanical Engineering, University of Southern California
RRB 203, Los Angeles CA 90089-1191
(213) 740-5359; fax: (213)740-7774; e-mail: browand@spock.usc.edu

Technology Development Manager: Lee Slezak
202-586-2335, Lee.Slezak@EE.DOE.GOV
Technical Program Manager: Jules Routbort
630-252-5065, routbort@anl.gov

Contractor: Lawrence Livermore National laboratory
Subcontract No.: B545349

Objective

Improve the performance of heavy trucks by reducing aerodynamic drag, and by increasing safety.

Approach

Improved use of aerodynamic design decreases truck drag and consequently improves fuel economy. However, decreasing truck drag places more stress on truck brakes. We show that manipulation of the cab extender angle can be used either to minimize drag or to increase drag when additional braking power is required.

Water spray from heavy truck tires is an important safety issue. The spray decreases the rearward visibility of the truck drivers. For automobiles in the immediate vicinity, spray obscures the roadway on either side of the truck.

Accomplishments

I. Manipulation of cab-extender angle

Wind tunnel drag measurements are made to study the effect of thin plates placed along the trailing edge of the tractor (cab). The plates can be inclined inward or outward from the alignment parallel to the side of the cab. The lowest drag position is with extenders aligned with the direction of the cab. Deflecting extenders outward increases drag, as might be expected. But surprisingly, deflecting the cab extenders inward results in a larger increase in drag. The cab extender angle can be adjusted to provide minimum drag in cruise, and an additional higher drag for braking situations.

II. Design and construction of a new apparatus for the study of spray formation from rolling tires

In the new apparatus, two tires are rolled in contact with one another, and water is injected from a specially designed injector placed just upstream of the contact patch. The speed of the injected water jet is the peripheral speed of the tires.

Future Direction

In an effort to get devices on the road, continue investigation of aerodynamic devices that do not present operational and maintenance issues

Initiate a program of study of tire spray using the newly constructed apparatus.

I. Manipulation of cab-extender angle

The variation of drag with varying cab-extender angle has been described in SAE Paper No. 2005-01-3527 entitled: Wind Tunnel Test of Cab Extender Incidence on Heavy Truck Aero-dynamics, by Charles Radovich.

A wind tunnel experiment has been conducted to determine the changes in drag and side force due to the presence and position of cab extenders on a model of a commercial tractor-trailer truck. The geometric variables investigated are the cab extender angle of incidence, the tractor-trailer spacing and the yaw angle of the vehicle. Three cab extender angles were tested—0º, 15º (out) and -15º (in) with respect to the side of the tractor. The wind tunnel models of both cab and trailer had the same width and height.

Cab extenders having a length of 25.4 mm were constructed. Expressed as a fraction of the trailer width, w = 154 mm, the cab extender non-dimensional length was 0.165. There was an extender on each side of the cab and one on the top. Two views of the tractor with extenders in place are shown in Figures 1a and 1b.

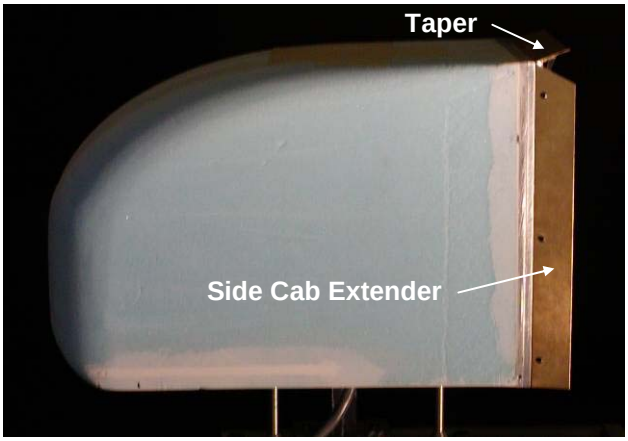

Figure 1a. Profile of tractor fitted with cab extenders.

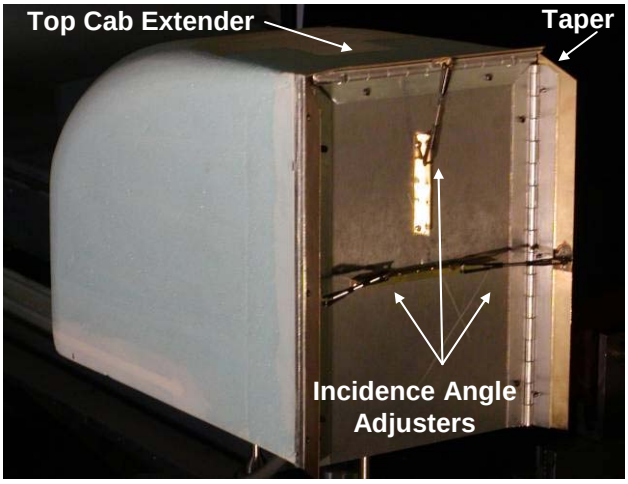

Figure 1b. Detail of cab extender attachment.

Cab extender angle settings of 0º, 15º (out) and -15º (in) were tested, as sketched in Figure 2. All data were obtained at a freestream velocity (U_∞) of 26 m/s. During the test, all three cab extenders were set with the same angle of incidence. As shown in figures 1a and 1b, the two side edges of the top cab extender and the top edge of both side cab extenders were tapered to allow the devices to fold inward for the -15º case without touching. This resulted in a

small gap between the extender edges at the 0º and 15º settings.

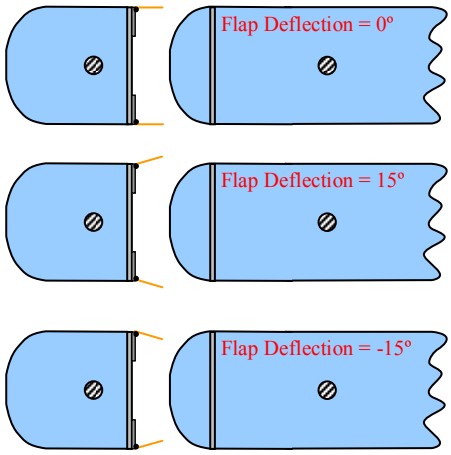

Figure 2. Cab extender flap angle settings.

The minimum drag coefficient was found for the tractor and trailer combination when the cab extenders were set to 0º angle of incidence with respect to the headwind. This result holds for all yaw angles with moderate gap spacing between the tractor and trailer, as in figures 3, 4, and 5.

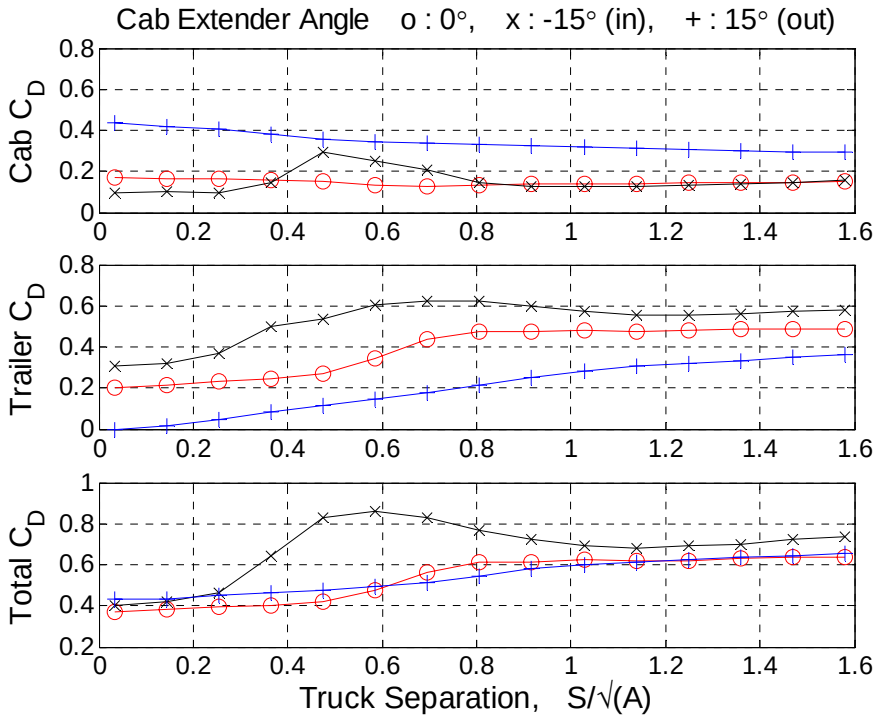

Figure 3. Yaw = 0º: Drag Coefficients for three cab extender angles

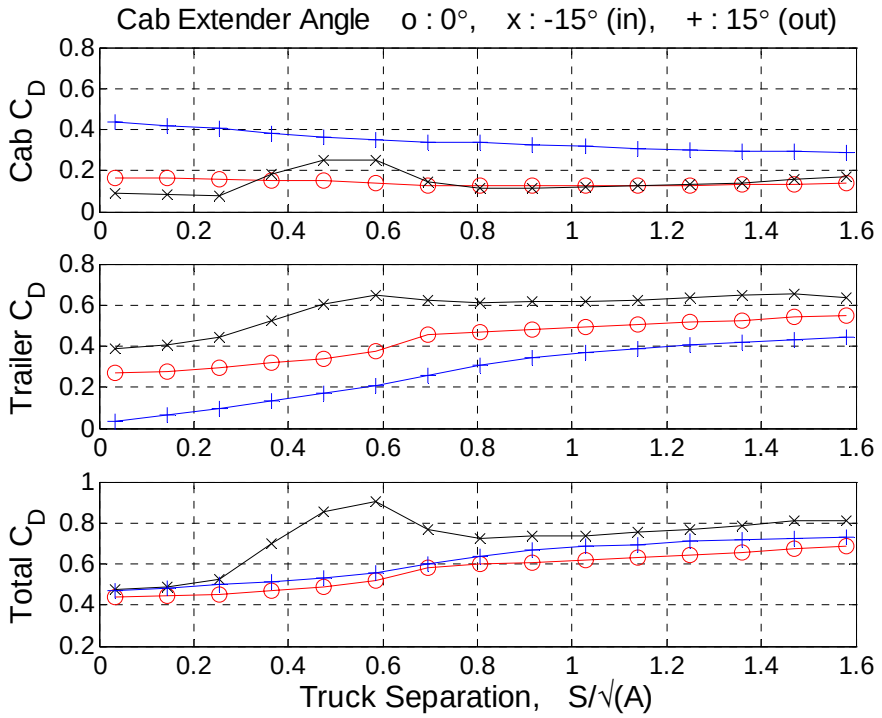

Figure 4. Yaw = 6º: Drag Coefficients for three cab extender angles.

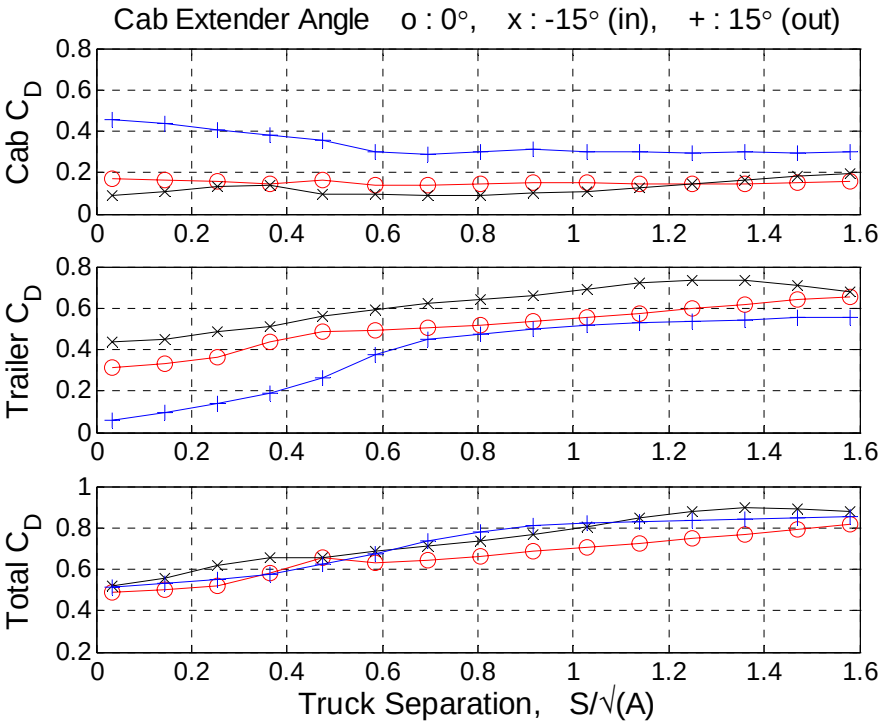

Figure 5. Yaw = 12º: Drag Coefficients for three cab extender angles.

When no trailer is present, the tractor has less drag with the cab extenders inclined inward at -15-degrees, as in figure 6.

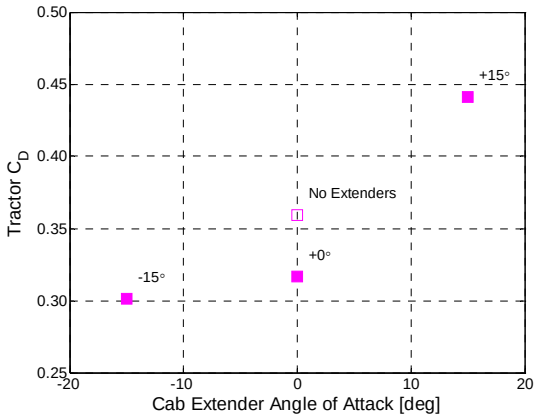

Figure 6. Tractor C_D – no trailer present.

This study suggests that commercial tractor-trailer trucks can benefit from adjustable cab extender settings; 0º when using a trailer and minus 15º (-15º) when no trailer is used. When no trailer is present, at 0º yaw, a -15º setting has approximately 5% less drag compared to having extenders at 0º, and 18% less drag when compared to a similar truck with no cab extenders installed.
Increasing the drag coefficient is also possible by deflecting the cab extenders in either direction. Similar to engine braking, this effect might be desired to reduce the vehicle speed without the application of brakes. At moderate tractor-trailer spacing, the 15-degree (out) and -15-degree (in) settings can increase C_D by about 10 - 20%, depending on yaw angle. At larger separations, the -15º setting can increase C_D by as much as 90%.

II. Design and construction of apparatus for the study of spray formation from rolling tires

A key factor in driving safety is driver visibility. Tires being driven through standing water create splash and spray which can decrease visibility for other drivers. Studying the formation of splash and spray will help in the understanding of how to maintain visibility.

Splash is water that is pushed out from the tire patch towards the sidewall of the tire. Spray is defined as the water forced into the tread pattern within the tire patch (contact patch) between the tire and the road. It is spray that we will be interested in here.

When tires produce spray, the water droplets form as a result of the break-up of jets and sheets of fluid.

The Tire Geometry in the Laboratory

In order to correctly model a tire rolling over a wet road, the physics of the tire patch must be understood. There are two reference frames applicable, as shown in Figure

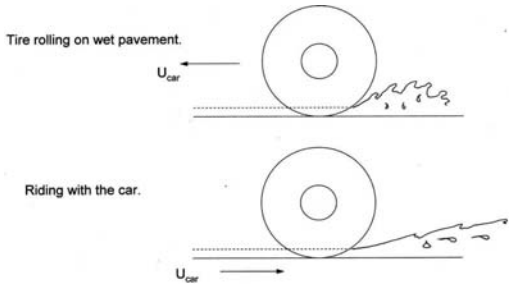

Figure 1. Two reference frames for tire rolling over a wet ground.

In the first reference frame, an observer watches a tire rolling along wet pavement. In this scenario, the tire moves at velocity U_{car} through stationary water. In the second reference frame, the observer rides with the car and sees water coming at the tire with velocity U_{car}. Now, using the principle of symmetry, the tire can be flipped so that a second tire represents the road, as shown in figure 2. This principle of symmetry, and a reference frame riding

with the car, is used to model the tire/water interaction in the laboratory.

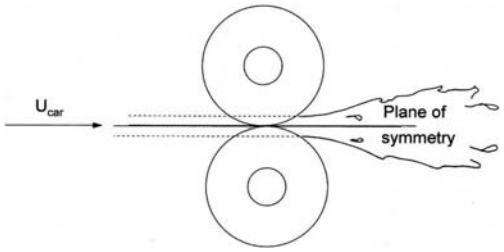

Figure 2. Using principle of symmetry, a second tire represents the road.

The Tire Spray Simulator

The experimental setup for capturing the formation of spray focuses on four main areas: the tire patch, the water jet, the imaging, and the lighting. The Tire Spray Simulator (TSS) machine met requirements for each of these four areas, as shown in figure 3 on the next page.

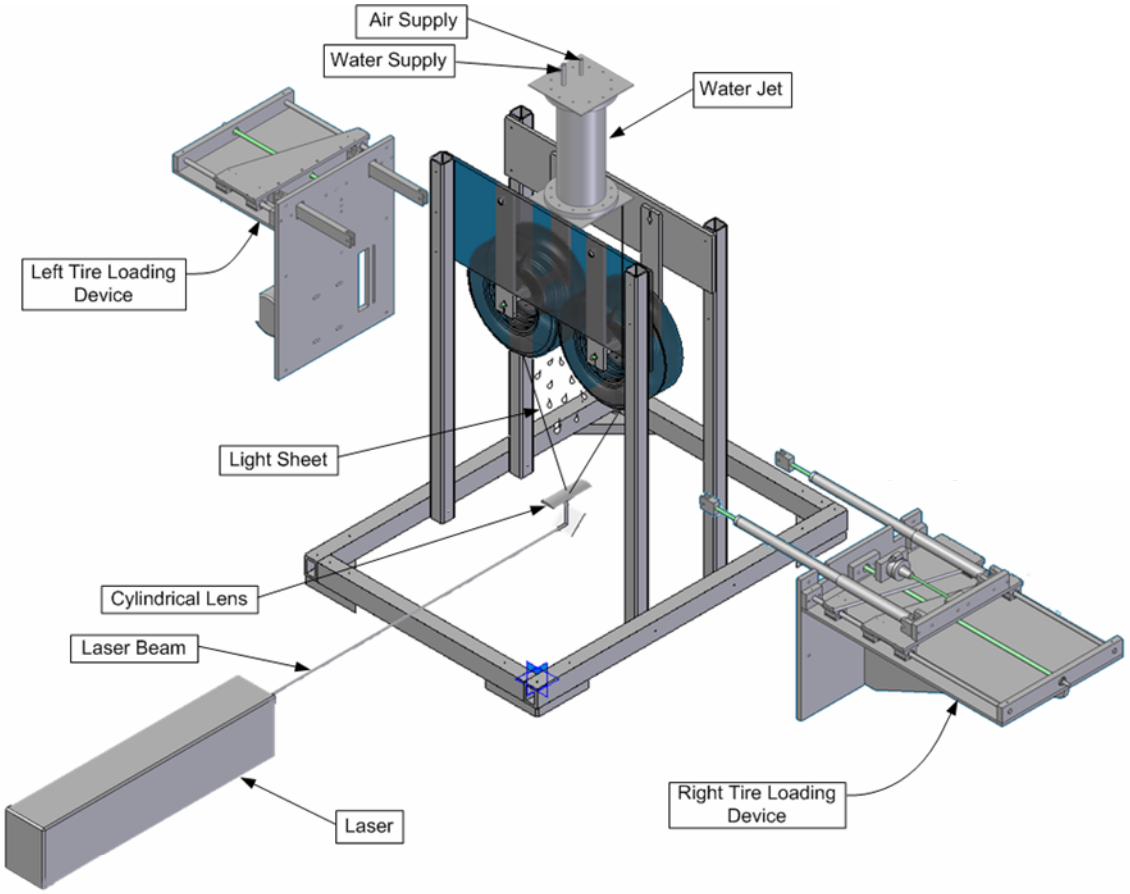

Figure 3. The Tire Spray Simulator.

The moving tire patch is created using one tire having a smooth surface to represent the road, and another tire with a circumferential groove to simulate the tread of a car tire. The tire patch is formed when the two tires are pressed and held together using the left/right tire loading devices. Two shock/spring dampeners, controlled by two stepper motors, regulate the force on the tire patch (contact patch). A 0-250 lbs Sensotech load cell loaded in-line with the dampeners measures this force. A 3-hp Leeson DC electric motor controls the rotation velocity of the tire to the left—the smooth tire in the present case. The second tire is driven by contact at the tire patch. A gear ratio of 30:21 is selected to properly step down the rotation of the tire. A 50 gage chain and chain-tensioner transfers rotational motion from the motor to the tires. Tires of varying grooves or tread patterns can be used to simulate different conditions.

In order to properly model the water coming into the tire patch, a jet of water traveling at the peripheral speed of the tire must be established. This is, by far the most difficult task. The water is stored in a pressurized stainless steel canister. Water and the air for pressurization enter at the top of the canister. A high-speed stepper motor drives a lead screw attached to a sliding

gate at the bottom of the canister, as in figure 4. A Teflon-sheet wraps around the gate, and actually provides a rolling contact with the seal at the exit nozzle. In operation, the stepper motor moves the sliding gate and the Teflon sheet rolls away from the exit nozzle. This process takes between 20 and 30 milliseconds. The gate remains open and water flows from the canister for a specified time, and the gate is closed. Nozzles of different sizes and shapes can easily be interchanged to allow tire treads of different sizes and geometries to be explored.

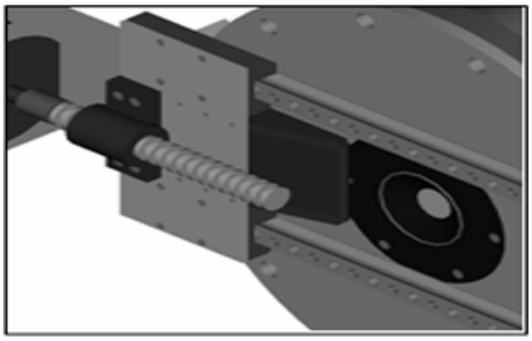

Bottom view of water jet, showing sliding wedge-shaped gate with leadscrew. A teflon sheet wraps around the wedge, sliding over the rounded nose as the gate is opened. The circular cutout receives nozzle inserts, allowing the nozzle shape to be easily changed.

Figure 4. Stepper-motor-controlled slider for precise water delivery.

Imaging

Image capture of the tire spray utilizes a high-speed digital video camera from Integrated Design Tools, Inc. (IDT). The camera has a resolution of 1260×1024 pixels. The camera has on-board memory of one gigabyte, or about 1000 images. On-board memory is expandable to 8 gigabytes. Framing rate and exposure time can be controlled independently. The smallest exposure time is approximately 1 micro-second (μs). The maximum framing rate is dependent upon the size of the image. The camera limit represents a maximum transfer rate of about 7 gigabits/second for 10-bit pixel information.

Both backlighting and a laser sheet are used to light the region of interest because they provided different views of the flow. Backlighting integrates all the water droplets between the frosted glass and the camera, although some of these features may be intentionally out of focus. In contrast, the laser sheet illuminates the features in a thin sheet of light—usually 2-3 mm in thickness. In the cases shown here, the sheet is perpendicular to the plane of tire rotation, and passes through the central symmetry plane of the tire. In principle, the light sheet can be moved laterally across the face of the tires (from sidewall to sidewall), and it can be broadened beyond the usual 2-3 mm.

We are presently using a Quantel Scientific, twin-tube Yag laser capable of 150 mJoules per pulse. The lasing time is approximately 5-10 nano-seconds, and the repetition rate is 10 Hz (pulses per second). The laser can be operated with one of the two tubes firing at 10 Hz, or with both tubes firing (10 Hz) with a prescribed time delay.

Results

Figure 5 shows the experimental tire orientation a second time, and defines

three cross-planes (A, B and C) at various distances downstream from the tire patch.

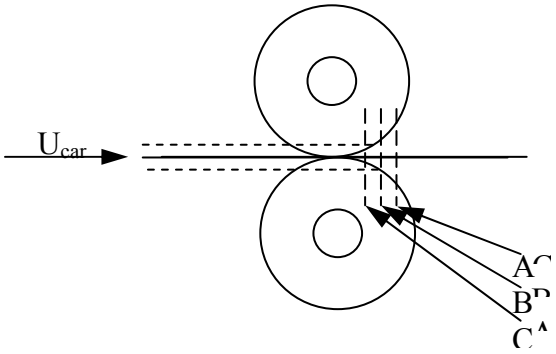

Figure 5. Tire orientation with three cross-planes A, B and C.

For the sake of the present argument, let both tires have the circumferential groove. Figure 6 shows what might be expected of the fluid at each cross-plane as it exits the tire groove (downstream from the tire patch). At section A, just beyond the tire patch, water completely fills the tire groove. Farther downstream at section B, the tires separate and are subjected to high accelerations. In a sense, the water is left behind as the tires move away from one another. Some of the water remains near the plane of symmetry as a jet, and some water remains in the grooves. At section C, the tires have moved farther apart, the central jet is more clearly defined, and the water remaining in the groove is connected to this central jet by a thin web. With increasing tire separation the web continually thins until breaks form and droplets are produced. Disturbances also act on the surface of the jet, and eventually break the jet into droplets.

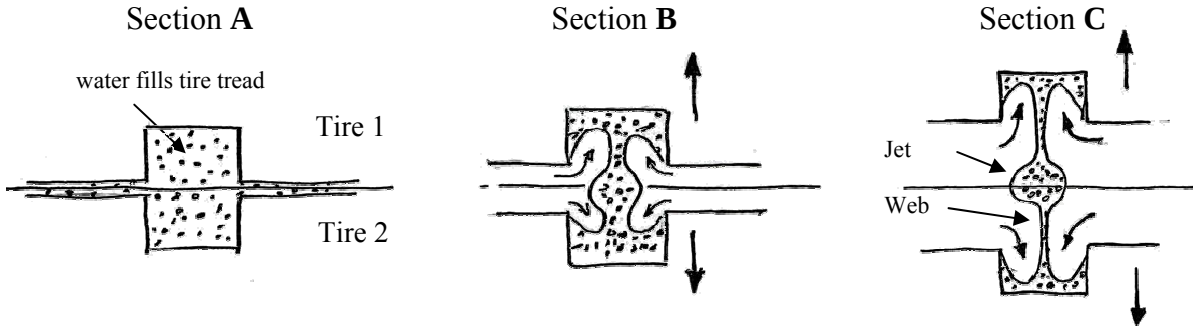

Figure 6. Expected behavior of water as it leaves the tire groove downstream from the tire patch.

If only one tire contains a groove, the situation is not materially different. Figure 7 gives a wide-angle view of the spray. Both tires are observed. The lower tire is the driving, smooth tire and the upper tire is the driven, grooved tire. Lack of symmetry about a central horizontal line is evident. In the case shown, the incoming water velocity has been matched to the peripheral speed of the tires. This makes the initial Weber number of the jet larger, and the flow appears more disturbed or fractured.

The central jet is seen as a nearly periodic row of (darkened) water blobs connected to the tires by ligaments. The ligaments are relatively thick regions, and may indeed be a developing wave structure. Breaks in the web appear on both sides of the central jet, but more appear on the lower side next to the smooth tire. The web probably thins most near the surface of the smooth tire, because replenishment from the groove is not possible.

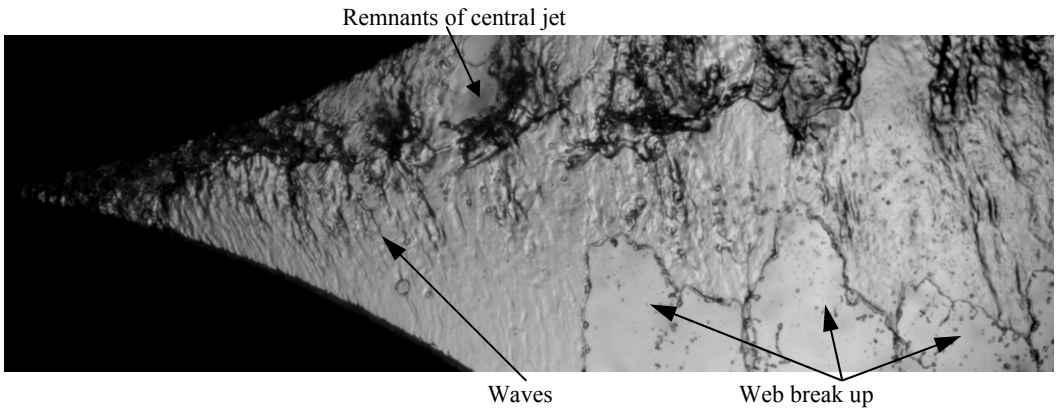

Figure 7. Spray from wider-angle perspective.

Figure 8 displays an image taken using a laser sheet. Similar to the backlight images, the web, central jet and connecting ligaments can be resolved. In addition there is a fine mist of extremely small droplets along the central plane in the picture. We believe these smallest droplets are a result of water forced between the tires themselves and into the contact patch. Digital particle imaging velocimetry (DPIV) is possible using images from this laser sheet technique.

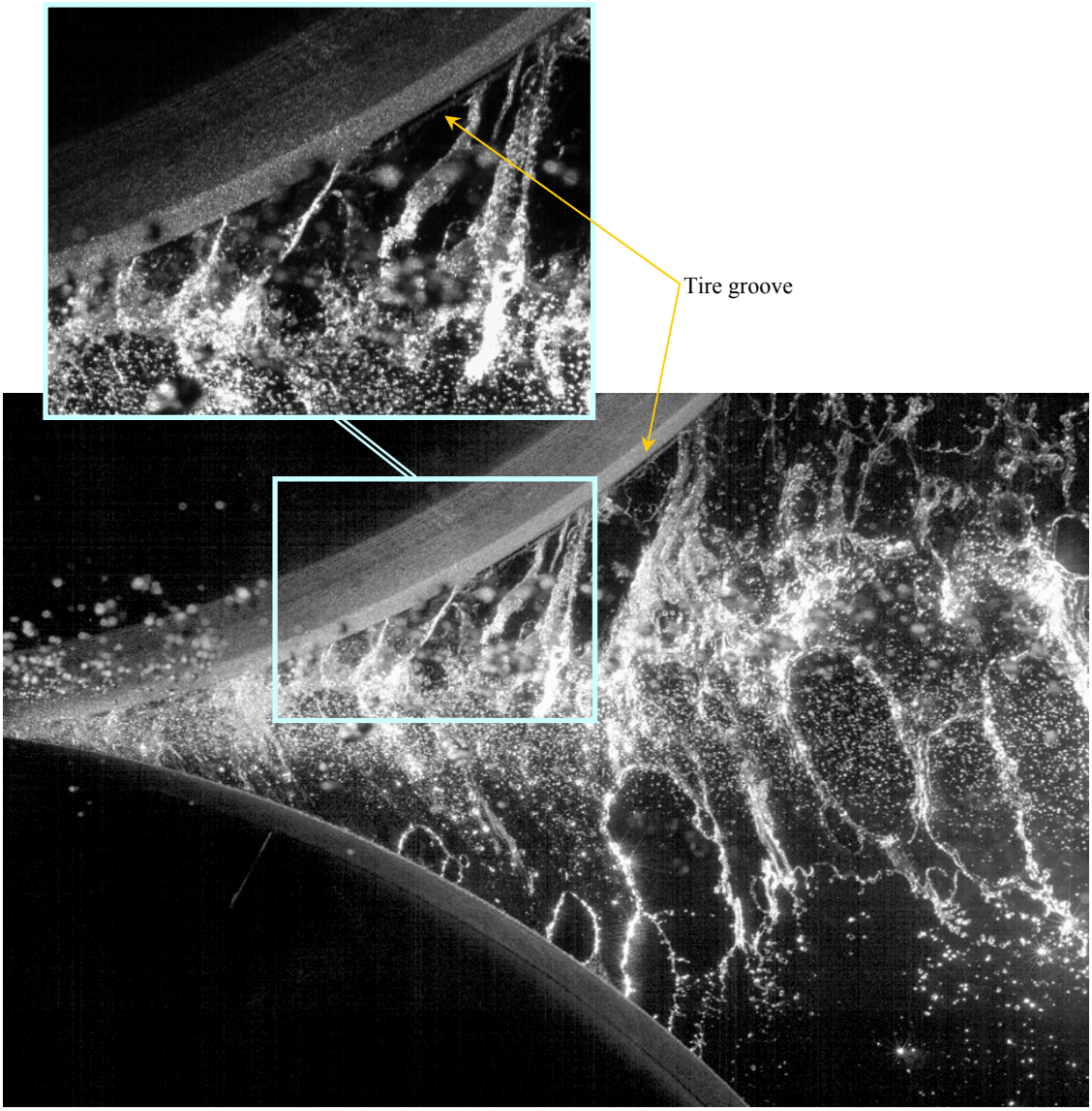

Figure 8. Spray image using a laser sheet (10 nano-second pulse time).

Conclusion

The Tire Spray Simulator (TSS) has demonstrated its usefulness in creating realistic spray. Qualitative results have been obtained with both the backlight and laser sheet procedures, and lead to an understanding of some the mechanisms behind the formation of jets and sheets, and of the eventual formation of droplets. The next step in analysis will be to measure droplet size and droplet velocity as a function of position within the spray field. Droplet sizes within the spray field are of first importance in themselves, but size information is also needed in order to resolve the velocity field according to size. We imagine evaluating droplet size in each image pair and filtering each image before the DPIV algorithms are applied.

APPENDIX C

Detailed Experimental Results of Drag-Reduction Concepts on a Generic Tractor-Trailer

Principal Investigator: Bruce L. Storms
AerospaceComputing, Inc.
M/S/260-1
NASA Ames Research Center
Moffett Field, CA 94035
(650)604-1356, fax: (650)604-4511, e-mail: bstorms@mail.arc.nasa.gov

Field Project Manager: James C. Ross
NASA Ames Research Center
M/S/260-1
Moffett Field, CA 94035
(650)604-1356, fax: (650)604-4511, e-mail: james.c.ross@nasa.gov

Technology Development Manager: Lee Slezak
202-586-2335, Lee.Slezak@EE.DOE.GOV
Technical Program Manager: Jules Routbort
630-252-5065, routbort@anl.gov

Participants
Dale R. Satran, James T. Heineck, Stephen M. Walker
NASA Ames Research Center

Contractor: NASA Ames Research Center
Contract No.: DE-AI01-99EE50559

Objective

- To investigate Reynolds-number effects on the flow field and resulting aerodynamic forces generated by a 1:8-scale model of a class-8 tractor-trailer configuration
- To provide quality experimental data on a simplified tractor-trailer geometry for CFD validation.

Approach

- To vary the total pressure of the wind tunnel thereby varying the Reynolds number from 500,000 to full-scale values over 6 million based on trailer width.
- Measure the forces and moments, surface pressure distribution, and off-body flow. Measurements were made at various yaw angles to study the influence of crosswind and to calculate wind-averaged drag coefficients. Several drag-reduction concepts were studied in order to document their potential benefit as well as their Reynolds-number sensitivity.

Accomplishments

- CFD validation data is now available for use by interested industry and government researchers

- Detailed experimental results were presented for several configurations of interest with the most promising tractor and trailer add-on devices.
- The results of the study were presented at the SAE 2005 Commercial Vehicle Engineering Conference in Chicago, IL on November 3rd (paper number SAE-2005-01-3525)

Future Direction

- Additional drag-reduction devices will be examined for under-body flow control/drag reduction
- NASA Technical Memo will be published summarizing the results from both the 12-Ft and 7x10 facilities

Introduction

For a typical heavy vehicle at a highway speed of 110 km/hr, the energy required to overcome aerodynamic drag is about 65% of the total expenditure (which includes rolling friction, transmission losses, and accessories). By altering the vehicle shape, it has been estimated that modern truck drag coefficients may be reduced by up to 50% resulting in an annual national fuel savings of eleven billion liters (Ref. 1). This large potential savings coupled with increasing fuel costs have spurred renewed interest in heavy-vehicle aerodynamics.

A significant number of experimental studies of heavy-truck geometries were conducted in the 1970's and 1980's (Ref. 2). The resulting first-generation drag-reduction technology currently in use includes cab shaping, cab-mounted deflectors, trailer front-end fairings, cab side extenders, and body front-edge rounding. The cab deflectors and side extenders accounted for the majority of the wind-averaged drag reduction reducing the pre-1980 drag level by about 25%. Other drag-reduction technologies that are not widely used include tractor-trailer gap seals, trailer side skirts, and rear boat-tailing. Each of these technologies produce a reduction of the wind-averaged drag coefficient between 0.03 and 0.10 which is about one-half the benefit of the first-generation technologies. However, the benefits of these devices are additive and the resulting net reduction is relatively large.

The aerodynamic drag reduction and fuel savings of various tractor and trailer modifications was previously summarized in Ref. 3. Since fuel consumption is the quantity of interest for commercial operators, a derivation of fuel consumption as a function of drag coefficient and road speed was provided. For trailer base flaps and skirts, the ranges of wind-averaged drag reduction were listed as 0.03 – 0.09 and 0.04 – 0.07, respectively.

More recently, a series of experimental and computational studies was funded by the Department of Energy (DOE), Office of Heavy Vehicle Technology. With the goal of CFD validation, the experimental efforts have focused on simplified geometries at 1:8-scale and below. Early experiments (Refs. 4-6) focused on the simplified geometry of the Ground Transportation System (GTS) model representative of a class-8 tractor-trailer with a cab-over-engine design. A 1:8-scale GTS model with no tractor-trailer gap and no wheels was first studied with the addition of several ogival boattails and slants to the base of the trailer (Ref. 4). The largest overall drag reduction of 10% was obtained by a 2.4-m ogive configuration (full scale). The addition of boattail plates to the same model resulted in a 19% drag reduction and PIV measurements behind the trailer document a significant reduction in the wake size due to the flow turning provided by the plates (Ref. 5). Variation of the tractor-trailer gap on a 1:15-scale model at zero yaw revealed relatively constant drag on the tractor while the trailer drag increased by a factor of three as the gap was increased from zero to 1.55*A**0.5 (Ref. 6).

Also part of the DOE effort, the Generic Conventional Model (GCM) of the current study was tested in two different facilities at the National Aeronautics and Space Administration's (NASA) Ames Research Center. This geometry included a tractor-trailer gap and a simplified conventional tractor geometry (detailed below). In the 7- by 10-Ft Wind Tunnel, measurements were made at a Reynolds number of 1.1 million. Of particular interest are the detailed PIV data in the tractor-trailer gap with and without side extenders and in the trailer wake with and without boattail plates (Ref. 7). A large subset of the configurations tested in the 7- by 10-Ft Tunnel were duplicated in the 12-Ft Pressure Tunnel to determine the effects of

Reynolds number variation (Ref. 8). For all configurations, Reynolds number effects were evident at high yaw angles (greater than □deg) where there was a significant reduction in drag at lower Reynolds numbers. However, this difference did not significantly affect the computation of the wind-averaged drag coefficients (at highway speeds) which employs data at lower yaw angles.

The goal of the present study is to provide detailed experimental results for the most promising and practical drag-reduction concepts tested on the Generic Conventional Model. In addition to the force, moment, and pressure measurements, off-body details were obtained using 3-D particle image velocimetry (PIV). The uncertainty in the PIV measurements was ±2% in the in-plane velocities and ±4% in the out-of-plane velocity. Measurements were made at various yaw angles to study the influence of crosswind and to calculate wind-averaged drag coefficients.

Experimental Setup

Measurements of the same model were conducted in both the 12-Ft Pressure Wind Tunnel and the 7- by 10-Ft Wind Tunnel at NASA Ames Research Center. Apart from the PIV data, the majority of the results presented in this report are from the 12-Ft Pressure Tunnel. The differences between the tunnels and the model installations are detailed below.

The 12-Foot Pressure Wind Tunnel can be pressurized from 0.25 to 6 atmospheres at Mach numbers from 0.1 to 0.5. The test section has a circular cross section 3.66 m in diameter with four 1.22-m wide flat surfaces centered about the horizontal and vertical centerlines. The RMS turbulence intensity in the test section was 0.27% and 0.52% at Reynolds numbers of 1 and 6 million, respectively. A ground plane was installed 53 cm above the tunnel floor providing a flat surface 3.05 m wide and 5.49 m long. Pressure taps were located on both the ground plane (2 rows of 64 taps) and the test-section walls (8 rows of 30 taps). A fairing was installed to isolate the model-support hardware from the air stream, and speed-correction probes were used to correct the facility speed due to the blockage of the ground plane and fairing. There was also an additional pitot-static probe installed on the upper left ceiling to measure the free-stream conditions in the test section. All of the data presented are referenced to the Mach number based on a wall tap located 1.88 m forward of the center of rotation at an azimuth of 60 deg from vertical (two o'clock looking downstream). Except where noted, all data were acquired at a Mach number of 0.15 which allowed for Reynolds number studies with no Mach-number effects. With the tunnel pressurized to six atmospheres, the Reynolds number was over 6 million based on the trailer width which is comparable to a full-scale truck driving at 120 km/hr.

The 7- by 10-Foot Wind Tunnel is a closed-circuit atmospheric facility incorporating a 4.57-m long test section with a constant height of 2.13 m and a nominal width of 3.05 m with a 1% wall divergence. The boundary layer thickness at the test section entrance is 5.3 cm which corresponds to a displacement thickness of 1.5 cm. The multiple turbulence-reducing screens in the circuit yield empty test-section turbulence intensities in the longitudinal, lateral, and vertical directions of 0.1%, 0.3%, and 0.3%, respectively, for a test condition of M = 0.22. These turbulence levels correspond to a RMS turbulence intensity of 0.25% and a turbulence factor of 1.2. For ease of comparison with CFD, the test section static pressure was obtained from a single wall pressure tap located at x/w = 4.5, y/w = 2.6, and z/w = -4.7. The 7- by 10-Ft data presented in this report are for Mach and Reynolds numbers of 0.15 and 1.1 million, respectively.

A photograph of the GCM baseline configuration installed in the 12-Ft Wind Tunnel test section is shown in Fig. 1. This 1:8-scale model is representative of a generic class-8 tractor-trailer with the engine in front of the cab. Designed for CFD validation, the model includes a number of geometry simplifications in order to facilitate grid generation and avoid the associated flow complexities. In particular, no effort was made to duplicate the complex geometry of the undercarriage of either the tractor or trailer (both were approximated by flat surfaces). Similarly, the wheel wells of the tractor were not modeled and only the portion of the wheels below the tractor lower surface were included (Fig. 2). Also, the tractor geometry (designed by the Calmar Research Corp.) is a streamlined shape representative of a modern tractor design while omitting most small-scale surface details and flow-through components. The trailer measures 13.7 m in length (full scale) with rounded front vertical edges

(20-cm full-scale radius). The tractor-trailer gap for this study was held constant at the full-scale equivalent of 1 m. The moment center on the model was specified as the point between the rear tractor wheels along the model centerline at the bottom of the trailer.

In the 12-Ft Wind Tunnel, the GCM was attached to the model-support hardware with four vertical posts that were 4.45 cm in diameter. The four posts were non-metric (i.e., their aero loads were not measured by the balance) with 0.75 mm of clearance as they passed through the trailer floor. The model was mounted with its wheels 3.8 mm above the ground plane and centered laterally in the tunnel. The center of rotation of the model was located 1.38 m aft of the tractor front bumper. The model frontal area of 0.154 m2 gives a solid blockage of 1.5%. The overall model loads were measured with a six-component balance (10-cm Task balance Mark 2B) that was mounted inside the trailer. The manufacturer-specified accuracy of the internal balance in the axial (drag) direction was ± 4.45 N, but the experimental data indicated repeatability on the order of ±2.2 N.

In the 7- by 10-Ft Wind Tunnel, the model was located at a position 13.33 cm downstream of the beginning of the test section. Mounted level in the test section, the bottom of the wheels were located 1.3 cm above the wind tunnel floor to account for the boundary-layer displacement thickness. Four cylindrical struts connected the model to the scale system and 3.8 cm diameter cylindrical fairings (non-metric) extended from the floor to within 0.63 cm of the bottom of the model. The model was mounted on the facility scale system that included a turntable for remote model positioning. Since the facility scales measure wind-axis forces (parallel and perpendicular to the axis of the wind tunnel), a coordinate transformation was employed to determine the body-axis drag (the force along the longitudinal axis of the model).

In both tunnels, the tractor was suspended from the trailer through a set of flexures and 2 load cells that measure the drag and yawing moment of the tractor alone. The specified accuracy of the load cells was ±2 N. The model was instrumented with 200 pressure taps on the tractor and 276 taps on the trailer. The surface pressures were measured with an electronically scanned pressure system and time averaging yielded an uncertainty in the calculated pressure coefficients of ±0.002 at Re = 6 million. There were also 12 unsteady pressure transducers mounted on the tractor rear surface, trailer front surface, and the trailer rear surface. A three-component PIV system was used to obtain horizontal-plane velocity measurements in the tractor-trailer gap and the trailer wake at 1/4, 1/2, and 3/4 of the trailer height (7x10 only). Details of the PIV system installation are presented in Ref. 9. The model was yawed through a range of angles between ±14 degrees.

Results and Discussion

Various add-on drag-reduction devices were tested on the bases of both tractor and trailer as well as on the trailer under-carriage. In this report, results will be presented for tractor side and roof extenders, trailer base flaps, and trailer skirts. Details of each device will accompany the discussion of the associated results.

The results presented below detail the body-axis forces and moments for the tractor-trailer combination and its components. This drag coefficient represents the force along the axis of the vehicle in the direction of travel. With the objective of CFD validation, no wall corrections were applied to the data and all coefficients were calculated based on the static pressure at a known point in the test section (as detailed above). Without wall corrections, the computed drag coefficients will differ from those of the equivalent model in free air. However, the measured differences between configurations should be representative of the effects of the associated geometric modifications.

Using the variation of drag with yaw angle, wind-averaged drag coefficients ( ) were computed using the SAE Recommended Practice (Ref. 10). This practice assumes that the mean wind speed in the United States of 11.2 km/hr has an equal probability of approaching the vehicle from any direction. This mean wind speed and the vehicle velocity were used to calculate a weighted average based on the variation in drag coefficient over a range of yaw angles. The wind-averaged drag coefficients reported in this paper were computed for a highway speed of 88 km/hr. Note that the uncertainty in the wind-averaged drag coefficient was less than the values listed in Table 1 due to the effects of averaging. In particular, the repeatability of the

wind-averaged drag for the baseline configuration was ±0.0004.

Except where noted, the data presented below are from the measurements conducted in the 12-Ft Pressure Wind Tunnel at a Reynolds number of 6 million. All data were acquired for increasing yaw angle. Details of the observed hysteresis were presented previously in Ref. 8.

A. Tractor Extenders

Similar to the components of a modern tractor aero package, side and roof extenders were attached to the rear of the tractor as shown in Figure 3. The extenders were 1/8-in thick (model scale) with four different lengths ranging from 30% to 60% of the tractor-trailer gap. As detailed previously (Ref. 8), the results indicated a consistent trend of increasing drag reduction with increasing extender length. The most effective side and roof extender length of 60% gap was chosen as the baseline for all subsequent comparisons in the current analysis. The wind-averaged drag (defined above) of this configuration was 0.422.

Since tractor aero packages frequently only include side extenders, the effect of the roof extender was investigated by testing the 60%-gap side extenders alone in the 7- by 10-Ft Wind Tunnel. The drag curves (Fig. 4) indicate that the addition of a roof extender provides a significant drag reduction at all yaw angles. The change in wind-averaged drag relative to the baseline for side extenders only was 0.009. The change in drag coefficient by component is illustrated in Figure 5. As expected from the drag curves, the drag on the tractor without the roof extender is increased relative to the baseline (side and roof extenders). The drag of the trailer, however, is reduced by removing the roof extender, likely as a result of the modified gap flow. The effect of the roof extender on the yawing moment (Fig. 6) is minimal with minor differences evident at the higher yaw angles. All other forces and moments (not shown) were relatively unchanged.

The effect of the extender length, as mentioned previously, indicated a general trend of increasing drag reduction with increasing extender length. This effect is illustrated at two Reynolds numbers for the 30% and 60% gap lengths in Figure 7. Relative to the 60%-gap baseline, the shorter extenders yielded an increase in wind-averaged drag of 0.003 and 0.011 for Reynolds numbers of 1.1 and 6.2 million, respectively. This difference suggests a sensitivity of the extender effectiveness to Reynolds number. Similar to the effect of the roof extender, the shorter extenders serve to increase the drag on the tractor while slightly reducing the drag on the trailer (Fig. 8). The shorter extenders also yield a significant decrease in the yawing moment that increases with yaw angle (Fig. 9). All other forces and moments (not shown) were relatively unchanged.

The GCM was instrumented with 476 surface pressure taps, many of which are located on the back of the tractor (39) and the front and back of the trailer (24 and 39, respectively). Figures 10-12 present pressure coefficient contours on these surfaces for the baseline configuration at yaw angles of zero and 10 deg. Note that all but three pressure taps were located on the left side of the model with clustering near the edges. For zero yaw, symmetry is assumed and the data are duplicated on the right side of the figure. For 10 deg, the right half of the figure includes data for the –10 deg yaw angle.

In both test facilities, particle image velocimetry (PIV) measurements were obtained in the gap between the tractor and trailer at yaw angles of zero and 10 deg. The 12-Ft Wind Tunnel results were previously reported for a configuration without side extenders (Ref. 8). In the 7- by 10-Ft Wind Tunnel, measurements were conducted with and without 50%-gap side extenders and the resulting stream traces (Fig. 13) indicate their effect on the gap flow. At zero deg, the flow fields with and without extenders are similar with two counter-rotating recirculation regions. Closer examination reveals that the presence of the extenders tend to move centers of these regions closer to the cab, minimize crossflow, and reduce the vertical velocity (Vmean) in the gap. At 10 deg, the stream traces without extenders indicate one recirculation region to the right with dramatic crossflow and downflow. The effect of the extenders is to reduce both crossflow and downflow (thereby increasing pressure), which results in a low-vorticity recirculation near the middle of the gap. A more detailed discussion of the PIV measurements is found in Ref. 9.

B. Trailer Base Flaps

As previously documented (Ref. 11), an effective method of aerodynamic boat-tailing is what will be referred to as base flaps. In this embodiment, the panels are attached to all edges of the trailer base

and angled inward. In the current study, measurements were made for a base-flap length of 63.5 cm full scale (non-dimensional length = l/A**0.5 = 0.20) at angles ranging from zero to 28 deg. The installation photo (Fig. 14) shows the base flaps with a 20-deg deflection mounted on the rear of the trailer. Note that the linkages connecting the flaps to the base were designed for easy angle change and are not representative of the full-scale hardware.

An analysis of base-flap effectiveness as a function of flap angle on the GCM (Ref. 8) indicated an optimum angle near 20 deg. However, other small-scale wind tunnel tests and road tests show the optimum angle to be closer to 15 deg (Ref. 11, 12). This difference is likely due to the absence of the lower base flap in the studies referenced above. In the current study, data will be presented for a base-flap angle of 16 deg due to the limited data available for the 20-deg deflection.

Relative to the baseline with side and roof extenders, the effect of the base flaps on the forces and moments is presented in Fig. 15-20. As indicated in Fig. 17, the base flaps provided a relatively constant drag reduction that increases slightly with angle of attack. The baseline drag curve for Re = 1 million is notably higher than that for Re = 6 million. The change in the associated wind-averaged drag was –0.087 and –0.079 for Reynolds numbers of 1 million and 6 million, respectively, suggesting some Reynolds-number sensitivity. These values are at the upper end of the range reported in previous studies (Ref. 3) that differ from the current configuration by the absence of the lower base flap. The base flaps also provided an increase in lift (Fig. 15) due to the downwash created by the flow turning of the top flap. The lift increase on the trailer is reflected by a corresponding pitching moment decrease (Fig. 18). Also, the addition of the base flaps resulted in larger yawing moments (more positive and more negative for positive and negative yaw angles, respectively, as shown in Fig. 19). The side force and rolling moment were relatively unaffected (Figs. 16 & 20). As expected, the change in the drag and yawing-moment coefficients by component (Fig. 21) indicate that the trailer is the source of the observed differences.

The trailer was instrumented with a line of pressure taps running axially along the centerline of the top and left side. The pressure distributions with and without base flaps are presented in Figs. 22-23 for yaw angles of zero and 10 deg. On both the top and side, the base flaps serve to reduce the pressure towards the rear of the trailer. The effect of the base flaps on the forward two-thirds of the pressure distribution was minimal. The pressures on the tractor (not shown) were unaffected. Hence, the base flaps have a relatively local effect on the truck pressure distributions. The pressure distributions at –10 deg (not shown) exhibit similar trends.

The differences in the pressure distributions on the back of the trailer with base flaps (Fig. 24) indicate significantly increased pressures relative to the baseline. At zero yaw, the increase in pressure is relatively constant with an average change in pressure coefficient of 0.14. At 10 deg, however, the increase in pressure is far from uniform with the greatest increase on the bottom half of the trailer base. The extremes of the pressure difference occur on the windward side of the trailer base. The pressures on the back of the tractor and front of the trailer (not shown) were relatively unchanged by the presence of the base flaps.

No PIV measurements were obtained in the wake of the base flaps due to technical difficulties encountered in the high-pressure environment of the 12-Ft Wind Tunnel. However, PIV data were obtained in the truck wake with and without boattail plates in the 7- by 10-Ft Wind Tunnel. Mounted perpendicular to the trailer base and slightly inset from the edge (see Ref. 8 for details), the boattail plates function similarly to the base flaps by turning the flow and reducing the associated wake size. The PIV images with and without boattail plates (Fig. 25) illustrate the how aerodynamic boat-tailing serves to reduce the wake size by deflecting the flow inward.

C. Trailer Skirts

Trailer skirts have been previously investigated (Ref. 3) as an effective add-on to minimize the crossflow under the trailer and shield the rear wheels. As shown in Fig. 26, the skirts extended from a short distance behind the tractor to just in front of the rear wheels. The skirts measured 0.355 truck widths in height allowing a full-scale ground clearance of 0.3 m.

The effect of the trailer skirts on the overall forces and moments is presented in Figs. 27-32. The

skirts significantly reduce the drag across the yaw range with the greatest reduction at the higher angles (Fig. 29). The associated change in wind-averaged drag relative to the baseline was –0.036. This value is at the lower end of the range reported in previous studies (Ref. 3) which is likely due to the simplified geometry of the GCM undercarriage. Due to time constraints, an analysis of Reynolds-number effects was not possible for this configuration. The skirts also provided a reduction in the normal force (Fig. 27) with a small corresponding increase in the pitching moment (Fig. 30) at most yaw angles. This is likely due to reduced pressure on the undercarriage due to vortical flow generated by the skirts under crossflow conditions. The skirts also yield small differences in the yawing moment (Fig. 31) with significantly greater variation at higher angles (unimportant at typical highway speeds). The side force and rolling moment were relatively unaffected (Figs. 28 & 32).

The effects of the skirts on the component drag and yawing-moment differences are presented in Fig. 33. Similar to that of the base flaps, the change in drag coefficient by component indicates that the measured drag reduction is due to the effect of the skirts on the trailer. However, the skirts also generate a smaller, but measurable drag increase on the tractor. The total difference in yawing moment for the skirts is approximately half of that generated by the base flaps. Unlike the base flaps, both the tractor and trailer contributed to the observed yawing-moment differences.

The axial pressure distributions on the side and bottom of the trailer (Figs. 34-35) illustrate that the general effect of the skirts is to reduce the pressures, especially on the bottom at ±10 deg. As suggested previously, the reduced pressures on the bottom of the trailer account for the reduced normal force generated by the skirts. Especially at high yaw angles, the windward skirt likely generates significant vorticity from the accelerated flow separating off the lower edge. The axial pressures on the side indicate slightly higher pressures on the forward third of the trailer except at –10 deg where the taps are on the leeward side. At mid-length on the side of the trailer, the skirts provide a noticeable decrease in pressure. The pressure distribution on the top of the truck (not shown) was relatively unchanged.

The contour plots of Figs. 36-38 show the effect of the trailer skirts on the pressure distributions on the back of the tractor and the front and back of the trailer. At zero yaw, there appears to be little difference on all three surfaces except for a slight increase in pressure on the back of the trailer. At 10 deg, a significantly larger increase in pressure is evident on the back of the trailer, especially on the right (leeward) side. A lesser increase in pressure is also observed on the front of the trailer, mainly on the upper half. A small decrease in pressure is also discernable on the back of the tractor, which accounts for the observed increase in tractor drag.

Although not tested directly in the current study, a previous study suggests that the combination of the trailer base flaps and skirts would yield a drag reduction equal to the sum of their individual effects (Ref. 3). If this is the case, a total drag reduction of 0.115 could be expected from the combination. The corresponding change in fuel consumption (also from the reference above) would be 3.68 liters/100 km.

Conclusions

Experimental measurements were obtained of a 1:8-scale generic class-8 tractor-trailer model in the NASA-Ames 12-Ft and 7- by 10-Ft Wind Tunnels. Data were acquired at a Reynolds number of 1 million in both facilities and at 6 million (equivalent to full scale at 75 mph) in the 12-Ft Pressure Wind Tunnel. Forces and moments, surface pressures, and 3-D particle-image velocimetry were employed to detail a baseline configuration representative of a modern aero package with and without trailer base flaps and trailer skirts.

The tractor side extenders were tested with and without a roof extender. The addition of the roof extender provided a significant drag reduction (0.009) by reducing the drag on the tractor while slightly increasing the drag on the trailer. The drag reduction of side and roof extenders was also found to increase with extender length. Apart from decreasing drag, the longer extenders also generated higher yawing moments. PIV measurements with and without extenders provided insight into the flow field and are also useful for CFD validation.

Relative to the baseline with 60%-gap side and roof extenders, the base flaps provided a sizable drag reduction (0.079) while increasing both normal force and yawing moment on the tractor. The

effectiveness of both the side extenders and base flaps were found to be sensitive to Reynolds number for the reported range of one to six million.

Trailer skirts also reduced the wind-averaged drag (0.036) while marginally reducing the normal force due to lower pressure on the undercarriage. Pressure distributions indicated significantly increased trailer base pressures with little effect on the tractor.

Assuming that the benefits are additive, the combined effect of the base flaps and skirts would correspond to a fuel savings of 3.68 liters/100 km. For more details and a list of references, please see the associated technical paper: SAE-2005-01-3525.

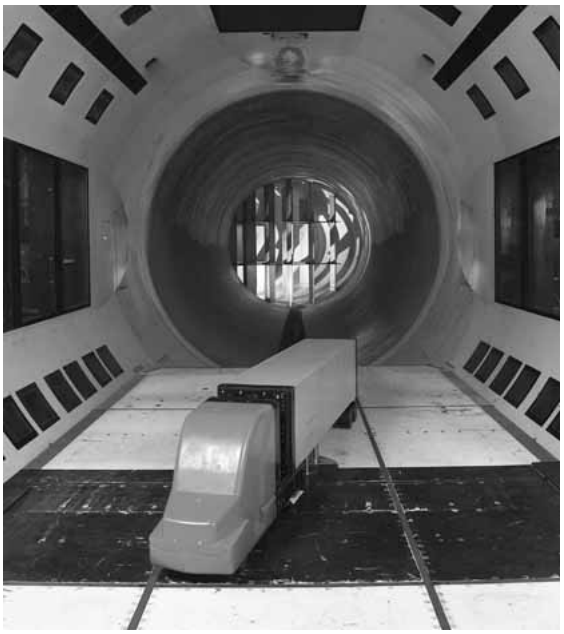

Figure 1: The Generic Conventional Model installed in the 12-Ft Pressure Wind Tunnel.

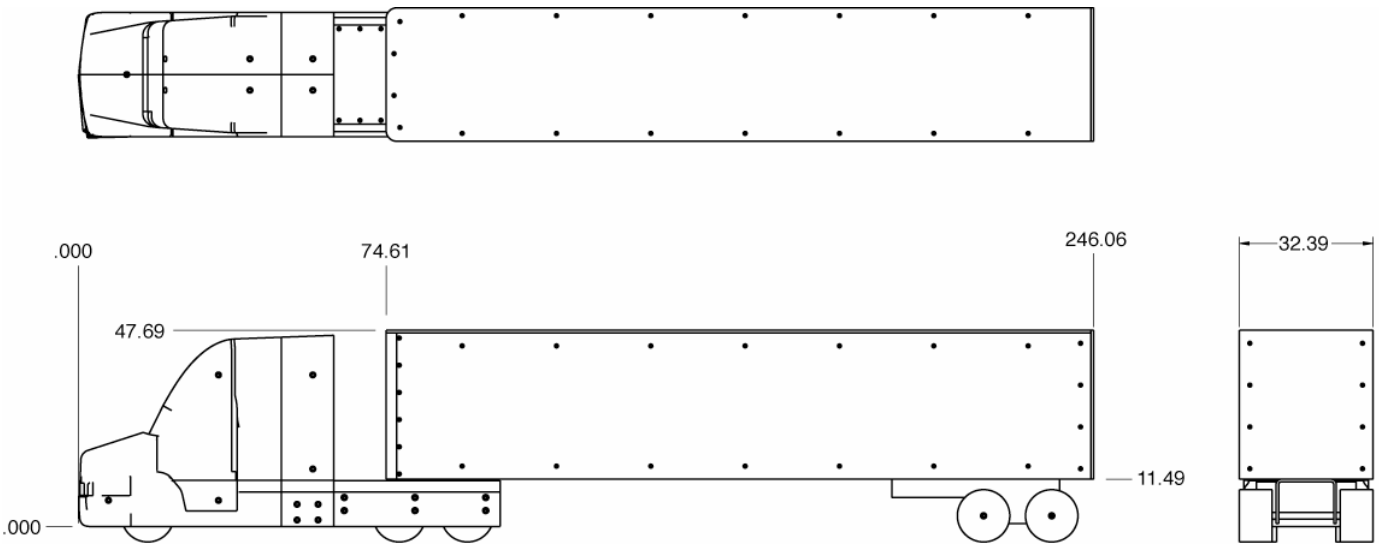

Figure 2: Three-view drawing of Generic Conventional Model (measurements in cm).

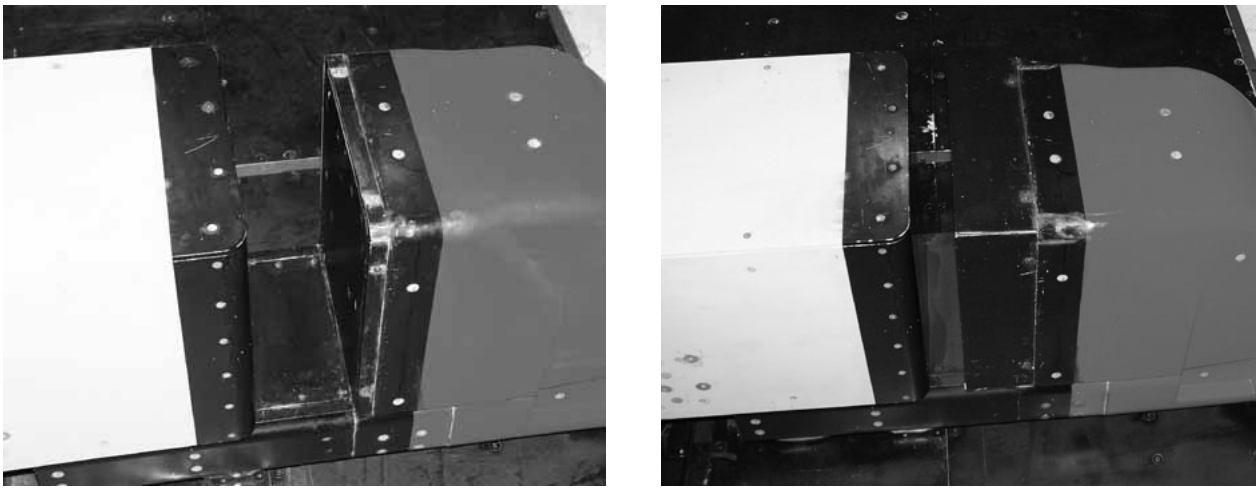

Figure 3: Close-up of tractor-trailer gap with and without side and roof extenders (60% gap).

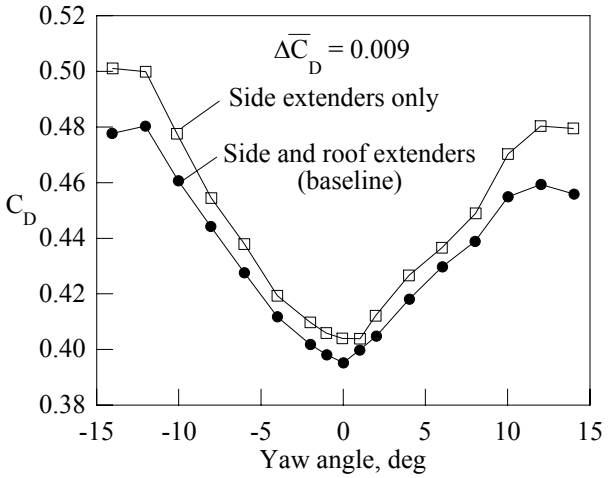

Figure 4: Effect of roof extender on drag coefficient (0.6g extenders, Re = 1.1 million, 7x10 Wind Tunnel).

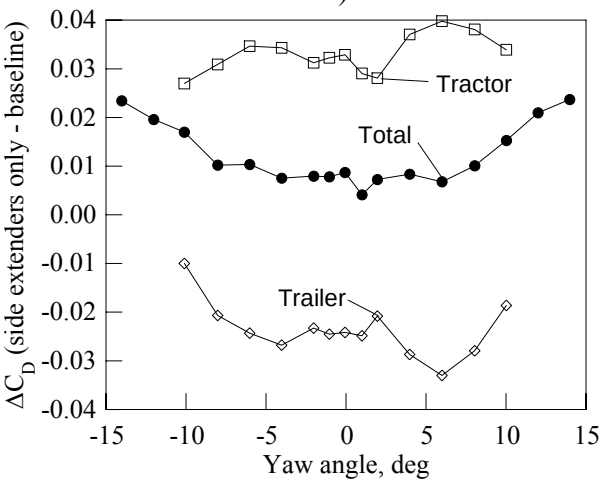

Figure 5: Effect of roof extender on component drag differences (0.6g extenders, Re = 1.1 million, 7x10).

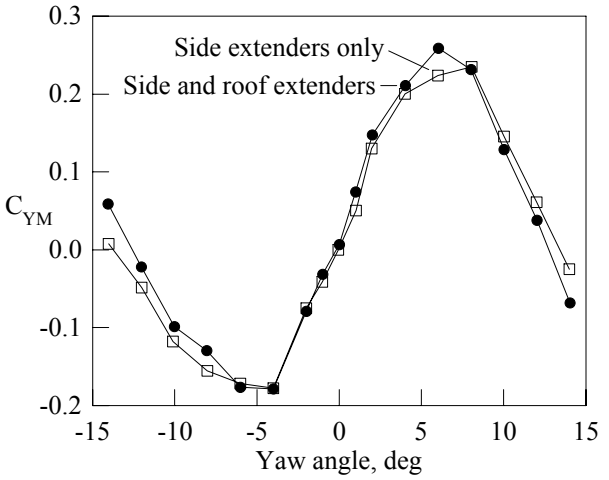

Figure 6: Effect of roof extender on yawing moment (0.6g extenders, Re = 1.1 million, 7x10 Wind Tunnel).

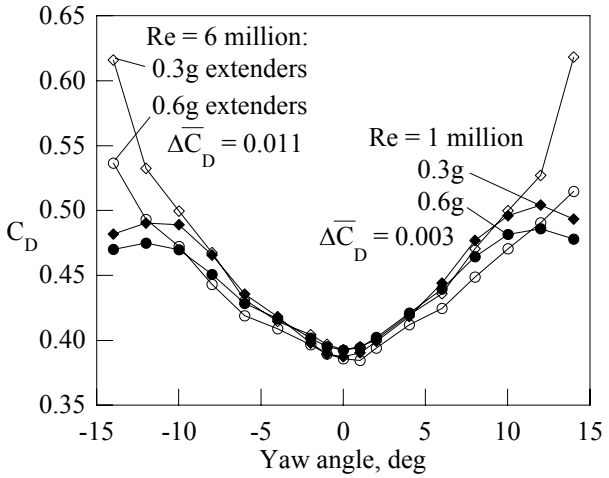

Figure 7: Effect of extender length on drag coefficient (baseline, 12-Ft Wind Tunnel).

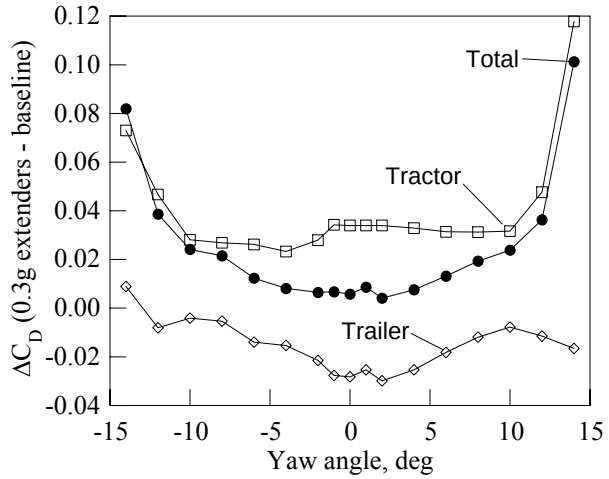

Figure 8: Effect of extender length on component drag differences (baseline, Re = 6 million).

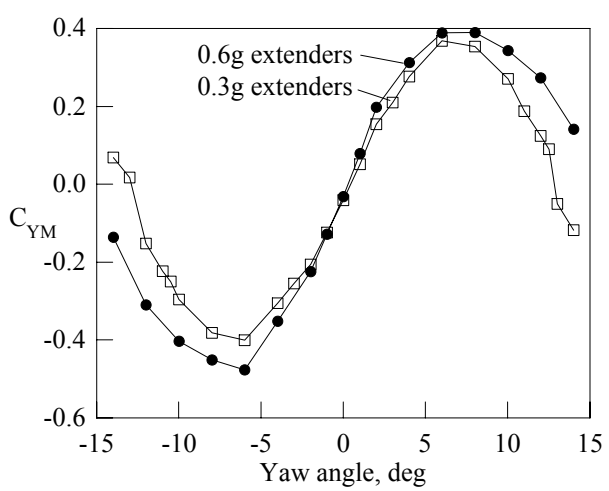

Figure 9: Effect of extender length on yawing moment (baseline, Re = 6 million).

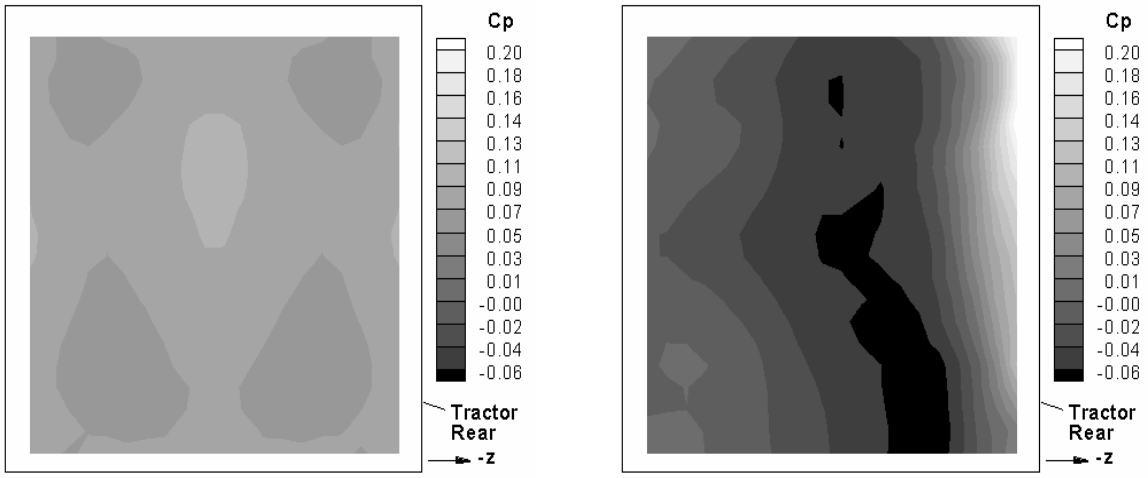

a) Ψ = 0 deg b) Ψ = 10 deg

Figure 10: Pressure coefficient contours on the back of the tractor with 0.6g side and roof extenders, Re = 6 million. Symmetry assumed for zero yaw. For Ψ = 10°, right half of image represents data at Ψ = –10°.

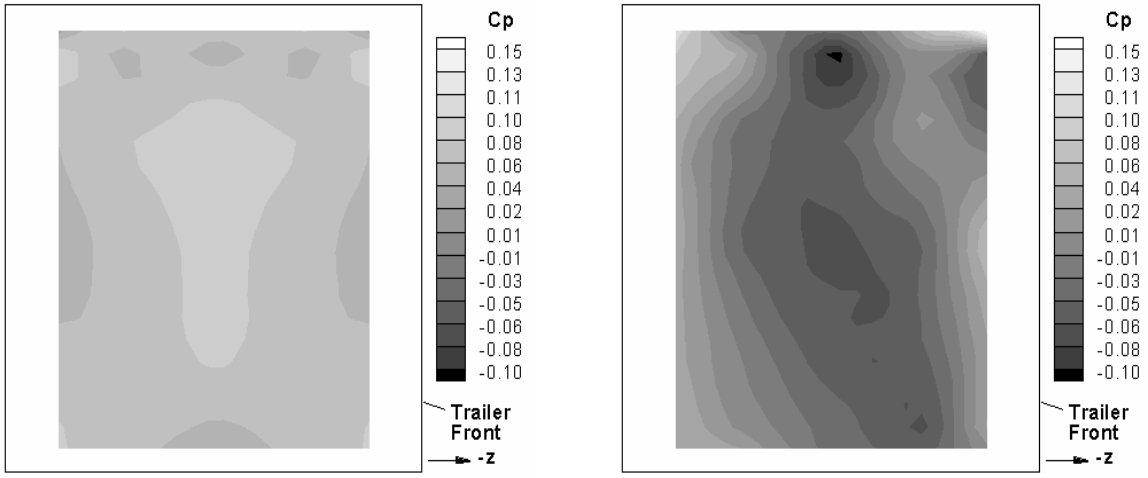

a) Ψ = 0 deg b) Ψ = 10 deg

Figure 11: Pressure coefficient contours on the front of the trailer with side and roof extenders, Re = 6 million.

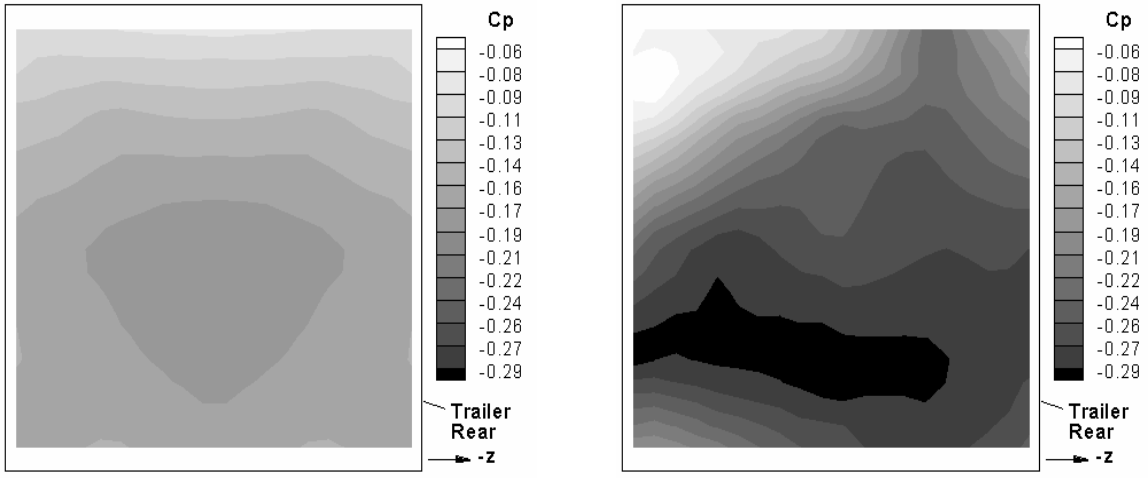

a) Ψ = 0 deg b) Ψ = 10 deg

Figure 12: Pressure coefficient contours on the back of trailer with side and roof extenders, Re = 6 million.

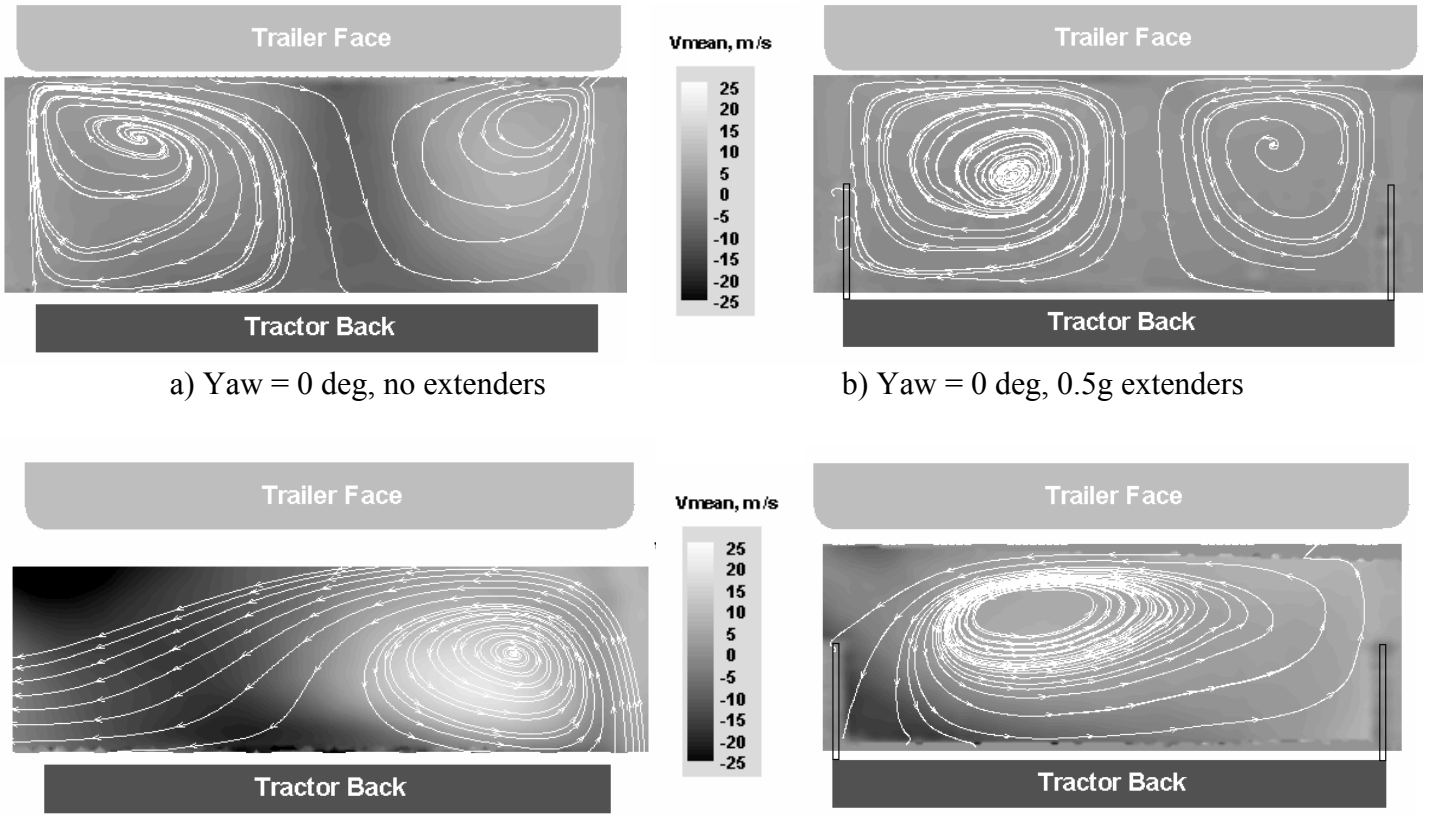

a) Yaw = 0 deg, no extenders

b) Yaw = 0 deg, 0.5g extenders

c) Yaw = 10 deg, no extenders

d) Yaw = 10 deg, 0.5g extenders

Figure 13: Partical image velocimetry data in the tractor-trailer gap with and without 0.5g side extenders. Images are shaded by out-of-plane velocity and flow is from bottom to top of the page (7x10 Wind Tunnel, Re = 1 million).

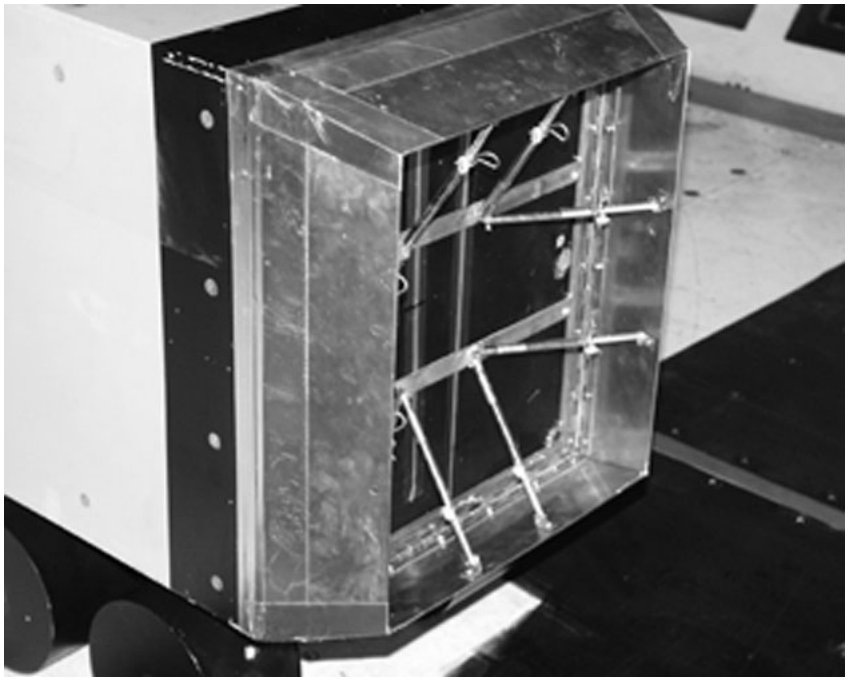

Figure 14: Base flaps installed on trailer base (flap angle = 20 deg).

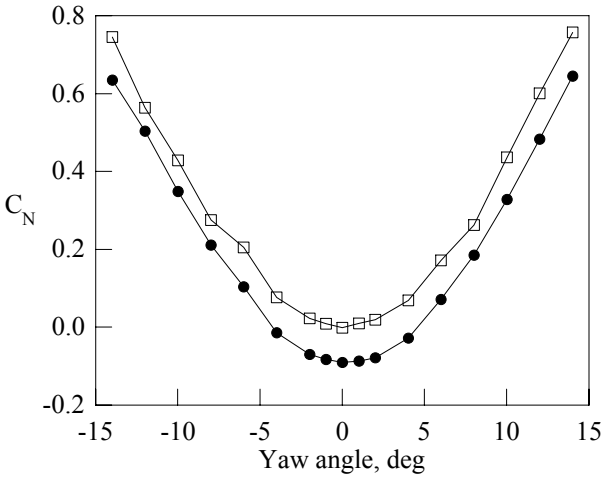

Figure 15: Normal force coefficient comparison (solid: baseline, open: base flaps, Re = 6 million).

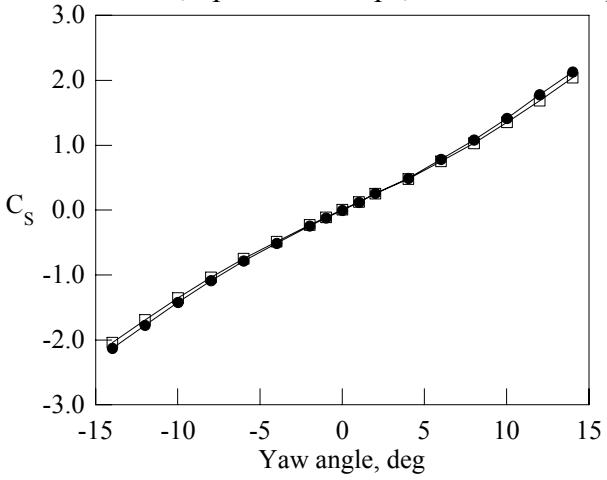

Figure 16: Side force coefficient comparison (solid: baseline, open: 16-deg base flaps, Re = 6 million).

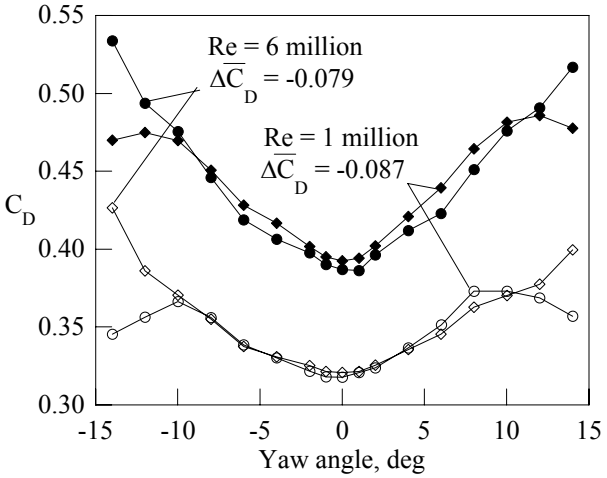

Figure 17: Drag coefficient comparison (solid: baseline, open: 16-deg base flaps).

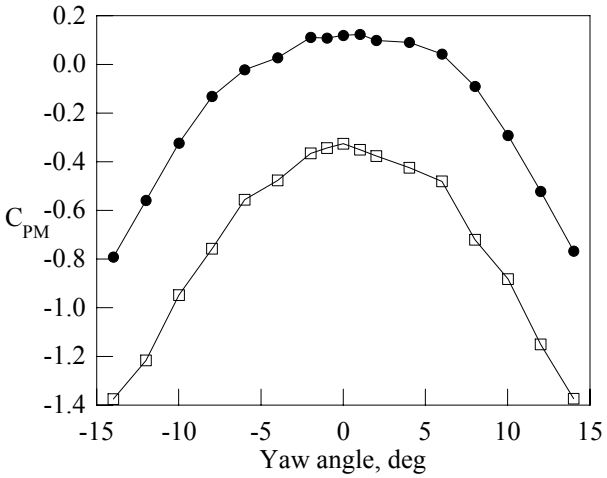

Figure 18: Pitching moment coefficient comparison (solid: baseline, open: base flaps, Re = 6 million).

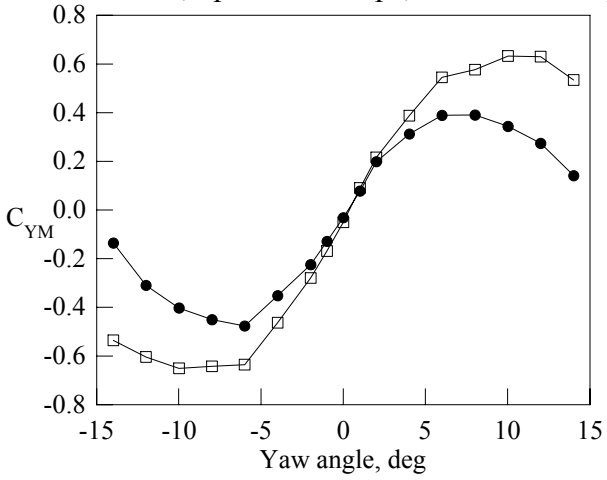

Figure 19: Yawing moment coefficient comparison (solid: baseline, open: base flaps, Re = 6 million).

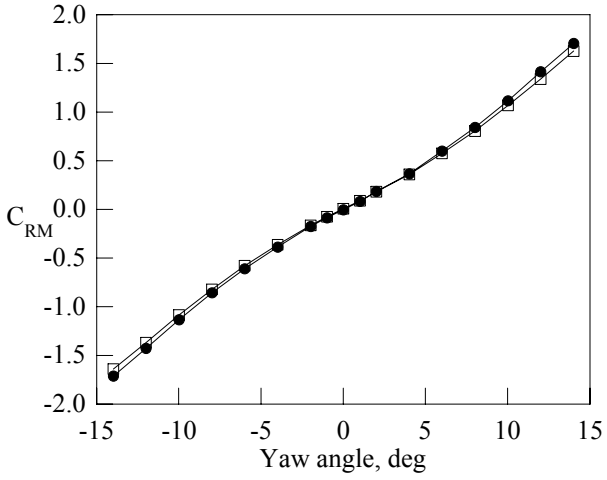

Figure 20: Rolling moment coefficient comparison (solid: baseline, open: 16-deg base flaps, Re = 6 million).

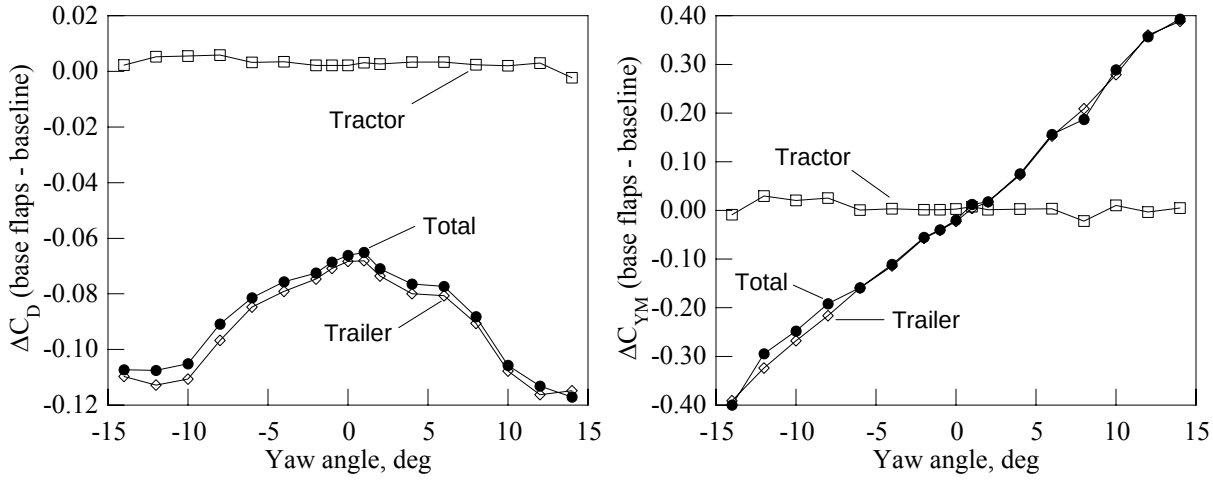

Figure 21: Effect of 16-deg base flaps on component drag and yawing-moment differences at Re = 6 million.

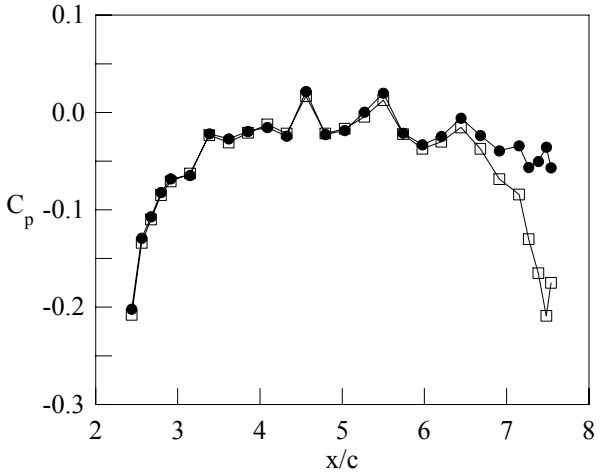

a) Ψ = 0°

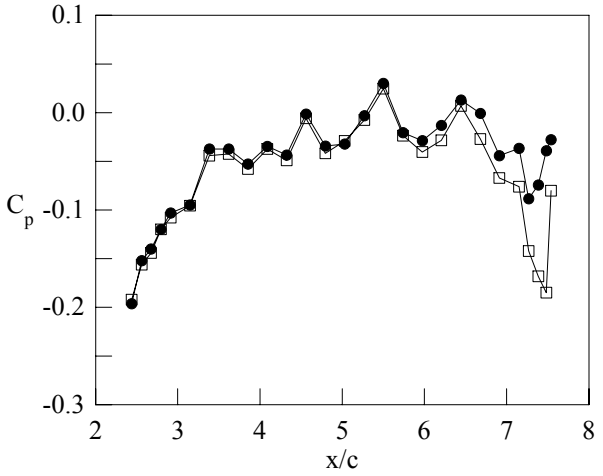

b) Ψ = 10°

Figure 22: Effect of 16-deg base flaps on trailer top centerline pressure coefficients, z/w = 0.0 (solid: baseline, open: base flaps, Re = 6 million).

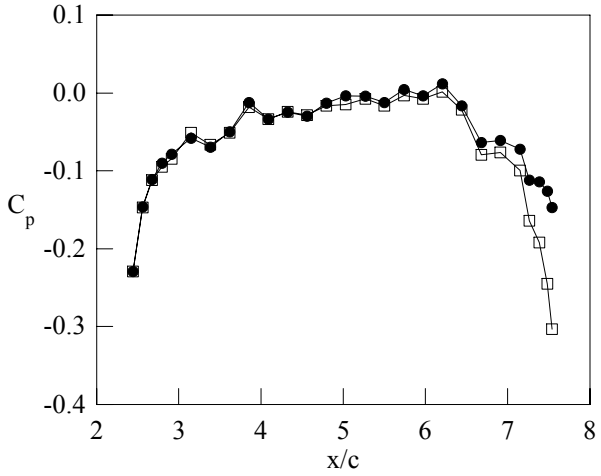

a) Ψ = 0°

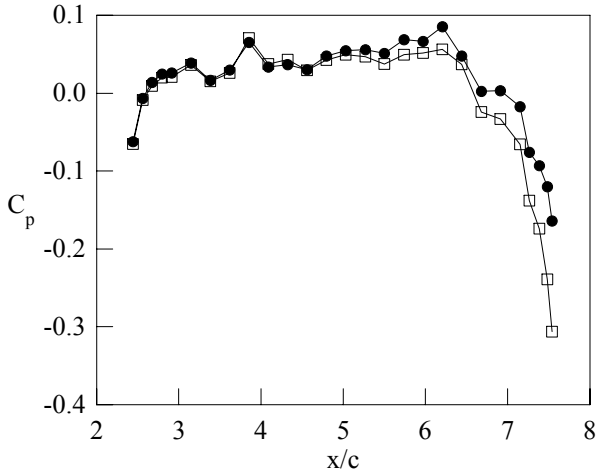

b) Ψ = 10°

Figure 23: Effect of 16-deg base flaps on trailer side centerline pressure coefficients, y/w = 0.9 (solid: baseline, open: base flaps, Re = 6 million).

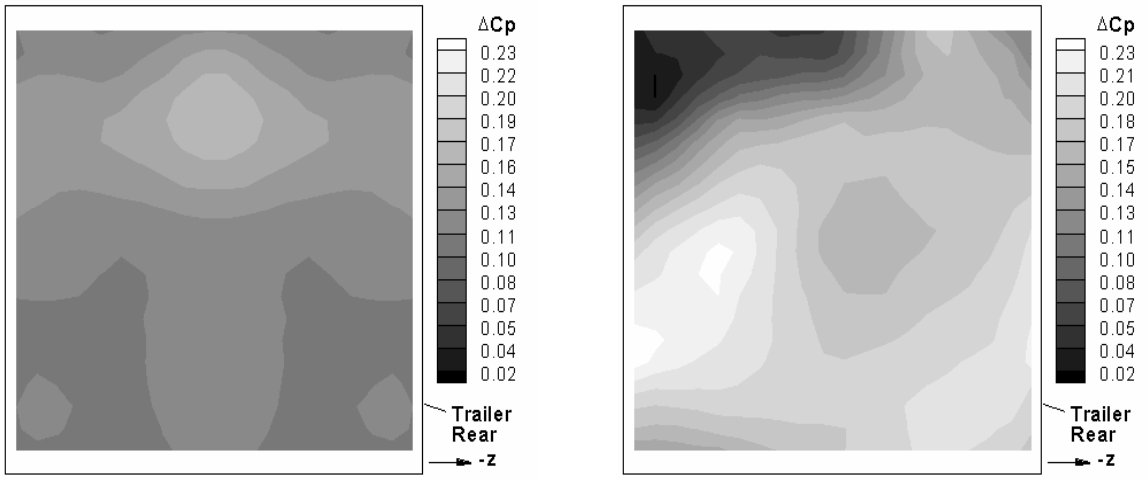

a) Ψ = 0 deg b) Ψ = 10 deg

Figure 24: Effect of 16-deg base flaps on the pressure distribution on the back of the trailer (relative to extender baseline), Re = 6 million. Symmetry assumed for zero yaw. For Ψ = 10°, right half of image represents data at Ψ = –10°.

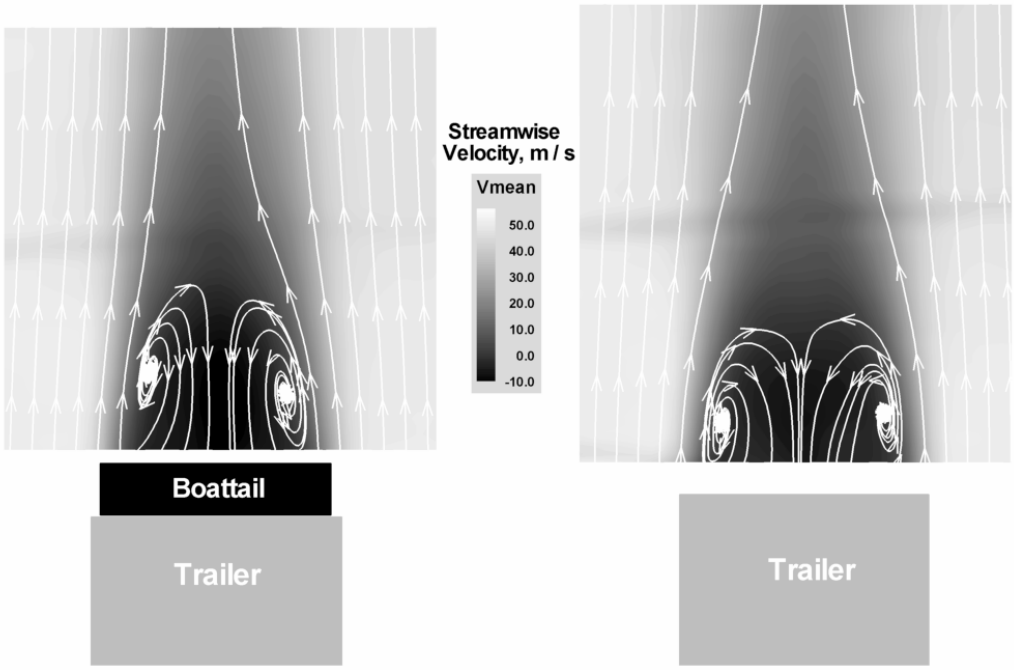

Figure 25: Partical Image Velocimetry data in the trailer wake with and without boattail plates. Images are colored by out-of-plane velocity and flow is from bottom to top (7x10 Wind Tunnel, Re = 1 million).

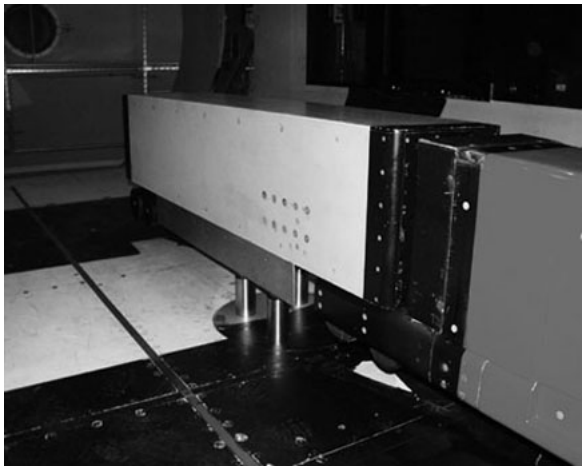

a) Front side of trailer with skirt (grey plate)

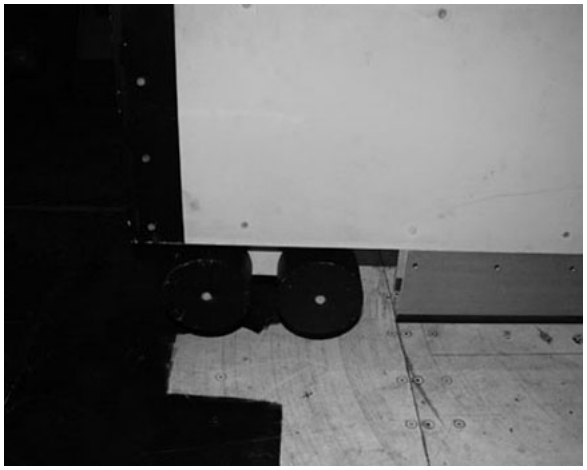

b) Rear side of trailer with skirt (at lower right)

Figure 26: Trailer skirt installation photos.

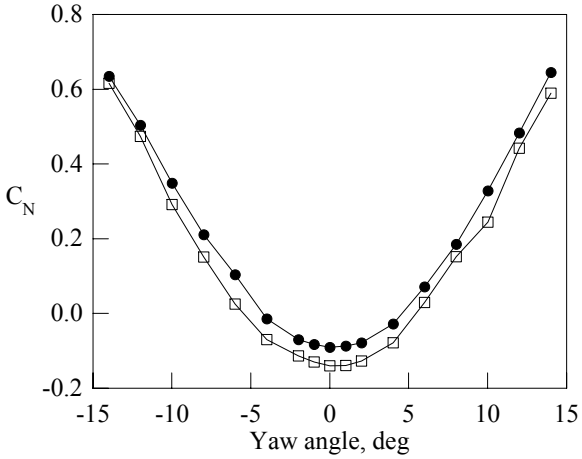

Figure 27: Normal force coefficient comparison (solid: baseline, open: skirts, Re = 6 million).

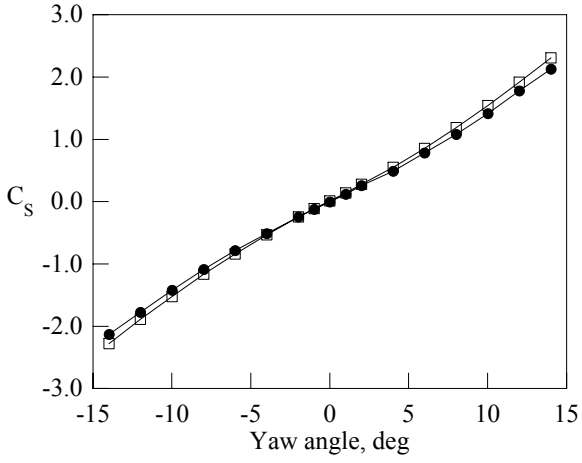

Figure 28: Side force coefficient comparison (solid: baseline, open: skirts, Re = 6 million).

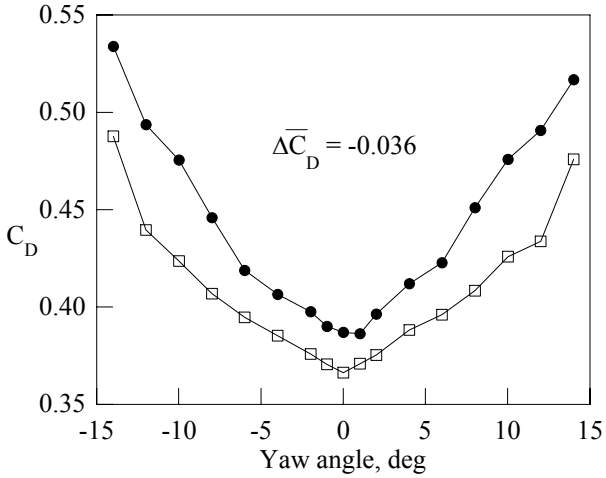

Figure 29: Drag coefficient comparison (solid: baseline, open: skirts, Re = 6 million).

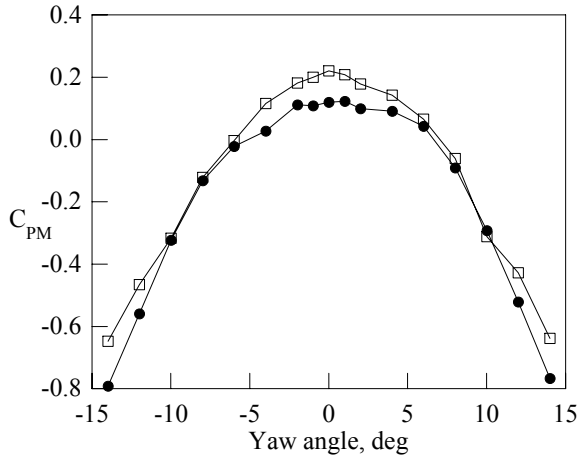

Figure 30: Pitching moment comparison (solid: baseline, open: skirts, Re = 6 million).

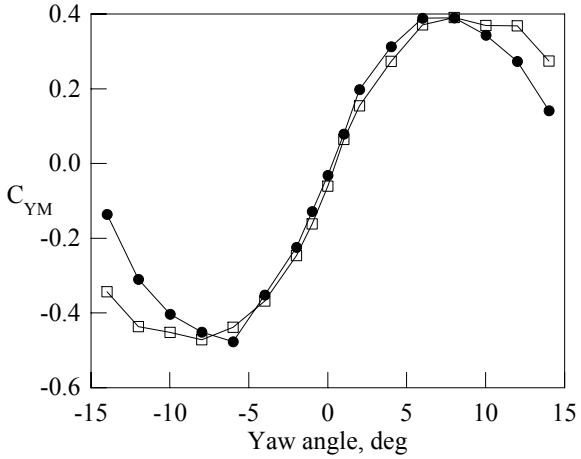

Figure 31: Yawing moment comparison (solid: baseline, open: skirts, Re = 6 million).

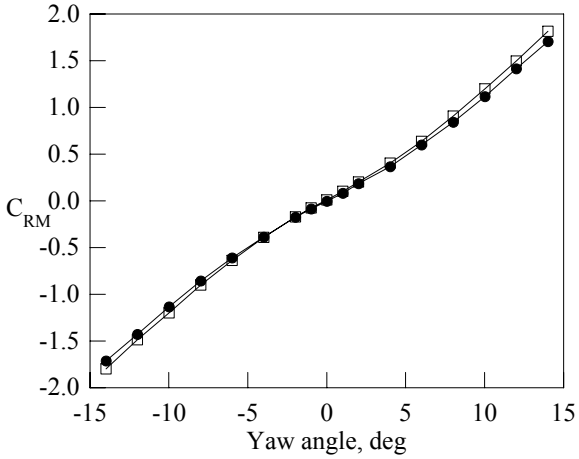

Figure 32: Rolling moment comparison (solid: baseline, open: skirts, Re = 6 million).

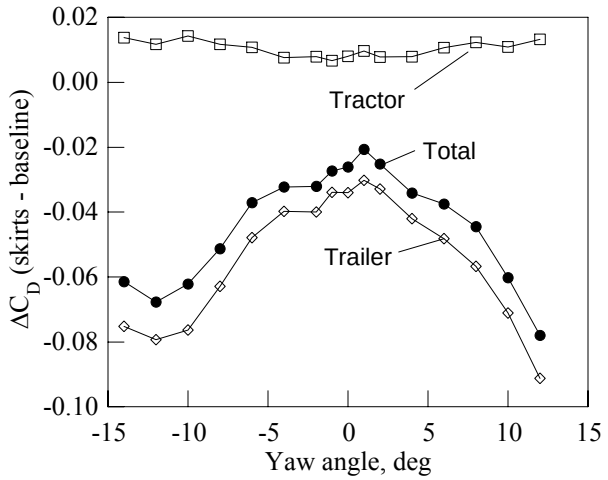

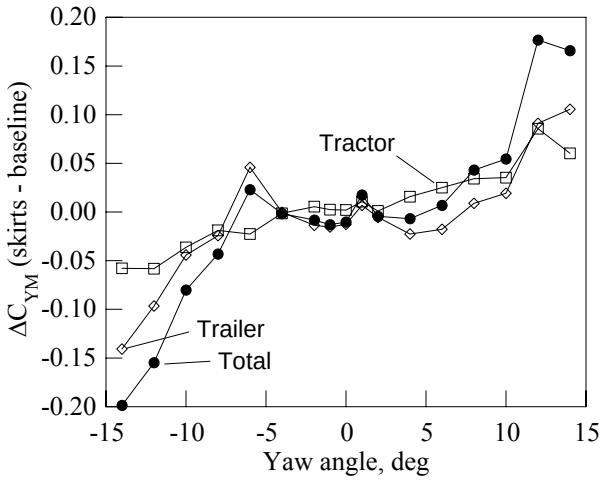

Figure 33: Effect of trailer skirts on component drag and yawing-moment differences at Re = 6 million.

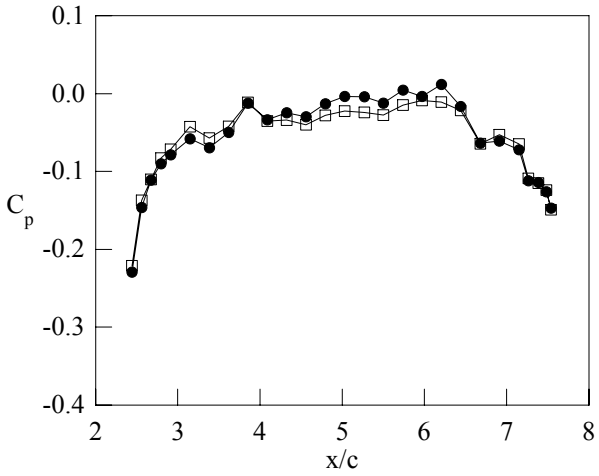

a) Ψ = 0°

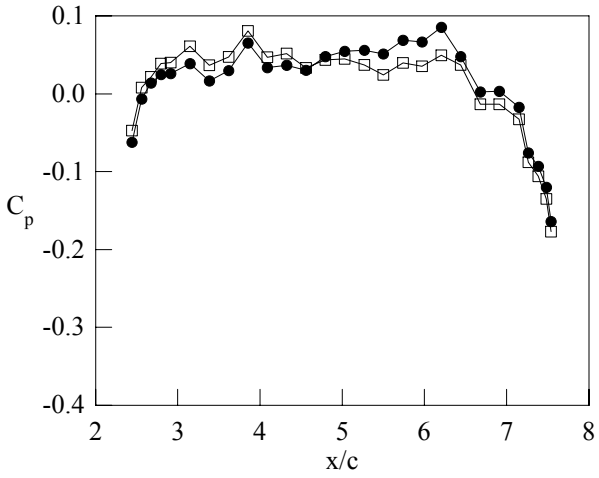

b) Ψ = 10°

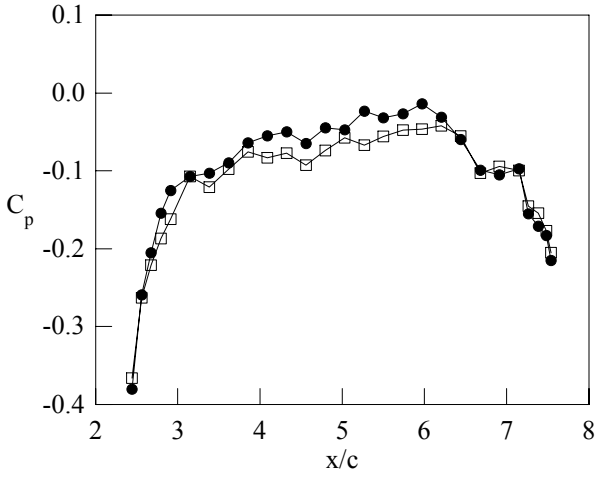

c) Ψ = -10°

Figure 34: Effect of trailer skirts on trailer side centerline pressure coefficients, y/w = 0.9 (solid: baseline, open: skirts, Re = 6 million).

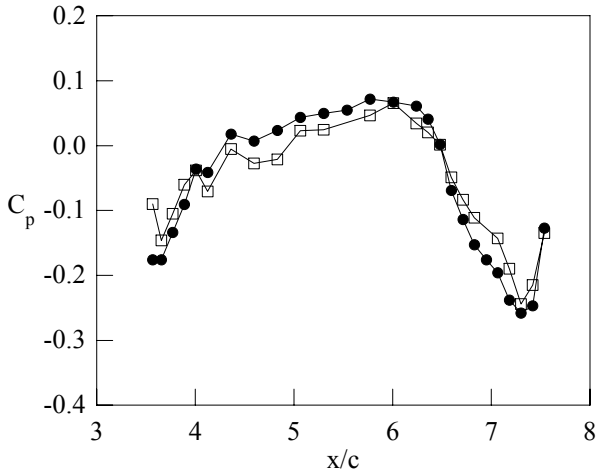

a) Ψ = 0°

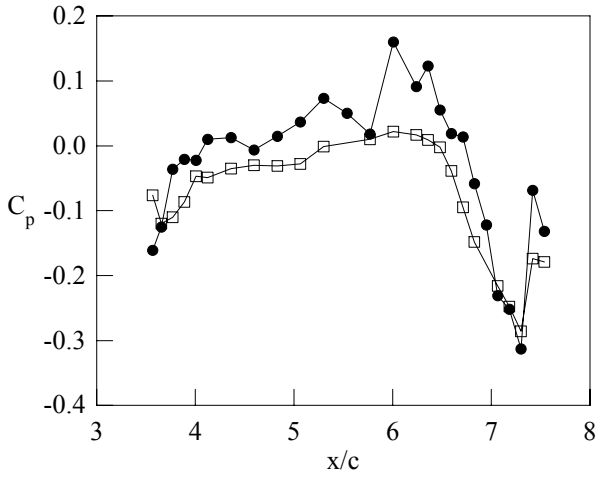

b) Ψ = 10°

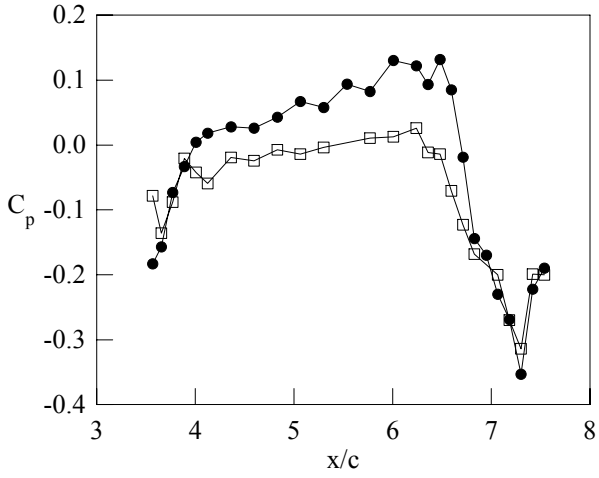

c) Ψ = -10°

Figure 35: Effect of trailer skirts on trailer bottom centerline pressure coefficients, z/w = 0.0 (solid: baseline, open: skirts, Re = 6 million).

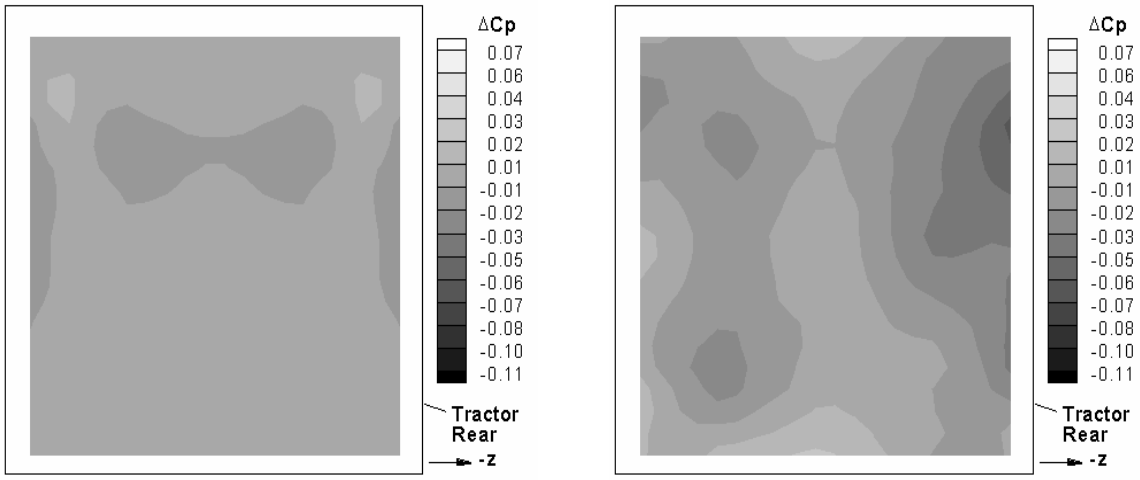

a) Ψ = 0 deg b) Ψ = 10 deg

Figure 36: Effect of trailer skirts on the pressure distribution on the back of the tractor (relative to extender baseline), Re = 6 million. Symmetry assumed for zero yaw. For Ψ = 10°, right half of image represents data at Ψ = –10°.

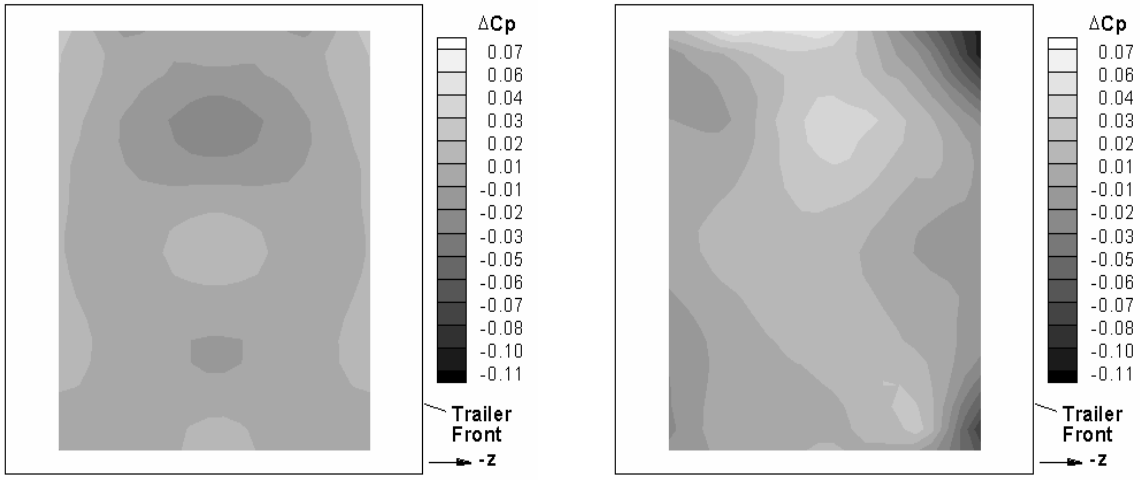

a) Ψ = 0 deg b) Ψ = 10 deg

Figure 37: Effect of trailer skirts on the pressure distribution on the front of the trailer (relative to extender baseline).

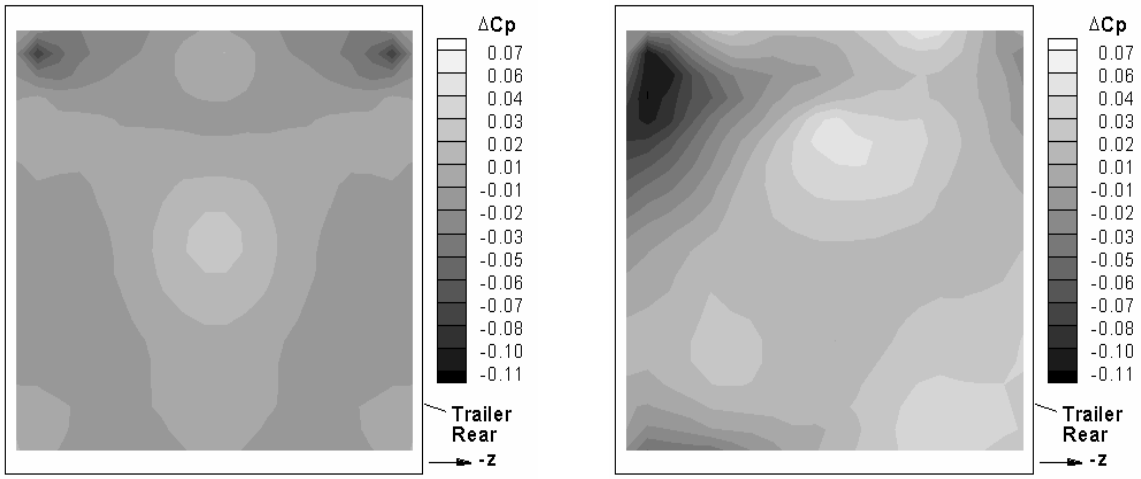

a) Ψ = 0 deg b) Ψ = 10 deg

Figure 38: Effect of trailer skirts on the pressure distribution on the back of the trailer (relative to extender baseline).

APPENDIX D

Commercial CFD Code Validation for External Aerodynamics Simulations of Realistic Heavy-Vehicle Configurations

Principal Investigator: W. David Pointer
Argonne National Laboratory
9700 S Cass Avenue, NE-208, Argonne, IL 60439
(630)252-1052; fax: (630)252-4500; email: dpointer@anl.gov

Technology Development Manager: Lee Slezak
202-586-2335, Lee.Slezak@EE.DOE.GOV
Technical Program Manager: Jules Routbort
630-252-5065, routbort@anl.gov

Participants
Suneet Singh, University of Illinois Urbana-Champaign
Tanju Sofu, Argonne National Laboratory
David Weber, Argonne National Laboratory

Contractor: Argonne National Laboratory
Contract No.: W-31-109-ENG-38

Objective

- Evaluate capabilities in standard commercial computational fluid dynamics (CFD) software for the prediction of aerodynamic characteristics of a conventional U.S. Class 8 tractor-trailer truck.
- Develop "best practice" guidelines for the application of commercial CFD software in the design process of Class 8 vehicles.

Approach

- Develop computational models of the experiments completed in the NASA Ames Laboratory's 7 ft. by 10 ft. wind tunnel using the Generic Convention Model.
- Compare the predictions of the computational models with experimental measurements of vehicle aerodynamic drag force and pressure field distributions.

Accomplishments

- Experimental measurements and computational predictions of the vehicle drag coefficient agree within less than 1 percent in the best case simulations at zero yaw. Experimental measurements and computational predictions of the pressure distribution along the surface of the vehicle agree well everywhere except the rear faces of the cab and the trailer.
- Evaluations of computational predictions of the vehicle at yaw angles greater than zero indicate that vehicle drag coefficients can be predicted with 5 to 10 percent of measured values.

Future Direction

- Confirm applicability of guidelines to real tractor trailer geometries as part of CRADA with PACCAR
- Consider alternate GCM configurations using various add-on devices to examine capabilities for the prediction of changes in drag coefficient

- Evaluate effects of changes in radiator size and effects of underhood flow on drag predictions as part of CRADA with Caterpillar, Inc.
- Suggest potential drag reduction design options based on knowledge gained from computational effort.

ABSTRACT

With rising oil prices, the issue of energy economy in transportation is getting much attention. At the same time, new emissions standards for tractor-trailer vehicles introduce additional challenges for the manufacturers to achieve improvements in vehicle fuel economy. As part of the U.S. Department of Energy Office of FreedomCAR and Vehicle Technologies' Heavy Vehicle Aerodynamic Drag Consortium, Argonne National Laboratory is currently developing guidelines for the use of commercial computational fluid dynamics (CFD) software to facilitate energy efficiency improvements through improved aerodynamic design of tractor-trailer vehicles. The development of these guidelines requires the consideration of the sensitivity of the accuracy of the analysis to the various modeling choices available to the end user. Early investigations focused on the sensitivity of the predictions of drag coefficients and surface pressure distributions for the standard configuration of the GCM at zero yaw to the size and structure of the computational mesh and the selection of turbulence model. Current assessments are focusing on the impact of these parameters on simulations of the standard GCM at yaw angles greater than zero and on the ability to predict the change in the drag coefficient when drag reduction devices are employed.

1 MODELING STRATEGY

This program will provide guidance for the use of commercial CFD software in heavy vehicle design, including the expected impact of grid resolution and structure on prediction accuracy, the impact of the RANS turbulence model formulation selected, the impact of considering only half of a vehicle to speed up initial simulations. These guidelines developed by this program intended to be generic advice for the application of a commercial CFD software package to the prediction of heavy vehicle aerodynamic drag coefficients. Since this market is currently dominated by finite volume formulations, the guidelines will focus upon software using this methodology.

Selection of Commercial CFD Software

Preliminary guideline development will be completed using the commercial CFD code Star-CD.[5] The Star-CD software was selected for this purpose largely because the code offers a great deal of the flexibility in computational mesh development with the ability to utilize polyhedral "cut" cells and recognize both integral and arbitrary interfaces between regions of the computational domain. Furthermore, user subroutines allow the user to implement significant modifications to most features of the code if such modifications are needed. It is anticipated that the applicability of the general guidelines to other commercial CFD codes, will be examined and that the extension of the guidelines to alternate commercial CFD software methodologies, such as Lattice-Boltzmann, will be pursued following the initial development stage.

1.1 SELECTION OF TRACTOR TRAILER GEOMETRY

The Generic Conventional Model[1] (GCM), developed by NASA Ames Research Center for scaled wind tunnel testing, is a generalized representation of a conventional U.S. tractor-trailer truck, as shown in Figure 1. The 1/8th scale model is approximately 2.5 m long by 0.3 m wide by 0.5 m high. The studies contained herein consider experiments that were completed in the NASA Ames 7 ft. by 10 ft. wind tunnel. Instrumentation included a force balance, 476 steady pressure transducers, 14 dynamic pressure transducers, and three-dimensional Particle Image Velocimetry (PIV). Data was collected at various Reynolds number values and yaw angles. The initial studies presented herein consider only the case using the standard configuration of the GCM with a vehicle-width based Reynolds number of $Re = 1.15$ million. Measurements using alternate configurations with add on devices will be used to evaluate whether computational modeling guidelines developed based upon these studies are sufficiently general to be applied in the evaluation of the aerodynamic characteristics of other vehicles under different operating conditions.

1.2 COMPUTATIONAL MODEL

The computational model employed in these studies was developed using the ES-Aero tool for aerodynamic drag simulation that is available as part of the Star-CD software package. The surface of the standard configuration GCM is defined using approximately 500,000 triangular surface elements based upon CAD data representations taken from optical scans of the actual model. A computational domain, which as external dimensions that are based on the cross-sectional dimensions of the wind tunnel, is developed based upon this surface definition using a semi-automated process that begins by creating a hexahedral mesh that is successively refined in smaller zones around vehicle, with integral cell coupling employed at the interfaces between zones. The dimensions of hexahedral elements that make up the zone immediately surrounding the vehicle are specified by user as the near vehicle cell size. The mesh elements near the vehicle surface are then further refined based upon local surface features identified by the user or selected automatically based on curvature or gap width. The user specifies a minimum allowable cell size that limits the refinement of the mesh in this step.

Using this locally refined hexahedral mesh, the original surface is "wrapped" by projecting the hexahedral mesh onto the original surface. The "wrapped" surface definition is then volumetrically expanded to create a subsurface which is used to cut away the portions of the locally-refined hexahedral mesh that fall inside the vehicle. A brick and prism cell extrusion layer is then created to fill the gap between the sub-surface and the "wrapped" surface. In this way, the polyhedral cut cells are removed some distance from the surface, and a consistent y^+ value between approximately 20 and 200, can be maintained regardless of grid resolution, insuring that the computational meshes are suitable for the turbulence models used in these studies. A final step further refines the wake region and the underbody region in order to better capture important flow features. An example of the mesh construction of the computational domain used in the GCM simulations is shown in Figure 2.

Using locally-refined, face-coupled computational domains with substantial numbers of non-hexahedral cells makes the standard practice of evaluating grid convergence by uniformly refining the entire mesh in all directions intractable. In the computational meshes used in these studies, two separate parameters determine the size of the mesh. Mesh sensitivity analyses included in these studies examine the effects of changes in the near-vehicle cell size and minimum cell size parameters on the prediction of the drag coefficient. However, this is not equivalent to the traditional grid convergence study because the grid is not uniformly refined in all directions throughout the domain and the vehicle surface definition cannot be exactly maintained for all models since the final surface definition is dependent upon the local refinement of the computational mesh.

Figure 1. Generic Conventional Model (GCM)

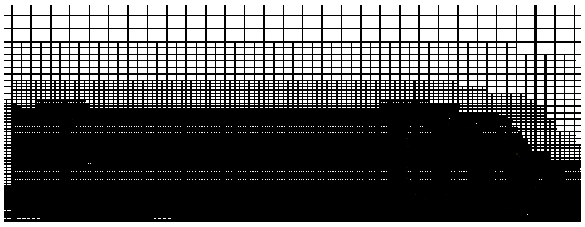

Figure 2. Example of computational mesh structure used in the simulation of the aerodynamic characteristics of the Generic Conventional Model (GCM).

1.3 COMPUTATIONAL REQUIREMENTS

Models are constructed using a 64-bit Itanium2 Linux workstation with 24 GB of RAM. The construction of the most coarsely-meshed models included in this study, from IGS data to final model, requires approximately 3 hours and peak memory usage is approximately 1.0 GB. The most finely-meshed models requires approximately 12 hours and the peak memory usage is approximately 5 GB. Since the automated mesh wizard included with the software package is used, little intervention is required by the user during this process. As with any software, initial models created by a novice user will likely require a larger initial time investment. All models employed in these studies are used as supplied from the automated tool with no manual repair or modification.

The Nuclear Engineering Division maintains a Beowulf cluster for performing engineering mechanics, fluid dynamics, and reactor engineering analyses. The cluster consists of three front-end (i.e., control) nodes and seventy-five compute nodes. One of the front-end nodes is a 32-bit servers contains dual Athlon MP 2.2GHz processors and 4 GB of memory. The two remaining front ends are 64-bit front-end servers: one with dual Itanium2 processors and 24 Gigabytes of memory, the other with dual Xeon processors and 8 gigabytes of memory. The cluster's file server provides nearly 1 Terabyte of home file system space. Each of the 75 compute nodes has a 3.2 GHz Pentium IV processor with 2 GB of memory. All of the machines in the cluster are interconnected via Gigabit Ethernet. All of the systems run RedHat Enterprise Linux.

2 BRIEF SUMMARY OF PRIOR RESULTS AT ZERO YAW

Initial studies focus on the prediction of the aerodynamic characteristics of the GCM at a yaw angle of zero. For this case, a preliminary mesh sensitivity study considering the effect of near vehicle cell size and minimum cell size on the accuracy of aerodynamic characteristics has been completed. Additional studies have considered the impact of turbulence model selection and the use of half vehicle versus full vehicle models.

2.1 BULK RESOLUTION SENSITIVITY

In previous efforts, five computational domains were generated based on the standard GCM configuration in order to evaluate the effects of the near vehicle cell size parameter on the prediction of the drag coefficient. Near-vehicle cell sizes of 16.0, 12.0, 10.0, 8.0 and 6.0 mm were considered. In each case, the minimum cell size resulting from local feature-based refinements is 12.5 percent of the near vehicle cell size. An additional restriction requires that a minimum of 16 elements are used to define any circle. In order to ensure that the quality of the vehicle surface is maintained, the cell layer immediately adjacent to the surface is refined to 25 percent of the original size prior to trimming. The computational domain characteristics are shown in Table 1.

In simulations using these models, a uniform inlet velocity condition and a zero gradient outlet condition were specified, and the standard high Reynolds number k-ε model was utilized. Convergence criteria were set so that 3000 iterations were completed, and all residuals fall below 10^{-4} by the 3000th iteration. Total computational time and clock time

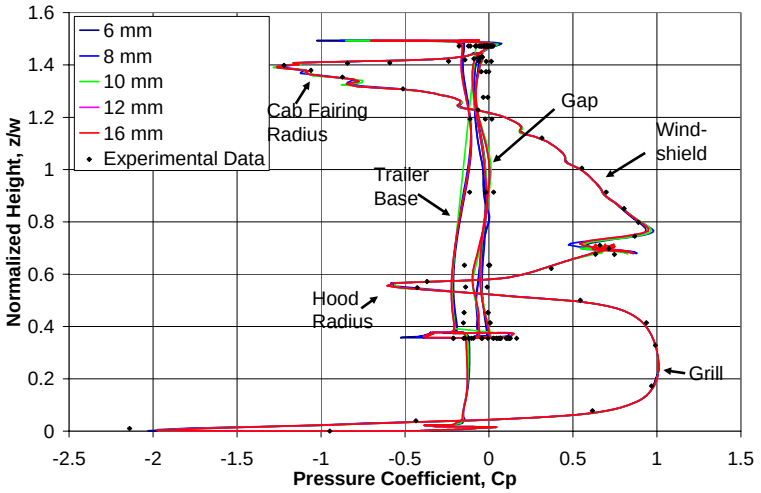

Figure 3. Comparison of predicted pressure coefficient distributions on the vehicle surface for various values of the near vehicle cell size parameter with experimental data for the GCM geometry.

when using 16 processors for each simulation are shown in Table 2. Predicted drag coefficients from each of the five cases are compared with experimental data from wind tunnel tests in Table 3. Pressure coefficient data was also extracted along the centerline of the vehicle for each case and compared with experimental data as shown in Figure 3. These comparisons show that the difference in the accuracy of the drag coefficient prediction as a function of the near vehicle cell size is a result of small differences in the pressure distribution over the entire surface rather than large localized differences.

2.2 NEAR WALL RESOLUTION SENSITIVITY

Following the assessment of the effects of the near-vehicle cell size parameter on the accuracy of the drag coefficient prediction, the effect of the near-wall cell size parameter was also considered. The near-vehicle cell size was set to 8mm and the minimum cell size for local refinement was reduced from 1mm to 0.5 mm. The change in the near wall resolution increases the number of computational elements from 3,282,426 to 4,264,232. The change in the computational mesh resolution results in a increase in the total CPU time from 610,958 seconds to 703,027 seconds. The change in the near-wall refinement parameter results in a reduction in the error of the drag coefficient prediction from 4.2 percent to 1.0 percent.

2.3 TURBULENCE MODEL SELECTION SENSITIVITY

In all simulations completed for the computational mesh sensitivity studies, the high Reynolds number k-ε turbulence model was used in conjunction with a standard logarithmic wall function for the prediction of turbulent kinetic energy and eddy diffusivity. While the high Reynolds number k- ε turbulence model is a robust general purpose turbulence model, the strong adverse pressure gradients and large flow recirculation regions associated with the GCM geometry may limit the applicability of steady state RANS modeling strategies. Using the computational mesh with a near vehicle cell size of 8 mm and a near wall cell size limit of 0.5 mm, simulations of the aerodynamic characteristics of the

Table 1. Summary of computational domain characteristics for evaluation of bulk cell size effects.

Near Vehicle Cell Size (mm)	Minimum Cell Size (mm)	Total Number of Volume Elements	Number of Volume Elements on Surface
16.0	2.0	1012338	73574
12.0	1.5	1737085	126119
10.0	1.25	2345640	175105
8.0	1.0	3282426	266666
6.0	0.75	5695622	400382

Table 2. Summary of computational cost for each case considered in the evaluation of bulk cell size effects.

Near-Vehicle Cell Size (mm)	Total CPU Time (seconds)	Total Clock Time (seconds)
16	206072	16454
12	390113	29392
10	417686	32182
8	610958	44967
6	2720956	188577

Table 3. Effects of Near-Vehicle Cell Size Parameter on Accuracy of Drag Coefficient Prediction.

Near-Vehicle Cell Size (mm)	Predicted Drag Coefficient	Error in Drag Coefficient
experiment	0.398	
16	0.449	12.0
12	0.441	10.3
10	0.418	4.9
8	0.415	4.2
6	0.405	1.7

Table 4. Results of the evaluation of two-equation turbulence models for prediction of drag coefficients for the GCM geometry.

Turbulence Model	Predicted Drag Coefficient	Percent Error in Prediction
Experiment	0.398	--
High-Reynolds Number k-epsilon Model	0.402	1.0
Menter k-ω SST model	0.401	0.8
RNG model	0.389	2.3
Chen's model	0.3919	1.61
Quadratic model	0.3815	4.32

Table 5. Drag coefficient predictions for full-vehicles.

Near-Vehicle Cell Size (mm)	Predicted Drag Coefficient	Percent Error in Prediction
16	0.441	10.3
12	0.426	6.7

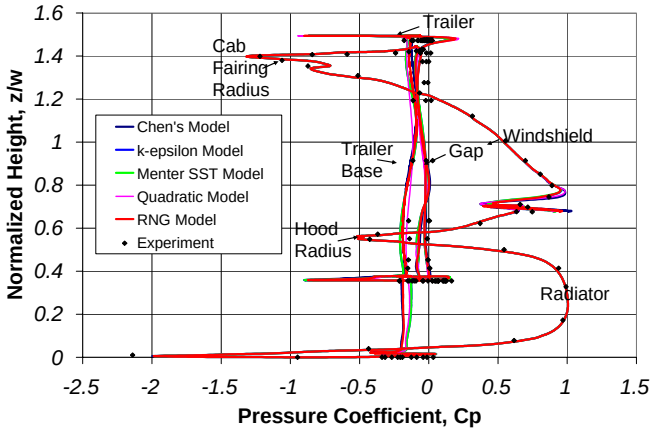

Figure 4. Comparison of predicted pressure coefficient distributions on the vehicle surface with experimental data for selected turbulence models.

GCM model were repeated using five steady RANS turbulence models and their associated wall functions: 1) the standard high-Reynolds number k-ε model with logarithmic wall function, 2) the Menter k-ω SST model, 3) the renormalization group (RNG) formulation of the k-ε model, 4) the Chen formulation of the k-ε model, and 5) the quadratic formulation of the k-ε model. Drag coefficients predicted using each of the selected steady-RANS turbulence models are shown in Table 4. Comparisons of the predicted pressure coefficient distributions when using the selected turbulence models are shown in Figure 4. The differences in the predicted drag coefficient are largely a result of localized discrepancies in the surface pressure coefficient predictions in the regions of separated flow, with the largest discrepancies appearing in the underbody region just behind the tractor.

2.4 HALF-VEHICLE VERSUS FULL-VEHICLE MODELS

In order to evaluate the effects of considering only half of the vehicle rather than the full vehicle, two models were created using the full vehicle geometry. These models use the same mesh parameter settings as the two coarsest models considered in the mesh sensitivity study. The full vehicle models are based upon near-vehicle cell sizes of 12 mm and 16 mm, with minimum near-wall cell sizes of 1.5 mm and 2.0 mm respectively. As in all previous studies, 3000 iterations were completed for each steady-state simulation and the convergence of the drag coefficient was monitored. As shown in Table 5, drag coefficient predictions show a slight improvement in agreement with experimental measurements when the full-vehicle model is used. The GCM geometry is in reality slightly asymmetric and the consideration of this geometric asymmetry is likely the primary difference in the models that contributes to these discrepancies.

3 RESULTS AT NON-ZERO YAW ANGLES

As an initial test of the general applicability of the lessons learned from the zero yaw angle sensitivity studies, the aerodynamic characteristics of the GCM were evaluated at yaw angles ranging from 1 to 14 degrees. In the wind tunnel experiments, three separate drag states are observed over this range. In the near-zero yaw range, drag, lift and side force coefficient values are all at their lowest values. Between 2 and 3 degrees, drag force coefficients rise rapidly to a higher drag state, presumably as a consequence of large separation zones forming on the leeward side of the vehicle. Between 10 and 15 degrees, drag force coefficients fall to a lower drag state, presumably because side forces grow to become the dominant forces in this range. Considerable hysteresis was noted in the experiments between yaw angle sweeps moving from positive to negative angles versus negative to positive angles.

3.1 YAW ANGLE SENSITIVITY OF NOMINAL MODEL

For each yaw angle, computational models were constructed using a near vehicle cell size of 8 mm and a near wall cell size of 1mm. Since the yawing of the GCM at angles greater than zero removes the option of considering only a half vehicle because there is no longer a symmetric plane, only full vehicle models were considered. All simulations use the standard high Reynolds number k-ε model with a logarithmic

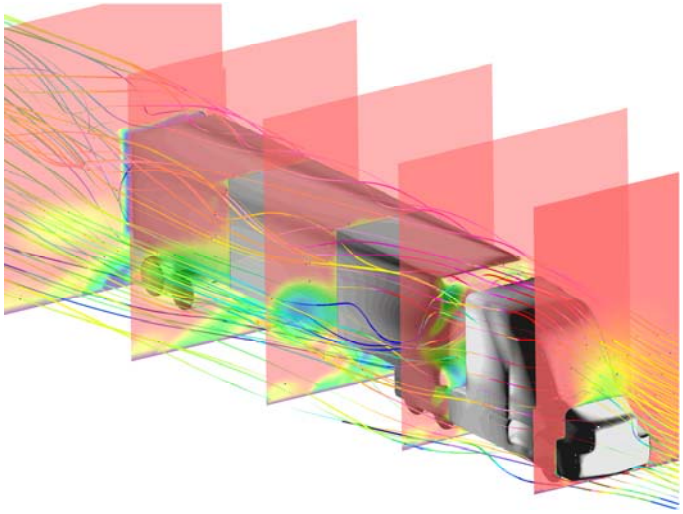

Figure 8. Streamlines showing predicted air flow across the surface of the GCM at a yaw angle of 10 degrees. Streamline color and translucent cutting planes indicate local velocity magnitude. Vehicle surface shading indicates pressure distribution

wall function. As in all previous studies, 3000 iterations were completed for each steady-state simulation and the convergence of the drag coefficient was monitored.

Predicted drag force coefficients are compared with experimental data from wind tunnel studies in Figure 5. Predicted drag coefficients appear to capture the jump from the low drag state to high drag state between 2 and 3 degrees. However, the low drag state predictions are much more accurate when compared to experimental data. Low drag state predictions exhibit less than 4 percent error while high drag state predictions exhibit errors of slightly more than 10 percent. Drag coefficient predictions do not appear to capture the observed drop to a lower drag state at higher yaw angles.

Predicted lift and side force coefficients are compared with experimental data in Figures 6 and 7, respectively. Both lift and side force predictions appear to capture the trends observed in the wind tunnel experiments well. Lift force coefficient predictions exhibit a maximum error of approximately 35 percent at zero yaw. Side force coefficient predictions exhibit a maximum error of approximately 15 percent at 4 degrees yaw.

At yaw angles greater than 2 degrees, large flow separation zones begin to form along the leeward side of both the tractor and trailer, introducing significant turbulent instability into the flow field. The instability is further exacerbated by the formation of a highly turbulent jet through the gap between the tractor and trailer which washes over the logical separation points on the leeward side of the trailer, extending the separation zone. While 2-D representations may illustrate the primary challenges in modeling the flow field surrounding the GCM at yaw angles greater than zero, the true complexity of the flow can only be visualized when considered in the 3-D as in Figure 8. It is anticipated that selective refinement of the separation regions or the application of a more rigorous turbulence modeling strategy may lead to improvements in predictive capability.

3.2 BULK RESOULTION SENSITIVITY OF PREDICTIONS AT NON-ZERO YAW ANGLES

To evaluate the sensitivity of aerodynamic coefficient predictions to changes in the near vehicle cell size, a parametric evaluation was completed using near vehicle cell sizes of 8 mm, 12 mm, and 16 mm as a basis for models of the GCM geometry at angles of 3, 6, and 9 degrees. Predicted drag coefficients are compared with experimental data in Figure 9. While the cases using the 8mm near vehicle cell size clearly capture the shape of the drag curve within a fairly consistent error, the coarser cases do not clearly show the same trend and the error band is not as regular. While this may indicate that the use of a smaller near vehicle cell size could improve the quality of the prediction, the resultant mesh would be too cumbersome to be of practical use in a design effort, and this possibility has not been considered in this study.

Predicted lift and side force coefficients are shown in Figures 10 and 11. As with the drag coefficient, the 8mm case appears to capture the shape of the lift force coefficient curve while the coarser models fail to predict the curve shape. For the lift force coefficient, the error band is fairly regular for the 8mm near vehicle cell size while the error in the prediction with the coarser models is more irregular. The error in the prediction of the side force appears to be relatively insensitive to the near vehicle cell size.

3.3 NEAR WALL RESOLUTION SENSITIVITY OF PREDICTIONS AT NON-ZERO YAW ANGLES

To evaluate the sensitivity of aerodynamic coefficient prediction to changes in the near wall cell size, a parametric evaluation was completed using a near vehicle cell size with near wall cell sizes of 1.0 mm, 0.5 mm, and 0.25 mm as the basis for models of the GCM at yaw angles of 3, 6, and 9 degrees. Predicted drag coefficients are compared with experimental data in Figure 12. The additional near wall refinement of the 0.5 mm case clearly provides an improvement over the nominal 1.0 mm case. However, the improvement that results from further refinement to 0.25 mm is minimal.

The predicted lift and side force coefficients are compared with experimental data in Figures 13 and 14, respectively. The lift force coefficient does not show the same consistent improvement as is seen with the drag coefficient, with larger errors seen for the 6 degree case. As in previous sections, the error in the side force coefficient prediction is small in comparison to the errors in the other coefficients.

3.4 TURBULENCE MODEL SELECTION SENSITIVITY OF PREDICTIONS AT NON-ZERO YAW ANGLES

To evaluate the effects of turbulence model selection on the accuracy of drag coefficient predictions at non-zero yaw angles, a parametric study was completed using the computational model with an near vehicle cell size of 8mm and near wall cell size of 0.5 mm. Three different turbulence models were considered: 1) the standard high-Reynolds number k-ε model, 2) the Menter k-ω SST model, and 3) the renormalization group (RNG) formulation of the k-ε model. All of these models were employed in conjunction with model-specific logarithmic wall functions.

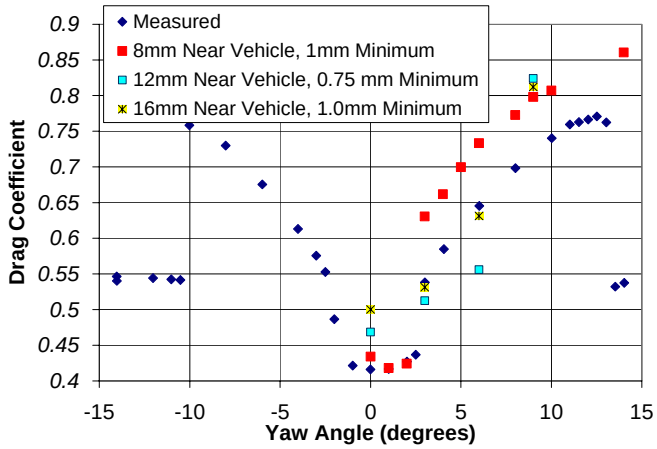

Figure 9. Comparison of Drag Coefficient Predictions as a Function of Yaw Angle and Near Vehicle Cell Size.

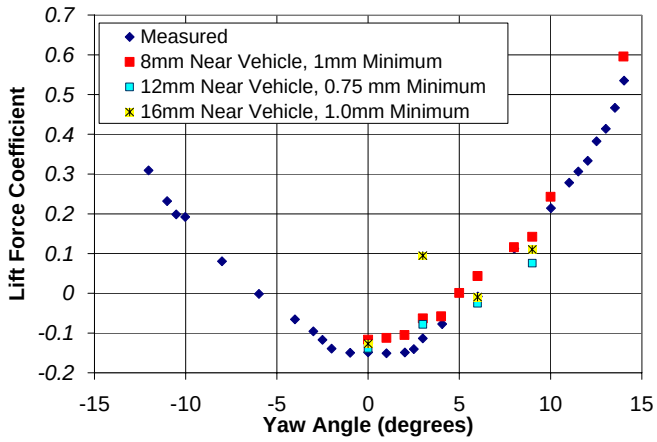

Figure 10. Comparison of Lift Force Coefficient Predictions as a Function of Yaw Angle and Near Vehicle Cell Size.

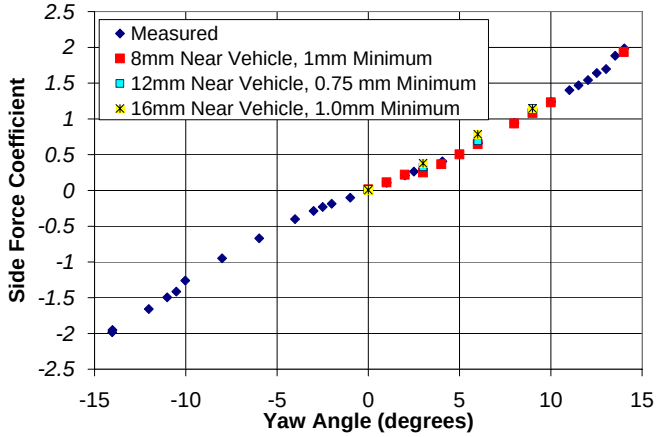

Figure 11. Comparison of Side Force Coefficient Predictions as a Function of Yaw Angle and Near Vehicle Cell Size.

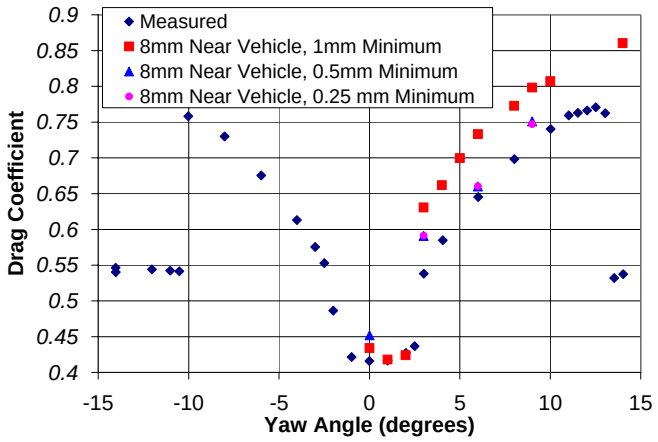

Figure 12. Comparison of Drag Coefficient Predictions as a Function of Yaw Angle and Near Wall Cell Size.

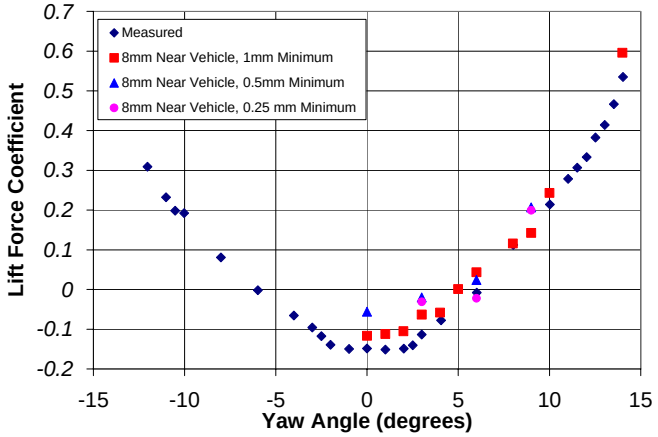

Figure 13. Comparison of Lift Force Coefficient Predictions as a Function of Yaw Angle and Near Wall Cell Size.

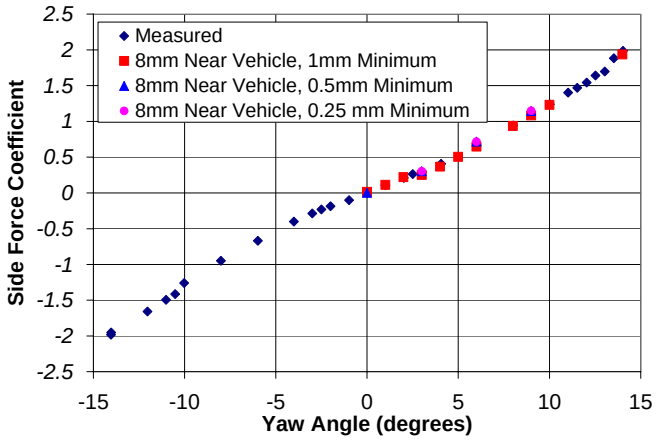

Figure 14. Comparison of Side Force Coefficient Predictions as a Function of Yaw Angle and Near Wall Cell Size.

Predicted drag coefficients are compared with experimental data in Figure 15. Lift and side force coefficients are compared with experimental data in Figures 16 and 17, respectively. In the prediction of drag coefficient, the high-Reynolds number k-ε model shows some advantage over the other models considered at higher yaw angles. The predicted drag coefficient typically exhibits an oscillatory behavior as a function of iteration number, and the difference between the Menter k-ω SST model and the renormalization group (RNG) formulation of the k-ε model is within the band of oscillation of the drag coefficient over the final 200 iterations. The accuracy of the lift force coefficient prediction appears to increase with yaw angle, with the largest errors seen at 0 degrees for this case. For both the lift force coefficient and the side force coefficient predictions, all three turbulence models appear to provide comparable performance.

4 CONSIDERATION OF ADD-ON DEVICES

As an initial test of the capability of the approach used in these studies to predict changes in drag coefficient when after-market drag reduction devices are employed, a modified version of the GCM was developed which incorporates an ogive boat tail based upon the inflatable boat tail design of Aerovolution, Inc. Aerovolution provided CAD data describing the surface of the boat tail, which was scaled to the match the rear face of the GCM trailer. Surfaces were created based on this description and merged with the GCM model to create the geometry shown in Figure 18. Using the methodology outlined above, three models were generated to assess the mesh sensitivity of the results and try to provide some feel for the accuracy of the solutions. The models use near vehicle cell sizes of 8 mm and 12 mm and near wall cell sizes of 1.0 mm and 0.5 mm. The standard high-Reynolds number k-ε model was used in all cases. The predicted drag coefficients are shown in Table 6. For the case with a near vehicle cell size of 8 mm and a near wall cell size of 0.5 mm, these results indicate a reduction in the drag coefficient of approximately 7 percent. At highway speeds, this would correspond to a fuel savings of approximately 3.5 percent. The predicted velocity field at the centerline of the vehicle with the boat tail device is compared with the velocity field for the standard GCM geometry in Figure 19. The device clearly reduces the size of the low velocity area (shown in blue).

that corresponds to the position of the recirculation zones behinds the vehicle. Futhermore, it significantly reduces the length of the wake behind the vehicle. Even if the fuel economy reduction is small, the device may reduce the impact of the vehicle's wake on the safety of automobiles traveling behind the vehicle.

Road test data has been requested from Aerovolution for comparison with the prediction results to confirm the accuracy of the solution.

5 CONCLUSION

These studies are the initial components of an on-going assessment of the capabilities for the prediction of heavy vehicle aerodynamic characteristics using current generation commercial computational fluid dynamics software. Based on the outcomes of these studies, guidelines are being developed for the immediate application of these current generation tools by the heavy vehicle manufacturing community. Initial assessments have shown that drag coefficients can be predicted within less than 1 percent of the measured value and the surface pressure distributions can be predicted with reasonable accuracy for vehicles at zero yaw angle, even when the standard k-ε type models and logarithmic wall functions are utilized. Near wall resolution appears to have more impact than bulk resolution on the accuracy of the results, indicating that resources should be focused in the near wall region. For the bare 1/8th scale GCM geometry, a near wall cell size of 1.0 mm overall and 0.5 mm in regions of geometric complexity, such as the hood vent, combined with a near vehicle cell size of 8 mm provides predictive accuracy for the drag coefficient on the order of 1 percent. As yaw angle increases to values greater than zero, predictive accuracy is somewhat eroded, but the prediction of general trends is still observed. It is anticipated that on-going sensitivity studies may lead to additional guidance for the consideration of tractor-trailer vehicles at yaw angles greater than zero. Additional studies will evaluate the applicability of these trends to more realistic geometries.

6 REFERENCES

Satran, D., "An Experimental Study of the Generic Conventional Model (GCM) in the NASA Ames 7-by-10-Foot Wind Tunnel," United Engineering Foundation Conference on the Aerodynamics of Heavy Vehicles: Trucks, Buses, and Trains, United Engineering Foundation, New York, 2002.

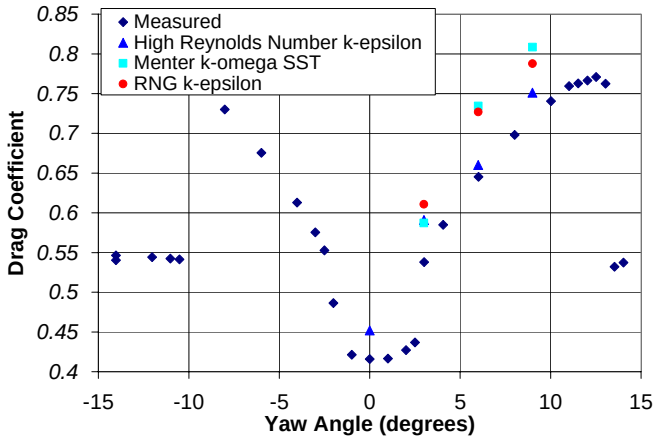

Figure 15. Comparison of Drag Coefficient Predictions as a Function of Yaw Angle and Turbulence Model.

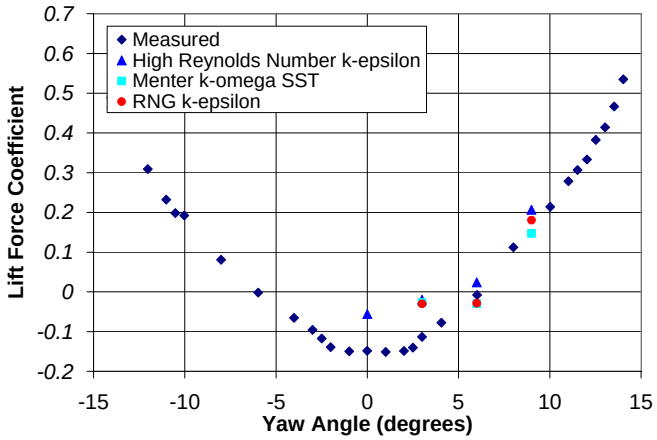

Figure 16. Comparison of Lift Force Coefficient Predictions as a Function of Yaw Angle and Turbulence Model.

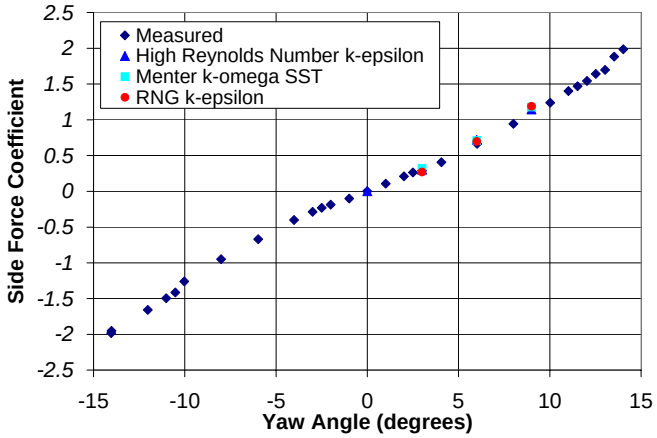

Figure 17. Comparison of Side Force Coefficient Predictions as a Function of Yaw Angle and Turbulence Model.

Figure 18. Modified GCM Geometry with Aerovolution's Inflatable Boat Tail Device.

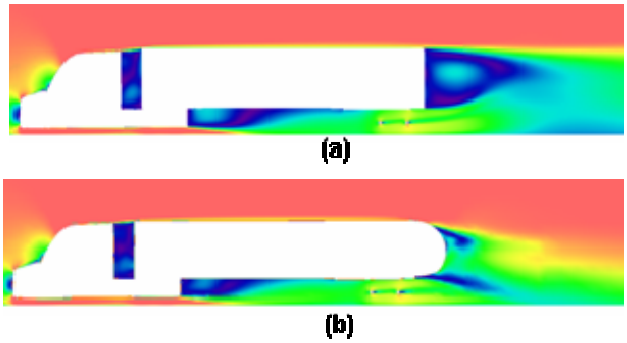

Figure 19. Comparison of Velocity Magnitude Predictions without (a) and with (b) the boat tail device installed.

Table 6. Drag coefficient predictions for vehicle with Boat tail device as a function of Mesh parameters.

Near Vehicle Cell Size	Near Wall Cell Size	Drag Coefficient
12 mm	2 mm	0.4179
8 mm	1 mm	0.4116
8 mm	0.5 mm	0.3975